CWP-240
February 1997

The Quality of the Surface-Consistency Assumption in Residual-Statics Estimation

Gabriel Perez

— Master's Thesis —
Geophysics

Center for Wave Phenomena
Colorado School of Mines
Golden, Colorado 80401
303/273-3557

ABSTRACT

Reflection data from land seismic surveys typically suffer from time-distortions, commonly attributed to anomalies in the velocity and thickness of the near-surface layers. These time-distortions are generally detrimental to the quality of the final seismic image. Residual statics are still present in the data after the application of field- and refraction-static corrections. Residual-statics problems are then related to rapid near-surface variations, beyond the resolution of previously-applied methods. The surface-consistency and time-invariance assumptions allow us to approach the problem of correcting for residual statics from a statistical viewpoint.

Reasons conventionally cited to support the validity of these assumptions are consistent with a ray-theoretical model of wave propagation in the near surface, ignoring the potential influence of wave-theoretical aspects. I study the magnitude and implications of that influence using measurements of time-distortions present in synthetic data generated by finite-difference acoustic modeling in subsurface models with a sinusoidal base of weathering. Albeit simple, the models considered are meant to address the essentials of the problem of residual statics.

I study the character of the time-distortions and the departure from surface-consistency as a function of the parameters of the near-surface. Even though it constitutes a simplification of a complex phenomenon involving the entire medium, viewing a given arrival at the receiver as the result of averaging information from a finite region in the medium (specifically, from the base-of-weathering) helps in understanding qualitatively the character of the time-distortions and its relation to the medium parameters. I estimate the size of that region along the base-of-weathering using the familiar concept of Fresnel zone.

Except when the weathering thickness is much smaller than the seismic wavelength, wavefront healing considerably reduces the size of the time-distortions for anomalies of short wavelength. For larger-wavelength anomalies, the time-distortions increase in magnitude with increasing offset due to ray-bending within the near-surface.

I quantify the errors in the surface-consistency assumption by comparing the time-distortions with those expected under that assumption. Consistent with experience, the quality of the assumption degrades with increasing ratio of spreadlength to reflector depth. The validity of the surface-consistency assumption is best for relatively long-wavelength anomalies in a weathering layer that is relatively thin. While the shortcomings in that assumption are largest where the weathering layer is relatively thick, wavefront healing limits the amplitudes of time anomalies in that situation. These results contrast with those for the quality of residual-static corrections computed as the solution to a general linear inverse problem, which is founded upon the assumption of surface-consistency. The quality of solution to that linear problem is better for short-wavelength anomalies, or equivalently, for large spreadlength.

Diffractions interfering constructively because of the regular sinusoidal shape adopted for the near-surface model, and other events such as multiples, act like noise that biases the estimates of time-distortions in this study. Although judged to be the most useful approach for this study, finite-difference modeling of wave propagation is troubled by issues of computational cost and accurate representation of interfaces. Also, the choice of a boundary condition at the earth's surface is most critical when attempting to simulate near-surface phenomena, with finite-differences or other methods.

Accurate modeling of wave propagation in the near-surface is still a largely unsolved matter. Our knowledge of the near-surface is still quite imperfect, both in the formulation of a proper model of wave propagation and in the definition and estimation of relevant physical properties.

TABLE OF CONTENTS

ACKNOWLEDGMENTS

I gratefully acknowledge the financial support of the national oil company of Colombia, Ecopetrol, and its research division, ICP, as well as the decisive support of Ariel Solano and Kurt Bayer. The former ICP director, Dr. Neftali Puentes, deserves recognition for his role in promoting the high-level training programs in geophysics and other areas that gave me the opportunity to become immersed in this fascinating science.

This research would not have been possible without the scientific and logistic support I got from the Center for Wave Phenomena and the friendship and help from all the professors, staff and fellow students in CWP. This research was partially supported by the Advanced Computational Technology Initiative (ACTI), subcontract number 4731U0015-2F, in conjunction with Los Alamos National Laboratory and industry partners. Computational support was provided by NSF under grant DMS-9505049.

I wish to thank Dr. Ken Larner for being my thesis advisor. Having had the privilege to work with him will remain a source of pride for me, besides my appreciation for his willingness to deal with my sometimes subjective and careless character. Dr. Larner's ability to make simple and get to the heart of the most intricate technical matters is the best lesson to learn from him.

Dr. Norm Bleistein and Dr. John Scales served in my committee and provided useful input for my research and the writing of this thesis.

Hermann Jaramillo and Gabriel Alvarez paved the way so that others like me just needed to follow them in our way here; they were also very helpful in many instances in my studies. Trino Salinas and the members of the "S-team" group provided useful comments and helpful discussions.

I learned by example from my parents Gabriel and Edelmira that the true heroes of daily life are those who get up everyday and work hard to meet their responsibilities.

The deepest gratitude goes to my wife Bertha Elisa, who has put up with me always giving me her love and support, even if it has meant changing her life time and again at the pace of my devious career. My sons Camilo Andres and Juan Fernando were always there reminding me that there is more to life than geophysics.

DEDICATION

To Bertha Elisa, who has given me so much that even as I try the hardest, I will never be able to correspond. To Camilo Andres and Juan Fernando, may this be the sort of example they need from their father.

With all of my love.

Chapter 1

INTRODUCTION

1.1 Reflection-time distortions: the surface-consistency assumption

Reflection data from land seismic surveys typically suffer from time-distortions commonly attributed to anomalies in the velocity and thickness of the near-surface layers. These time-distortions are generally detrimental to the quality of the final seismic image. The conventional approach to the correction for these distortions considers them as static (i.e., time invariant), surface-consistent trace-dependent time shifts associated with vertical travel paths in the near-surface.

These assumptions are suited to the common situation where the velocity of waves in the weathering layer is low compared to that in the sub-weathering; the departure from vertical raypaths should also be small, and the near-surface layer thin, with only minor lateral variations in thickness and velocity. The assumptions also imply that wave-theoretical influences on time-distortions can be ignored. Practical methods developed to correct for time-distortions induced by propagation through the near-surface generally work well in estimating short-wavelength components (wavelength smaller than the spread length) of static corrections where the subsurface is relatively uncomplicated and at least approximately layered.

1.2 Implications of geologic complexity

As dictated by the realities of the hydrocarbons and mineral resources business, exploration is being conducted for targets of increasing complexity and difficulty, where tools such as reflection seismology are being pushed toward their limits. In areas of complex geology, characterized by large lateral and vertical velocity variations, the assumptions of surface-consistency and time-invariance of the time-distortions can be in error; on the other hand, conventional methods for statics estimation based on normal-moveout (NMO) correction might fail because of the inadequacy of the NMO assumption, due to the occurrence of multi-valued or non-hyperbolic moveout.

The issues of non-hyperbolic and multi-valued moveout have been addressed by Tjan (1995), who proposed the introduction of prestack depth migration followed by stack and multi-offset modeling in the estimation of reference traces. Tjan tested the method, with promising results, for complex synthetic data from the Marmousi dataset, which was simplistically contaminated in a surface-consistent manner with pseudo-random, low-cut filtered (i.e., wavelength components larger than the spread length were suppressed) static shifts. The question could be raised then, as to the performance of the prestack-migration-based approach in the presence of more realistic,

expectedly non-surface-consistent, time-distortions.

In all justice, the same question should be posed of any other static-estimation method based on the surface-consistency assumption. In fact, we should not limit ourselves to consideration of a particular method but rather leap toward generality by consideration of the more fundamental question of the validity of the surface-consistency assumption itself, and of the relative importance, for surface-consistency (or for departure from surface-consistency, for that matter), of some of the factors mentioned earlier, such as the magnitude and variation in thickness and velocity of the weathering layer.

To my knowledge, this question has not been addressed in a systematic study but rather has been left to confirmation in practice. Even if static-estimation methods based on surface-consistency do yield robust and useful solutions most of the time in common practice, we still have little feeling for the magnitude of the errors we are incurring with that assumption. Probably in many situations, residual-statics errors influence mainly subtle features such as the quality of individual stack traces or wavelet character, and important differences might be difficult to observe at first hand. As previously observed, reflection seismology is increasingly being used in situations where departure from some of the above-stated conditions for the validity of the surface-consistency assumption is ever more likely. On the other hand, independent of the degree of geological complexity, we can presume that, for the rapid variations in near-surface conditions addressed by residual-statics, wave-theoretical aspects should have some distinguishable influence. What is the magnitude of that potential influence and what are its implications, are other valid and interesting questions.

1.3 A model of the near-surface?

To examine the validity of the surface-consistency assumption, somewhat realistic time-distortions should be generated by a modeling procedure. Here, questions arise as to how to define a velocity model of the near-surface, and what modeling algorithm to use, so that the generated distortions resemble those found in field data.

One difficulty in doing the velocity modeling is that our knowledge of the near-surface geology and structure is still quite imperfect, despite its tremendous importance to the nature and quality of surface seismic recordings. Even if a plausible model of the near-surface could be built, the question would still exist as to whether or not the results of specific studies would be general enough to allow drawing some useful conclusions. The problem is certainly complex, and the most general formulation would surely involve a large number of parameters; an alternate approach would be to choose simple models, characterized by a few key parameters, in hopes that in that case, clear and unambiguous relationships can be established between the results and the model parameters.

As to the choice of modeling algorithm, if we wish to have the chance at observing wave-theoretic phenomena, we should direct our search toward a full-waveform solution of the wave equation. A finite-differences, two-way wave-equation solver offers

an opportunity to model wave propagation with some degree of accuracy.

1.4 Purpose and scope of this thesis work

Wiggins et al. (1976) presented a now-classic study on the quality of surface-consistent residual static solutions as a function of spatial wavelength via an eigenvector analysis. That analysis, however, remained fully within the assumption that near-surface-induced time anomalies are surface-consistent. Thus, the problem as defined was a linear one. If the wave-theoretic anomalies were a linear function of the shape of the near-surface, then what we learn from studies with a simple sinusoidally-varying near-surface could be used to build expected time-distortions for more complicated models. We cannot expect to be as fortunate as that since the problem of near-surface-induced time anomalies is nonlinear. I hope nevertheless, to be able, as proposed above, to use simple models to characterize the influence of some key parameters.

Following that idea, in this thesis I study the validity and implications of the surface-consistency assumption through consideration of wave-theoretic time-distortions for plane reflectors in 2D models whose near-surface layer structure is simply sinusoidal, as illustrated in Figure 1.1. For problems that are linear, one can understand them through use of sinusoidal variations. Although the problem here is nonlinear, the hope is that we can still gain some general understanding from a study involving weathering layers whose base is sinusoidal. I perform a number of modeling tests involving variation in the parameters describing the near-surface. In a further abstraction of the problem, I attempt to draw general conclusions from the time-distortions observed on just a single shot-record for each test. Wave-theoretic anomalies are obtained by finite-difference simulation on a sufficiently fine computational grid, for the wavelengths considered; the pertinent details are presented in Chapter 3 .

The nature of the time-distortions and the implications for surface-consistency are characterized in terms of the observed dependence on parameters of the model, specifically, the geometry of the sinusoidal-shape layer, seismic wavelength and layer velocity. I compare the wave-theoretic time anomalies obtained for a number of specific model parameters with those expected under the assumption of surface-consistency, to qualify the validity of that assumption.

Figure 1.2 presents an example of a shot record generated for one of the models. I will purposedly omit any discussion on the details of how the data were generated, and on particular parameters; a thorough discussion of those aspects is given in Chapter 3. Let us rather examine some general features in the data.

The near-surface layer for the velocity model used to generate the data in Figure 1.2 has a sinusoidal variation with 400-m wavelength; the time-distortions induced in the reflection just below 1.0 s are clearly visible as an oscillating departure from a standard hyperbolic reflection-shape; similar distortions are indeed present in the first arrivals (head waves).

The solid-line curve in Figure 1.3 presents my estimate of the time-distortions

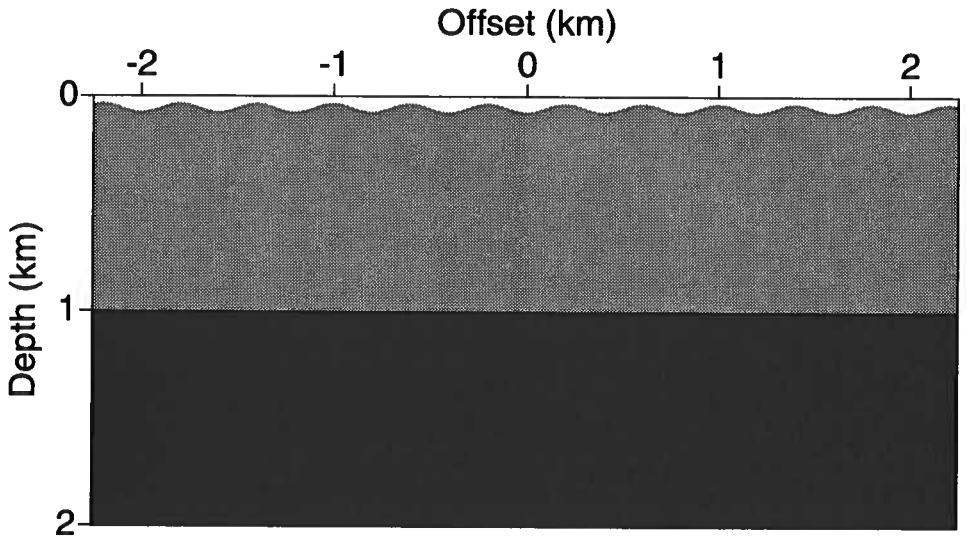

FIG. 1.1. Schematic depth section depicting general model consisting of a sinusoidal base-of-weathering and a deep reflector. Darker shading indicates higher velocity.

present in the reflection from the data in Figure 1.2, due to the occurrence of the variations in the near-surface layer. Here again, a discussion with details on how these time-distortions are estimated is postponed for Chapter 3. Also shown in dotted-line, are the distortions that one would expect to have if these distortions were purely surface-consistent and attributable to vertical raypaths in the weathering layer. It can be seen that the variations in the time-distortions are largely periodic, with a wavelength similar to that in the near-surface variations; the separation between the solid and dotted curves indicates a departure from surface-consistency that in this case increases with increasing offset.

Figure 1.4 shows the time-distortions estimated for the data from a similar model which differs in that the wavelength of the sinusoidal base-of-weathering is a much shorter 50 m. The differences from Figure 1.3 are notable, though similarities also exist. First, the 50-m wavelength of the near-surface variations for Figure 1.4 is also roughly that observed for variations in the time-distortions. The time-distortions in Figure 1.4, however, exhibit significant departure from those that would be obtained under the assumption of surface-consistency. The departure is much larger than that observed for the time-distortions in Figure 1.3, and interestingly, it is of opposite sense, i.e., it *decreases* with increasing offset.

The brief excerpt, just presented, from some of the results that I will examine in greater detail later on is intended to illustrate issues I will address. For example: what are the reasons for the differences in character between the time-distortions presented in Figures 1.3 and 1.4? Quite likely it must be related to the change in the wavelength

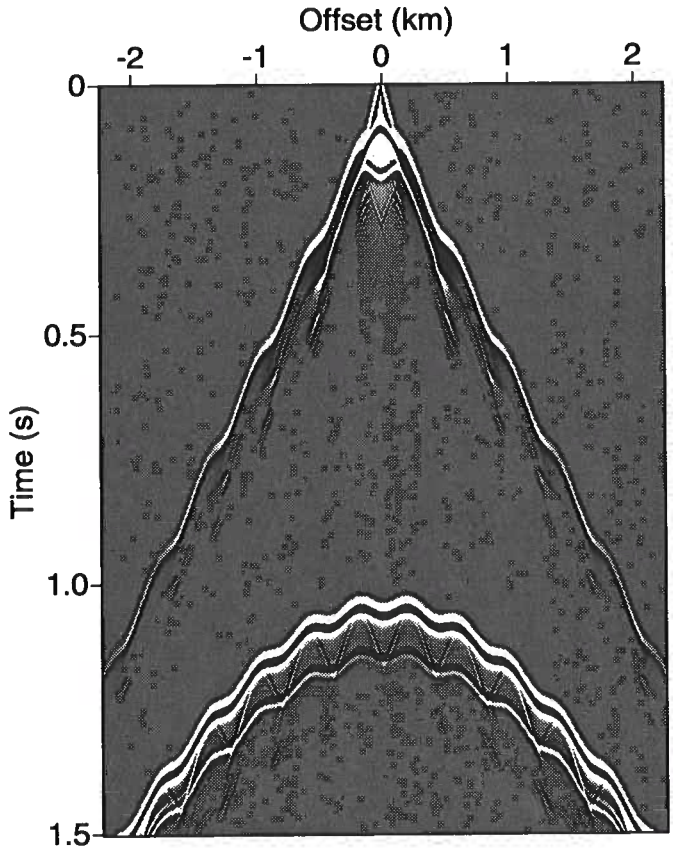

FIG. 1.2. Synthetic shot record generated for a 3-layer model featuring a sinusoidal variation in the shape of the base-of-weathering interface. The reflection just after 1.0 s zero-offset time comes from the horizontal interface between the second and third layers.

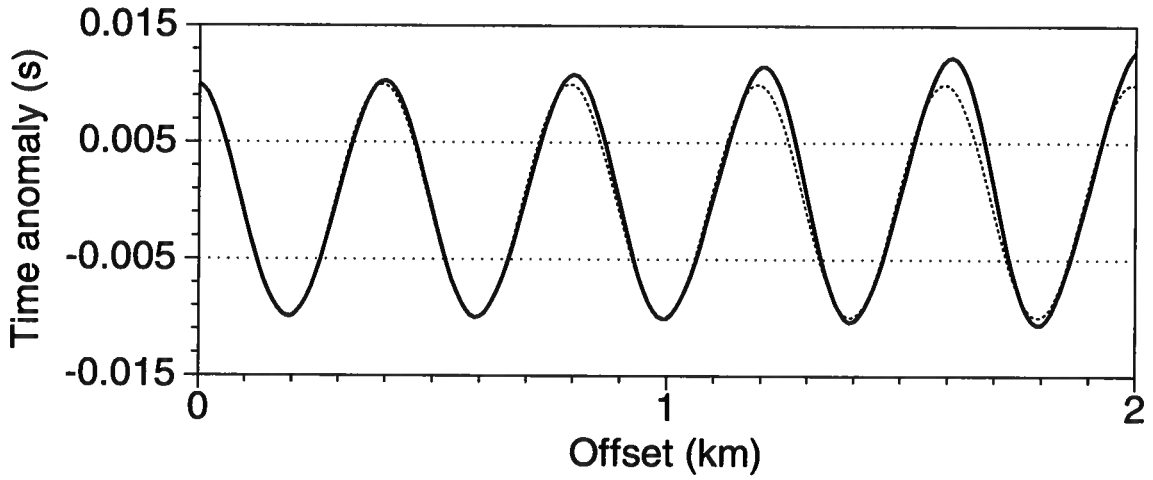

FIG. 1.3. Solid line: time-distortions estimated for the reflection in Figure 1.2. Dashed line: the corresponding surface-consistent statics. This convention is followed in similar plots throughout the thesis.

in near-surface variation, but, other than that what can we say? How large is the departure from surface-consistency in one case as compared to the other? How can we quantify that departure? What lessons can be learned on the relationship between the extent of that departure and variations in the model parameters? Taking care of these issues in some detail will be the purpose of the work in the succeeding chapters.

1.5 Content overview

In Chapter 2 , I review the main ideas concerning estimation of static corrections in seismic data processing practice, placing the subject of residual-statics estimation in a general context. I introduce the key issues to be addressed and provide some background to support the approach followed in the study.

Chapter 3 is devoted to the study of modeled wave-theoretic time anomalies. First, I briefly discuss the motivation and limitations of the choice of a sinusoidal model for near-surface variations. Then I describe in detail the generation of synthetic shot records and the estimation of reflection-time anomalies for 2D acoustic earth models featuring a sinusoidal variation in the thickness of the near-surface layer. We shall see the data and the corresponding time-anomalies for a number of modeling tests involving variation in one or more of the parameters considered. I also discuss the implications of some issues related to practical implementation of finite-difference modeling, such as the choice of a boundary condition at the model boundary corresponding to the earth's surface, and the procedure for representing interfaces in the velocity model on a discrete grid.

Chapter 4 is devoted to the study of the influence on the character of the time-distortions and on the departure from surface-consistency, of variations in the near-

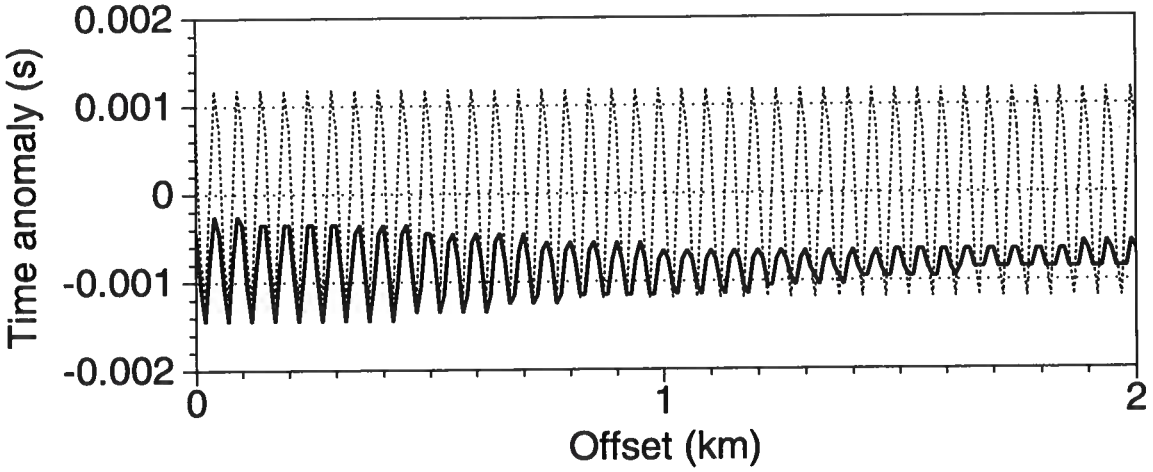

FIG. 1.4. Time-distortions estimated for data from a model featuring a 50-m wavelength variation in the near-surface.

surface parameters. I characterize the dependence on those parameters of wave-propagation phenomena influencing the generation of the time-distortions. I quantify the extent of departure from surface-consistency of the wave-theoretic time-distortions and discuss the implications for the validity of the surface-consistency assumption.

In Chapter 5 I explore the implications of reflector dip for the character of the time-distortions and the departure from surface-consistency.

Finally, in Chapter 6 I summarize the contributions of this work to the understanding of implications and quality of the surface-consistency assumption and give general conclusions. Chapter 7 is devoted to a discussion on open questions and recommendations for future work.

Chapter 2

THE ESTIMATION OF STATICS CORRECTIONS IN SEISMIC DATA PROCESSING

The purpose of this chapter is giving an overview of the basic issues related to estimation of statics corrections, as well as the main approaches existing in common seismic data processing practice, their scope and limitations. My goal is to provide a general context for the subject of this research, introducing the key issues to be addressed (specifically, those related to residual-statics problems) and supporting the relevance of the approach followed in this study.

2.1 Near-surface-induced distortions and image quality

As previously stated, reflection-time distortions are typically present in land-acquired seismic data. If not properly corrected for, these might severely degrade the quality and resolution of the final seismic image. Relative time shifts among the traces in a common-midpoint (CMP) gather would cause the reflection events to be misaligned, thereby both impairing the ability of the stacking to enhance the primary signal and corrupting wavelet character. On the other hand, time-shifts among the traces of different CMP gathers, not related to the true configuration of reflectors in the subsurface, would yield a distorted structural picture. Although such time-distortions can be caused by structural complexity in the deeper subsurface, often they arise from irregularities in the near-surface.

Typically in onshore exploration areas, the land surface is covered with a relatively thin layer of poorly consolidated material of anomalously low seismic velocity, commonly referred to as the weathering layer; rapid variations in the physical properties of this upper layer will introduce large distortion of reflections from depth. Near-surface layers could be viewed as a filter whose response depends on the path of the seismic wave: variations in surface elevation, near-surface thickness or velocity, result in phase and amplitude distortion of the propagating wavefront (Taner et al., 1974). The accurate estimation of this filter is difficult in practice, mainly because of the low definition of near-surface structure provided by conventional seismic exploration techniques, which are aimed at deeper targets in the subsurface.

The presence of low- or high-velocity layers does not pose special time-distortions problems by themselves. Those rather arise from the anomalous variation in the velocity and thickness of the near-surface, and from the limitations in our ability to accurately define those variations and compensate for them. Lateral variations are particularly challenging for conventional CMP processing, more suited to a laterally invariant, layered earth model.

2.2 The surface-consistency assumption

Conventional methods to correct for near-surface-induced distortions avoid the complex problem of estimating the full wave-theoretical near-surface filter response by making simplifying assumptions (Hileman et al., 1968; Taner et al., 1974; Wiggins et al., 1976): corrections are estimated as simple time-invariant (i.e., static) delays introduced to the seismic traces. Furthermore, these are assumed to be "surface-consistent" i.e., a single time delay is assigned to each particular surface location, regardless of the details of wave propagation (see Figure 2.1).

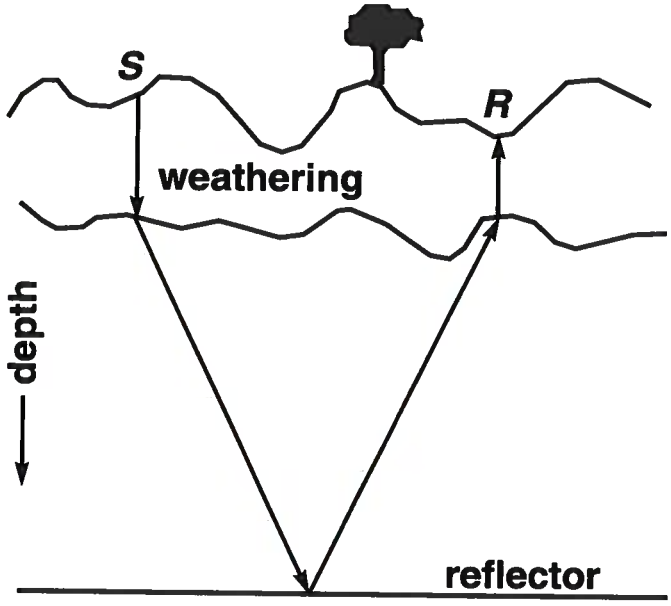

FIG. 2.1. Surface-consistent statics model: if waves propagate as vertical rays through the near-surface, time-distortions will be a single time-invariant delay for each shot (S) or receiver (R) position.

Those assumptions, which allow us to approach the problem of correcting for near-surface-caused time anomalies from a statistical viewpoint, are consistent with a model of vertical travel path of seismic energy through the near-surface; they also imply that wave-theoretical influences on time anomalies can be ignored (Larner et al., 1996). Vertical propagation is approximately correct if the velocity of the weathering layer is much lower than that in the sub-weathering; other factors that are often cited to favor the validity of the assumptions are (Marsden, 1993a): small source-to-receiver offsets, small surface elevation changes and the presence of a thin weathering layer. It is clear how these factors influence the extent of departure from vertical travel path for a ray-theoretical model of propagation; it is not so clear, however, how they relate to the wave-theoretical aspects of the problem. As previously stated, addressing

implications of wave-theoretical aspects for the validity of the basic assumptions of conventional static-estimation methods is the purpose of the present work.

2.3 The correction for near-surface-induced time-distortions in practice

A comprehensive solution to the problem of correcting for near-surface-induced distortions in reflection data is far from being achieved routinely in seismic data processing, even if those distortions are simplistically assumed to be only time delays among traces. If treated as such, corrections are estimated to conceptually move the shots and receivers from their surface locations to a common reference surface (the datum plane), at a depth expectedly beneath the distorting action of the near-surface. A number of methods for estimating corrections have been developed that make simplifying assumptions or address partial aspects of the problem, thereby yielding only partial solutions. Typically, the practical approach is to combine several methods to get as complete a solution as possible. Some of the key issues for estimation of corrections for time-distortions are briefly discussed next, with emphasis on how those issues are addressed in common practice.

Most commonly, vertical wave propagation through the near-surface is assumed. Simple methods, referred to as field statics approaches (Yilmaz, 1988), aimed mostly to correct for variations in surface topography, apply a vertical time-shift computed using an assumed near-surface propagation velocity (replacement velocity) or velocities estimated from additional field measurements.

In refraction-based methods (Farrell and Euwema, 1984; Marsden, 1993b), a layered velocity model of the near-surface is estimated by modeling the first arrivals in the recorded traces as head-waves. After estimation of the velocity model, the model is used to compute a vertical time-shift correction. Turning-ray tomography methods have been recently developed (Zhu et al., 1992; Stefani, 1995) to overcome the limitations of the layered-model assumption, by modeling first arrivals as resulting from propagation of continuously refracted turning-rays in a medium with horizontal and vertical velocity variations; vertical time-shift corrections ("tomostatics") are again applied in these approaches.

Again, all these conventional methods estimate the static-correction for each trace as a single time-shift consistent with vertical propagation through the estimated near-surface velocity model. Several methods have been proposed to overcome the limitations of the vertical-propagation assumption for the estimation of corrections. Kin and Jacewitz (1984) present a method to obtain dynamic (i.e., time-variant) corrections from ray-tracing traveltimes: corrections are estimated for a number of reflectors depending on raypath geometry in the subsurface and near-surface, and then interpolated between the reflectors and applied to the CMP data. The velocity model of the near-surface is estimated by an iterative, interactive interpretation procedure. Bloor (1996) computes similar dynamic corrections, estimating a velocity model by a linearized inversion approach in which the model estimate is iteratively updated to fit traveltimes observed in the data to those predicted from ray-tracing.

Wave-equation datuming (Berryhill, 1979; Berryhill, 1984) is a method in which the extrapolation to a datum of the surface-recorded seismic data is done propagating the wavefield following a Kirchhoff-integral formulation of the wave equation. Originally proposed to solve water-layer replacement problems in marine data, it has been applied also in land situations (Schneider et al., 1995). McMechan and Chen (1990) and Rajasekaran and McMechan (1995a) implicitly perform the extrapolation by incorporating the details of the near-surface in the velocity model used in prestack reverse-time common shot migration; Rajasekaran and McMechan (1995b) postulate that the velocity model required for those processes can be obtained from a combination of refraction- and reflection-traveltime tomography.

2.3.1 Residual statics problem

The methods to estimate corrections for near-surface-induced time-distortions are far from being perfect, for several reasons. As we have seen, a number of approaches implicitly assume a vertical wave propagation model, and even though they work generally well in practice, they are nevertheless inexact. Even if more accurate (though still approximate), wave-equation-consistent approaches are followed, they are only as good as the associated near-surface velocity model. Velocity estimation, for a wave equation-based or any other approach, is also imperfect.

As a result, it is common experience that even after the application of some of the methods mentioned above, the data are still not free of time anomalies (Yilmaz, 1988; Marsden, 1993c). These *residual-statics* problems occur because of variations in the near-surface that are not accounted for by the applied corrections. Compensating for residual-statics problems is then, essentially beyond the scope of those approaches: residual static anomalies are corrected for by using data-driven, statistical correlation techniques. If residual-statics are not corrected for, reflections will be misaligned after NMO correction, yielding a less-than-optimum stack trace. In the so-called reflection-statics estimation methods (Hileman et al., 1968; Taner et al., 1974; Wiggins et al., 1976), this observation is used to compute source and receiver surface-consistent residual-static corrections from measurements of relative time-shifts within the traces of each CMP gather.

2.3.2 Anomaly wavelength

A conceptual distinction can be made between spatial components of time-anomalies according to the scale of their variation relative to the length of the seismic cable (Wiggins et al., 1976; Yilmaz, 1988); this distinction indeed has geophysical significance. Short-wavelength components, those whose wavelength is smaller than the spread length, will impair the alignment of reflections within the traces in a CMP gather, thus deteriorating wavelet character and stack quality. On the other hand, long-wavelength components, with a wavelength larger than the length of the spread would yield relative misalignments within traces of different CMP gathers, thereby influencing the integrity of the structural picture.

Also, the performance of different static-corrections estimation methods is highly dependent on the wavelength of different components of the solution: in particular, surface-consistent reflection-based statics estimation techniques are capable of accurately solving for short-wavelength variations, but perform poorly in handling long-wavelength variations (Wiggins et al., 1976). Refraction-based methods, on the other hand, are considered to be more suited to solve for long-wavelength components of the solution (Yilmaz, 1988; Marsden, 1993b).

As we have seen, residual-statics estimation methods are intended to solve for time-distortions not accounted for by previous or alternative application of deterministic corrections. Refraction-based and similar techniques should potentially solve for long-wavelength components, so it seems reasonable to expect that residual-statics are related to rapid variations in the near-surface, beyond the resolution of previously applied methods (Yilmaz, 1988). This assumption will guide the choice of depth models used to study residual-statics-related issues in what follows.

Chapter 3

MODELING WAVE-THEORETIC TIME ANOMALIES

In this chapter, I generate synthetic seismic data that contain reflection-time distortions due to the occurrence of anomalous variations in the near-surface layer. The near-surface anomalies considered are simple sinusoidal variations in the shape of the base-of-weathering interface. Time-distortions are estimated by a crosscorrelation procedure, for a number of modeling tests involving variations in the model parameters. I also discuss some issues related to the implementation in practice of finite-difference modeling in this thesis, such as the choice of a boundary condition in the model boundary representing the earth's surface and the representation, in a discrete grid, of the contorted interfaces of interest in this study.

3.1 The choice of a near-surface model

In any study involving simulation of seismic-waves propagation, an essential requirement is that of defining the properties of the medium through which propagation is to occur; specifically, a velocity model of the medium is required. This velocity model should contain any feature whose influence on the outcome of the simulation is of interest for the purposes of the study. For the subject at hand, that of residual-statics estimation, the discussion in Chapter 2 made the case that the models to be considered should feature short-wavelength lateral variations (i.e., of a wavelength smaller than the length of the seismic cable) in the near-surface layer.

Hopefully, those models should also have some appeal to reality. Unfortunately, even though it strongly influences the quality and nature of the data acquired in surface recordings, our knowledge of the near-surface is still quite imperfect, both in terms of what is a realistic picture of the variation of physical properties, and what is a proper model of wave propagation through it. A main reason for this is that the acquisition and processing methods of conventional exploration seismology are better suited for the study of deeper targets in the subsurface.

Even if a detailed realistic model of the near-surface could be built, the question would arise as to whether or not it would be adequate to allow drawing some general conclusions from the results of specific studies. I have pursued a different approach to the matter of defining a prototype velocity model for investigating reflection-time distortions due to variations in the near-surface. I have chosen to implement simple models characterized by a few parameters in hopes that clear and unambiguous relationships can be established between the results and the model parameters. Although simple, those models, as stated above, should feature short-wavelength lateral variations in the near-surface layer so as to address essentials of the residual-statics

problem.

In their classical study of residual static corrections as a general linear inverse problem, Wiggins et al. (1976) could learn much about the quality of the statics solution as a function of spatial wavelength of the statics variations via an eigenvector analysis. Their analysis had the advantage that the surface-consistency assumption turns the problem into a linear one. This is not the case for this study about the quality of the surface-consistency assumption itself, where differences in time anomalies that honor the wave-equation and those computed under the assumption of vertical ray propagation through the weathering layer are not linearly related to the shape of the near-surface. Nevertheless, I believe — again, with the hope of establishing sound relationships between the results and the model parameters — that much can be learned about the quality of the surface-consistency assumption by considering models featuring simplified lateral near-surface variations of a sinusoidal shape.

As exemplified in Figure 1.1, the general depth model in this study is characterized by a plane free-surface, a homogeneous weathering layer (velocity V_1) bounded below by a cosine-shaped interface with spatial wavelength D, amplitude h and mean thickness z_w, and a second homogeneous layer (velocity $V_2 = 2000$ m/s) bounded at its base by a plane interface, which is horizontal (depth $Z = 1000$ m) in most of our tests. A third layer (velocity $V_3 = 3000$ m/s), below this interface, completes the model. The size of the model is 4500 m in width and 2000 m in depth.

3.2 Finite-differences computations

A number of choices exist as to algorithms for simulating seismic-wave propagation; they differ in scope, accuracy and computational cost.

Analytical solutions are accurate, within the limitations of the approximations involved in deriving a wave equation, on which all the methods are based; however, those are available for only a limited number of relatively simple cases, sometimes involving additional approximations. Combee (1994, 1995), for example, has derived series expressions for the distortions in the wavefield due to elliptic-shape near-surface anomalies in the neighborhood of the source or the receiver.

Ray-tracing methods allow for the consideration of a wider variety of earth models, but those are restricted to situations in which the scale-length of the model is large compared to the seismic wavelength (Bleistein, 1984); that might not be the case for the study of near-surface-related phenomena, in which it is desirable to consider a wide variation in magnitude of parameters such as the thickness of the weathering layer z_w or the wavelength of lateral variation D, ranging from a fraction of the size of a typical seismic wavelength to several times that size. Further consideration is given to the pertinence of ray-theory to help understand near-surface-related wave phenomena later in this and the next chapters. Practical implementations of Kirchhoff-type algorithms are based largely on ray-tracing and suffer, therefore, from similar limitations.

Finite-difference methods are known to be accurate provided that costly requirements in the grid- and time-step-sizes are met. Cost considerations certainly influenced

the scope and development of this work, but accuracy was considered a must. A finite-difference solution of the two-way wave equation was highly desirable for the modeling studies in this thesis. The algorithm used is the explicit, fourth-order in space and second-order in time, acoustic-wave-equation modeling code of Fei and Larner (1995). I did not, however, use their optional implementation of a flux-corrected transport algorithm aimed to alleviate numerical dispersion problems. To that end, I chose to follow the conventional approach of selecting a sufficiently fine grid-step size, so as to accurately represent the seismic wavelengths being considered; in fact, as discussed in Section 3.5.3, a fine grid is primarily necessary in order to describe the sinusoidal-shaped base of the weathering.

3.2.1 A typical test

I performed a number of simulation tests on models with the geometry illustrated in Figure 1.1; different tests typically involved differences in the parameters that define the sinusoidal base-of-weathering interface (i.e., the values of D, z_w and h). The geometry and model parameters for the tests performed are further illustrated in Figure 3.1. As suggested there, I will use the notation $D/z_w/h$ in what follows to refer to different tests involving particular choices of values for those parameters; for example, the reference 400/25/20 concerns a particular test in which $D = 400$ m, $z_w = 25$ m and $h = 20$ m.

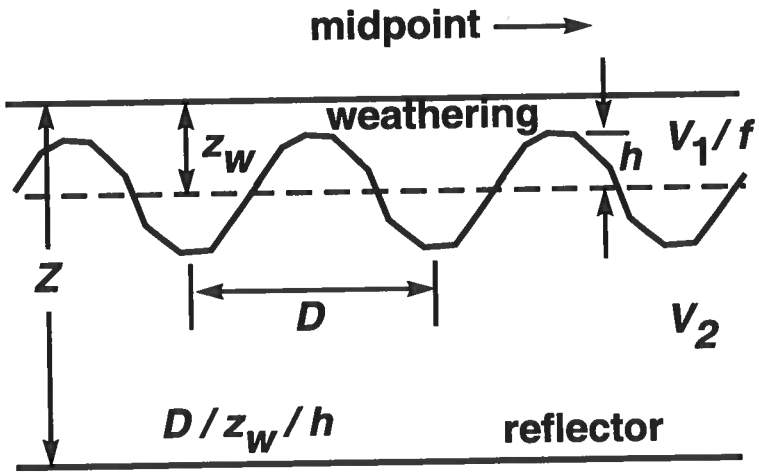

FIG. 3.1. Parameters describing the geometry of the depth models in the study. The notation $D/z_w/h$ will be used throughout this thesis.

A grid-step size of 2.5 m was selected for most of the tests performed. Standard references (Alford et al., 1974) give an accuracy requirement of at least 5.5 points per wavelength for the algorithm used, so this grid size should be sufficiently fine for frequencies up to about 70 Hz (seismic wavelength λ_1 around 14.0 m in the upper

layer); the dominant frequency in most of the tests is 30 Hz. Even for lower frequencies this fine grid is convenient so as to ensure that whatever time anomalies are observed, are governed solely by wave propagation and are not influenced by numerical artifacts from the computational algorithms. Moreover, a fine grid is necessary in order that the sinusoidal shape of the near-surface lower boundary be accurately characterized, as discussed in Section 3.5.3. This is a key reason why the flux-corrected-transport feature of Tong Fei's code did not need to be invoked.

The standard stability requirement for the finite-difference scheme used is (Alford et al., 1974) $\Delta t \leq \sqrt{3/8}\ \Delta x / v_{max}$, where Δt is the time-step for wavefield updating, Δx is the grid-step size and $v_{max} = 3000$ m/s, is the maximum velocity in the model. This condition yields a maximum value of 0.51 ms for the time-step; I used a 0.5 ms time-step in all the tests in this work.

Each test involved the computation of a single shot record, with source position centered on the upper boundary of the model. Absorbing boundaries implemented following the approach of Clayton and Engquist (1977) were used in the top, bottom and side boundaries of the model. The implications of the choice of boundary condition for the top boundary representing the earth's surface are discussed in Section 3.5.1.

I used an impulse as the input source signature so that seismograms characterized by any desired wavelet could be obtained by simply convolving the output with that wavelet. In all of the studies presented in the succeeding chapters, I used symmetric (zero-phase) Ricker wavelets with various desired peak frequencies. Unless otherwise noted, that frequency is 30 Hz in the results presented in this thesis.

The finite-difference algorithm was implemented in a way such that an output trace was recorded at every grid position along the top boundary, simulating a single-receiver recording, receivers being spaced every 2.5 m along the earth's surface; the source was also conceptually placed at the earth's surface. A typical test computed a total of 1.5 s recording time. Given the fine grid in space and time required for the modeling, calculation of a single shot record took 70 minutes of CPU time running in a single processor on a Silicon Graphics Power Challenge computer with 256 Mb total memory.

3.3 A look at the data

Let's examine some of the synthetic data generated in the tests. First, in Figure 3.2, which is a repeat of Figure 1.2, observe several events: the refraction first-arrival from the corrugated base-of-weathering; the reflection from that interface, arriving later than the first-arrivals and becoming quite weak past about a 0.5 km offset; and, of most interest, the time-distorted reflection from the deep horizontal reflector, with apex just below 1.0 s. A relatively weak, but still clearly visible source-related multiple (some 0.1 s later than the primary reflection) as well as weak receiver-related multiples (the large-moveout events visible between the primary and the source-related multiple) evidence imperfections in the performance of the absorbing boundary in the top surface of the model.

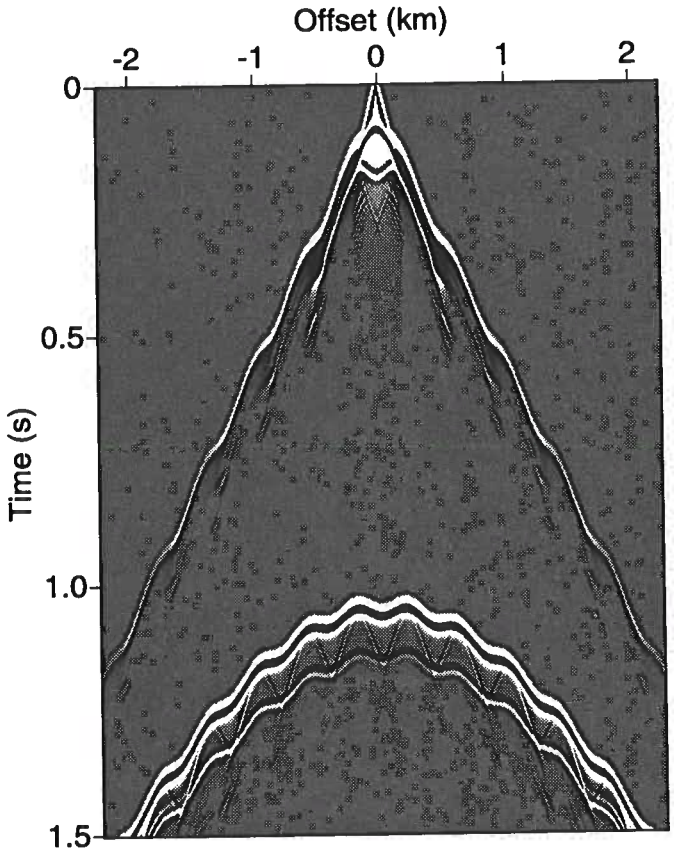

FIG. 3.2. Synthetic shot record generated for a depth model as illustrated in Figure 1.1, with a $D = 400$ m, $z_w = 25$ m, $h = 20$ m geometry for the sinusoidal base-of-weathering interface. The source signature for this and similar data plots in this thesis is a 30-Hz peak-frequency Ricker wavelet.

The wavelength $D = 400$ m of the sinusoidal base-of-weathering interface for the data in Figure 3.2 is several times larger than the size of the dominant seismic wavelength in the near-surface layer but is still much smaller than typical values of the length of the seismic spread; commonly, spreadlength is chosen with a magnitude comparable to the depth of the reflector of interest, which for the generic model of Figure 1.1 is $Z = 1000$ m.

The association of the time-distorted reflection in Figure 3.2 with the anomalous lateral variations in the near-surface becomes clear if we examine a case in which no such variations exist. Figure 3.3 presents a synthetic shot record generated for a model featuring a horizontal base-of-weathering interface at a depth $z_w = 25$ m, the mean depth of the sinusoidal interface for the data in Figure 3.2 (in other words, the depth model differs from the one in Figure 1.1 in that $h = 0$ here).

The time-distortions we will be concerned with in the course of this work are exemplified by the oscillating departures in traveltime we observe in the reflection

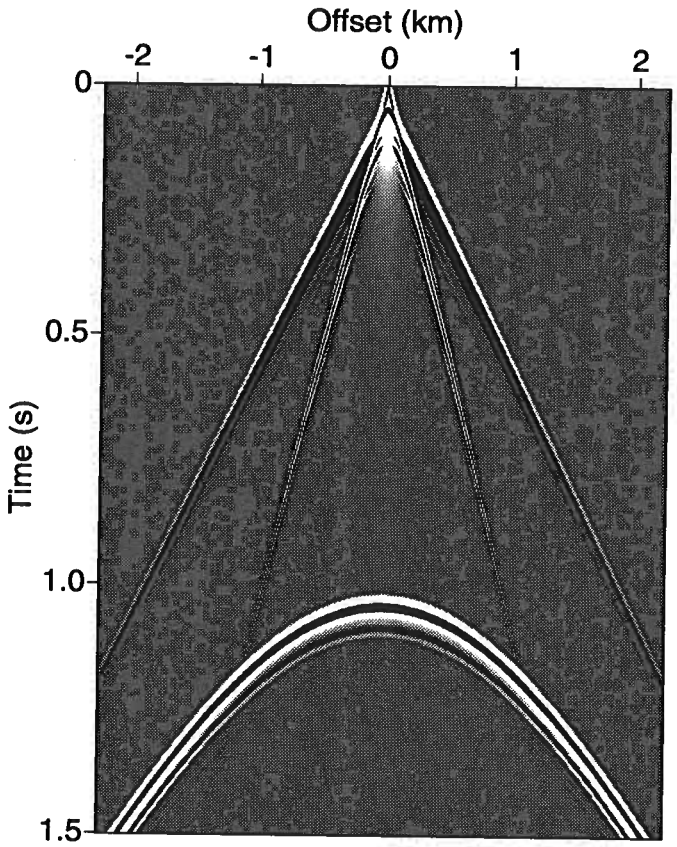

FIG. 3.3. Synthetic shot record generated for a depth model similar to that in Figure 1.1, but with a horizontal base of weathering, i.e., $z_w = 25$ m, $h = 0$.

from Figure 3.2, compared to the more-nearly hyperbolic moveout in the reflection in Figure 3.3. As already observed in Chapter 1, the periodicity of this departures bears some relation to that in the corrugated base of weathering.

Comparison of the shot records in Figures 3.2 and 3.3 brings out a couple of key elements that highlight issues concerning residual-statics methods in practice. First, the time-distortions are a departure from the moveout of some reference reflection. Second, this reference moveout is not strictly hyperbolic, i.e., the presence of the thin low-velocity near-surface layer, even in the absence of lateral variation, introduces some departure from perfect hyperbolic moveout. For insight into residual-statics problems, our interest should focus mostly on the short-wavelength anomalies related to the sinusoidal variations introduced in the near-surface layer. By referencing reflection times in data such as in Figure 3.2 to those in reference-model data such as in Figure 3.3, we reduce the influence of such longer-wavelength variations as a factor in this study.

Let's examine some more data. Figure 3.4 shows the shot record generated for a model with a shorter $D = 50$ m, compared to that in Figure 3.2, other parameters

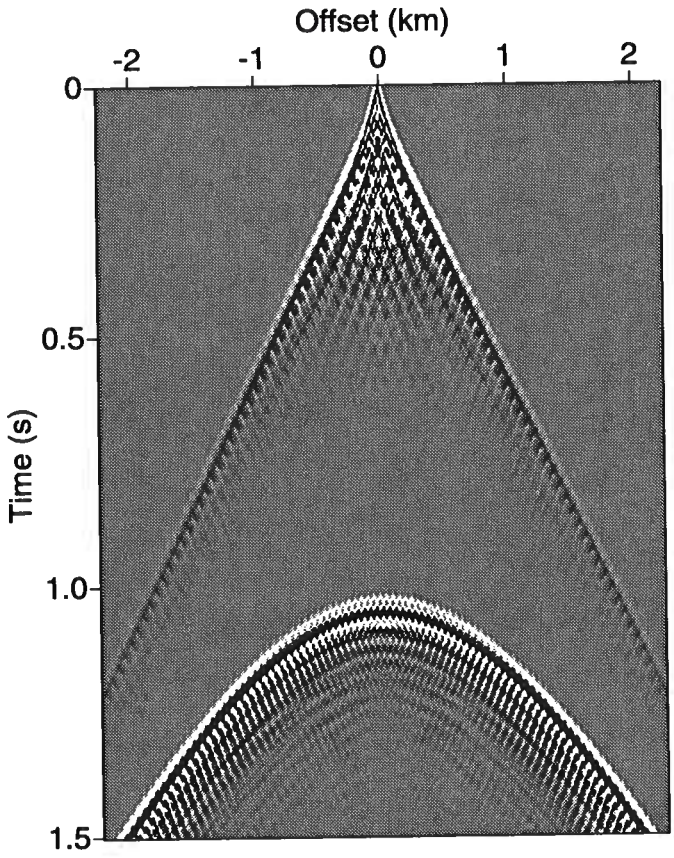

FIG. 3.4. Synthetic shot record generated for the 50/25/20 model

being unchanged. Note that a 25-m group interval, which is quite common in current seismic acquisition practice, would sample the 50-m-wavelength anomaly at Nyquist wavenumber. Thus, as residual-statics variations go, this is a very-short-wavelength anomaly.

Several differences are evident between the data in these two figures. In Figure 3.4, the first arrivals and the primary reflection from the deep interface are clearly visible. Following both of them, we can also observe a complex mix of interfering reflection and diffraction events, those following the first arrivals being weaker than the ones following the deep reflection. These events are related to the presence of the corrugated base of weathering. A careful examination reveals time-distortions in the primary deep reflection, but interestingly, these are much smaller than those observed in Figure 3.2. This is an example of the general behavior that a reduction in D (such as in the near-surface model associated with the data in Figure 3.2 as opposed to that in Figure 3.4) where other parameters are unchanged, introduces both relatively strong diffractions from the sinusoidal base of the weathering and a reduction in the amplitude of the time-distortions.

Figure 3.5 shows the computed shot record for a model in which the corrugated

base of weathering has deepened to an average depth $z_w = 100$ m while keeping $D = 50$ m and $h = 20$ m, unchanged with respect to Figure 3.4. For this thicker weathering, the head waves are much weaker than before. Moreover, the mix of reflection and diffraction events arising from the sinusoidal interface, arriving after the relatively weak first breaks, is not only much stronger but more coherent here (i.e., a number of individual large-moveout events can be distinguished whose mutual interference makes up the complex overall pattern). Time-distortions on the deep primary reflection are hardly visible; they must be small in this case. Thus, an increase in z_w seems to give rise to a further reduction in the size of the time-distortions.

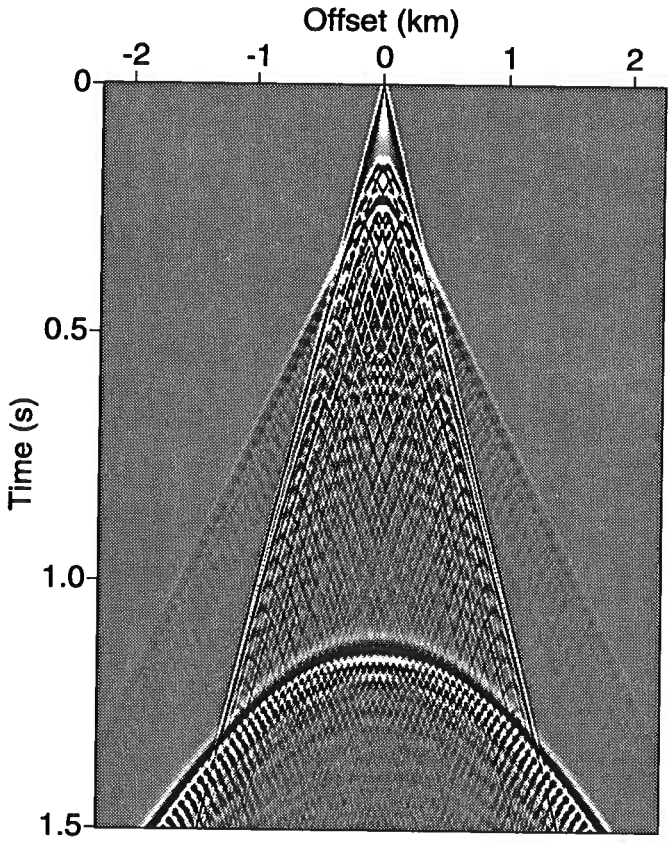

FIG. 3.5. Synthetic shot record generated for the 50/100/20 model

3.3.1 Discussion

Let me conjecture on possible reasons for the differences in the datasets presented here. First, while it seems plausible to postulate that the traveltimes in the main reflection events in Figure 3.2, including the multiples, might be predicted by ray tracing, this is absolutely not the case for the other datasets portrayed here. Figure 3.6 presents the result of generating the data for the 400/25/20 model using CSHOT, a

ray-tracing modeling program (Docherty, 1991). The timing of the main events seen in Figure 3.2, including the source- and receiver-multiples for the deep reflection and the first arrivals, is reproduced quite well.

Ray-tracing succeeded in reproducing main features in the finite-differences results for values of D as small as 100 m; attempts to reproduce the data for some of the models with a smaller $D = 50$ m yielded results that differed substantially from those obtained with the finite-differences modeling. In particular, the time-distortions in the ray-traced data failed to reproduce those estimated in the finite-difference data; this is exemplified in Figure 3.7. In all the tests comparing finite-difference and ray-tracing results, the peak frequency of the source wavelet again is 30 Hz; i.e., the seismic wavelength is around 33 m. This means that the scale-length of the problem (the magnitude of D) is close to the size of the seismic wavelength; a rule-of-thumb for the validity of ray-theory is that the scale-length of a problem must be at least three times as large as the seismic wavelength (Bleistein, 1984). That is indeed the case for $D \geq 100$ m, for the 30 Hz frequency.

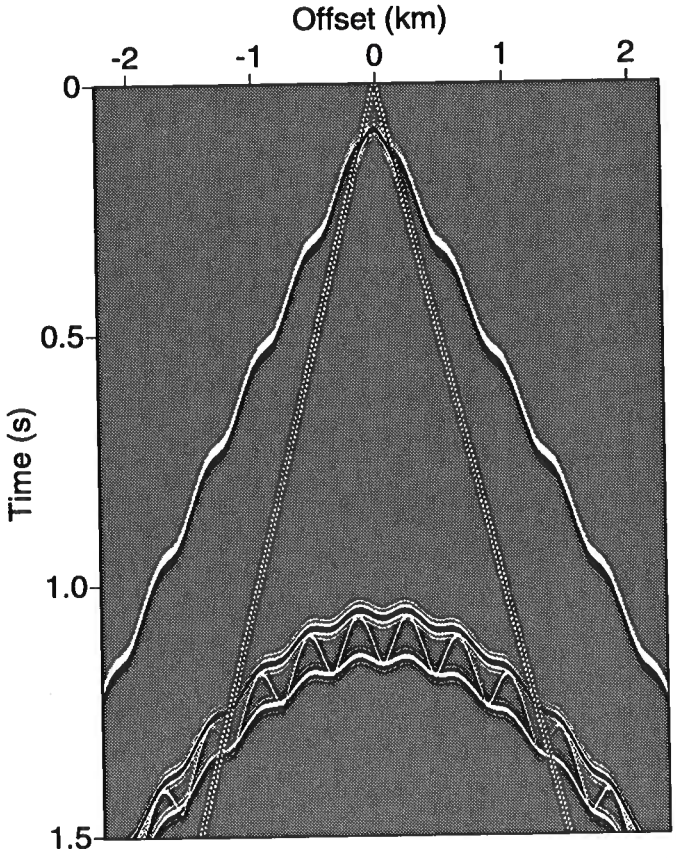

FIG. 3.6. Ray-trace-generated synthetic shot record for the 400/25/20 model

As the model changes in going from Figure 3.2 to Figure 3.4, the value of D has

decreased while h kept constant; the sinusoidal features on the corrugated interface have become steep (i.e., the ratio h/D is relatively large) and thus the interface is less smooth, thus giving rise to a relatively large amount of energy scattered from that interface, i.e., the "diffraction" events observed in Figure 3.4. Some "smoothing" or "wavefront healing" occurs as well for the energy reflected from the deep interface, as manifested in the reduction in the size of the time-distortions in the primary reflections. This phenomenon is related to the reduction in the magnitude of D relative to the seismic wavelength.

Finally, the further reduction in the magnitude of the time-distortions observed in the data in Figure 3.5 results from increased healing of wavefronts resulting from the increase in the thickness of the weathering.

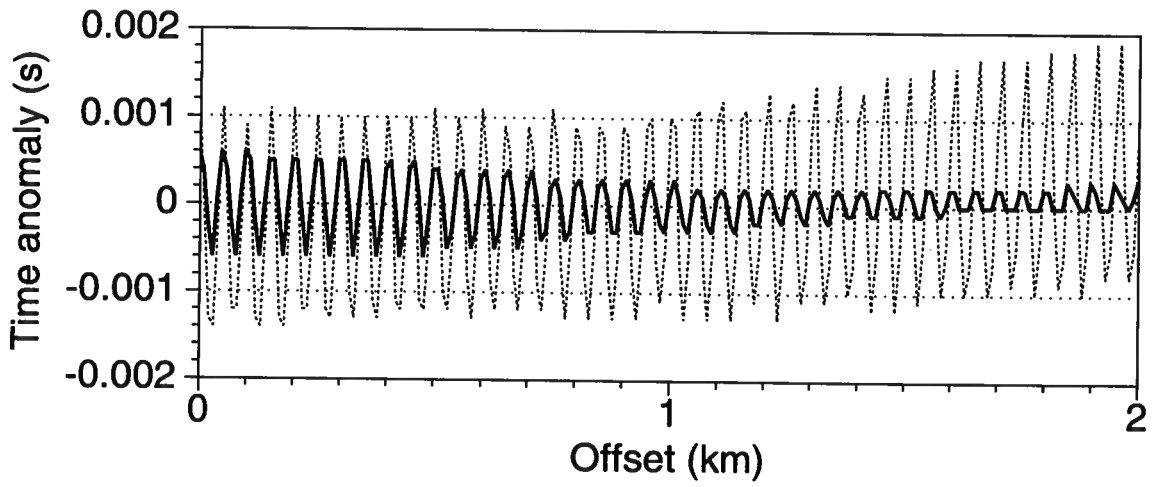

FIG. 3.7. Significant differences between finite-difference and ray-tracing results for the relatively lower values of D. Solid line: time-distortions estimated from data generated by finite-difference modeling for a model with $D = 50$ m, $z_w = 25$ m and $h = 2.5$ m. Dashed line: their counterparts for ray-trace-generated data.

3.4 Estimation of time anomalies

The first step in studying the nature of the time-distortions induced in the data is to measure the time-distortions seen on the deep reflection in the shot records. I compute quantitative values for time anomalies such as those seen in the data examples in Section 3.3 by comparing the time-distorted reflection in each test with a reference. That reference is the reflection obtained from a synthetic shot record for a subsurface model in which the sinusoidal-shape interface has been replaced with a horizontal interface at the mean depth z_w of the corrugated interface (i.e., one for which $h = 0$). I compute the crosscorrelation of corresponding traces on the two shot records,

over a 0.6 s window encompassing the deep reflection of interest; the result of such a calculation is exemplified in Figure 3.8 for the 400/25/20 model.

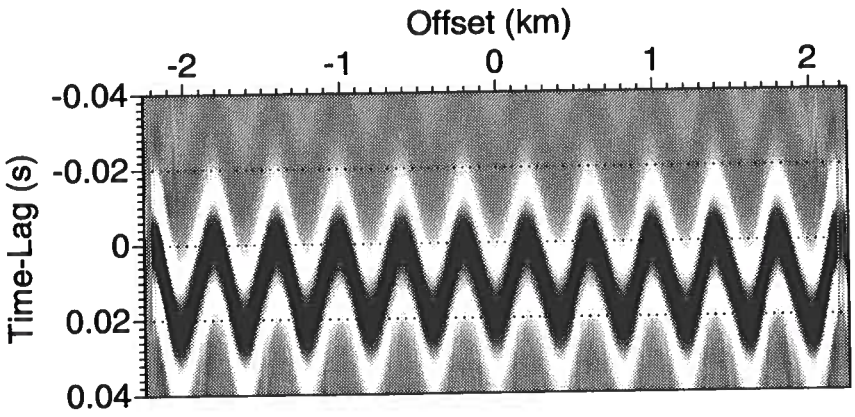

FIG. 3.8. Crosscorrelation of the data generated for the 400/25/20-model from Figure 3.2 and the reference data from Figure 3.3.

To obtain time-distortions as a function of source-to-receiver offset, such as those shown in Figure 1.3 and repeated here as Figure 3.9, I pick the time-lag of the maximum crosscorrelation value (crosscorrelation peak) by scanning crosscorrelation functions such as those in Figure 3.8. The time-lag window for picking crosscorrelation peaks is narrow (typically 10- to 80-ms long), and centered around the zero-lag sample.

For comparison in that and similar figures throughout the thesis, the dashed lines show the time anomalies computed simplistically as vertical receiver statics (i.e, computed as the difference in vertical traveltime between the sinusoidal and flat base-of-weathering depth models, at receiver locations). Specifically, the vertical shot static (which is computed in a way similar to that for receiver-statics, but at the shot location) is subtracted from the total static (the sum of shot- plus receiver static), to obtain the quantities in dashed-line in Figure 3.9. The magnitude of the vertical shot-static is also subtracted from the raw picked time-lags (i.e., the time-lag values obtained by picking the maxima in crosscorrelation traces such as those in Figure 3.8) to obtain the values of time-distortion such as those displayed in Figure 3.9. For the particular case portrayed there, the shot static is quite close to the mean value of the raw picked time-lags, so the solid curve in Figure 3.9 is close to zero-mean. That might not be the case when the time-distortions in the data depart significantly from the statics (such as in Figure 3.10 below).

Time-distortions for all of the tests performed varied with offset in ways similar to one or another of the representative time-distortion curves presented in this section.

First, as in Figure 3.9, when D is large compared to the seismic wavelength, the time-distortions are similar to the statics (the solid and dashed curves are close to one another), with differences growing mildly with increasing offset. As discussed in Section 3.3 this is the regime in which ray-theory is valid. Indeed the increasing

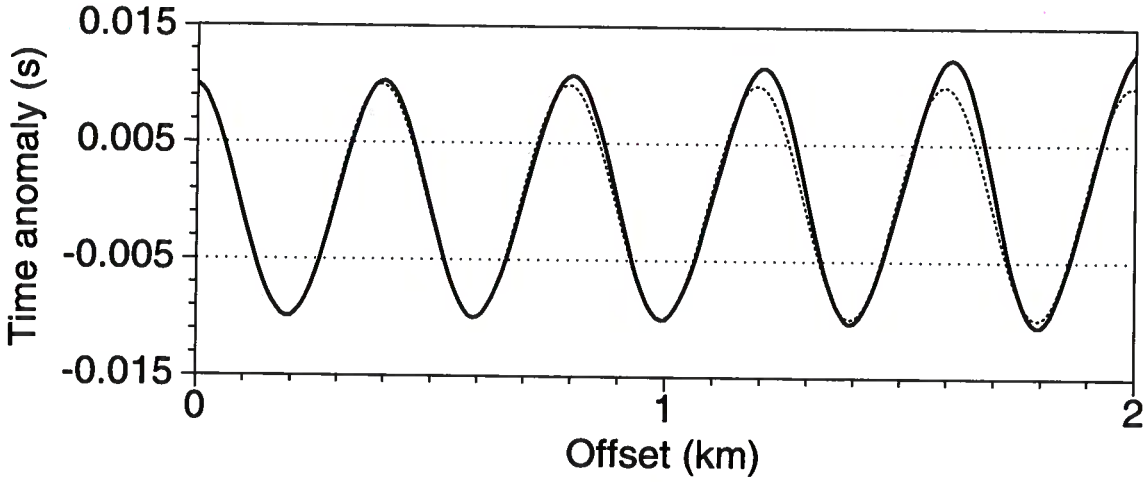

FIG. 3.9. Solid line: time-distortions estimated for the reflection in Figure 3.2. Dashed line: corresponding surface-consistent statics. This convention is followed in similar plots throughout the thesis. The wavelet is Ricker with a 30-Hz peak frequency. Only the anomalies for positive offset are shown since the anomalies are symmetric with offset.

departure of the two curves with increasing offset is due to the simplistic use of vertical raypaths in the computation of surface-consistent statics. Raypaths depart from vertical in the near-surface, increasingly for increasing offsets. Moreover, the departure between the computed time-distortions and the statics is larger for the peaks than for the troughs in the time-anomaly-curve in Figure 3.9 (i.e., the greater difference between the solid and dashed lines around a 1.6 km offset, compared to that at 1.8 km). This is due to the difference in the length of the slant raypath through the low-velocity layer as the ray emerges from different positions along the sinusoidal interface: this length is largest for a ray emerging from a trough and smallest for one emerging from a peak in the base of weathering (a minimum in the time-distortions or statics curves corresponds to a peak in the sinusoidal shape of the base of the weathering, and conversely for a trough in that interface).

Figure 3.10 exhibits a characteristic yet quite different from that seen in Figure 3.9. For Figure 3.10 the model has a smaller $D = 50$ m, but maintains the ratio $D/h = 20$, as well as the value of z_w. The magnitude of the computed time-distortions is much smaller than that of the vertical statics, decreasing with increasing offset. A "wavefront healing" phenomenon is present in this case, with action that becomes stronger for increasing offset. Such wave-theoretical phenomena become important as the seismic wavelength becomes large compared to the wavelength D of the corrugated base of weathering. Also observed in the time-distortions of Figure 3.10 is an overall negative shift in the mean value of the distortions. Below, we will look more closely into these features.

In Figure 3.11, the magnitude of h has increased to a larger 20 m compared

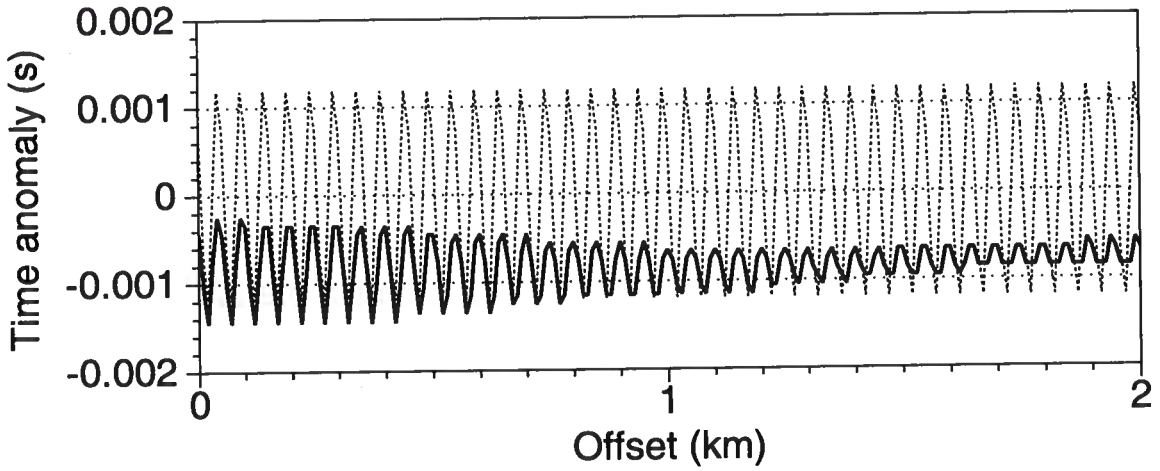

FIG. 3.10. Time-distortions estimated for the data from the 50/25/2.5 model.

to 2.5 m in Figure 3.10; again we see a reduced amplitude of the computed time-distortions, compared to that of the corresponding statics, for offsets up to about 1.0 km, beyond which the size of the measured distortions increases abruptly. In Section 3.3, we observed that the shot record corresponding to Figure 3.11 (see Figure 3.4) contained a notable level of diffracted and scattered events related to a relatively large value of the ratio h/D; a window of that data is presented here as Figure 3.12. The constructive interference of the regular pattern of diffractions originating from the corrugated base of the weathering is indeed a shortcoming of the sinusoidal model.

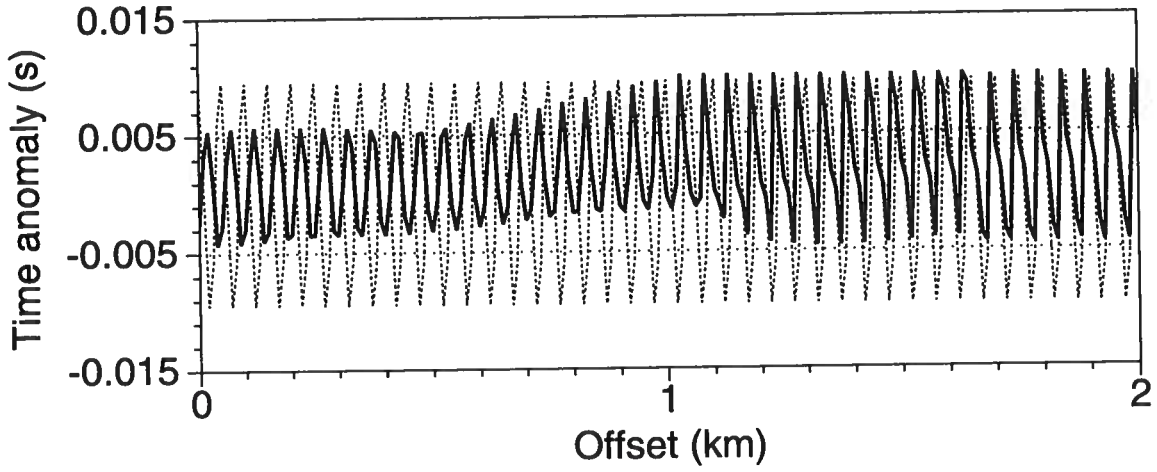

FIG. 3.11. Time-distortions estimated for the data from the 50/25/20 model.

The level of noisy diffractions and scattered energy in the data in Figure 3.12 is large enough to interfere with the event of interest, distorting the wavelet and

biasing the computation of crosscorrelation and thus the picking of meaningful time-distortions. This is an example of cycle-skipping problems common in the picking of crosscorrelation maxima for noisy data. Due to cycle-skipping and other problems, the computed time-distortions can be a poor estimate of the time-distortions that are truly representative of near-surface-induced distortions in reflection times. Results similar to those in Figure 3.11 are obtained even after several tests involving reduction in the size of the crosscorrelation and picking windows (down to 100 ms for the crosscorrelation window and 30 ms for the picking window) in attempts to avoid including the diffractions.

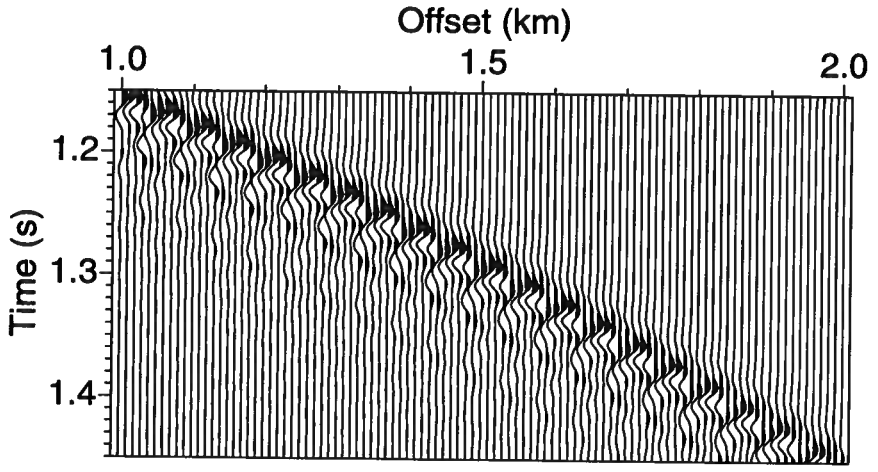

FIG. 3.12. A window of the shot record generated for the 50/25/20 model presented in Figure 3.4, between offsets 1.0 km and 2.0 km, and times 1.15 s and 1.45 s. Observe the repetitive diffraction events dipping down to the left, interfering with the reflection, distorting the wavelet shape and creating ambiguities as to the correct event to pick, in some traces.

In Figure 3.13, the depth of the base-of-weathering interface has been increased relative to that for Figure 3.11, to $z_w = 50$ m. Figure 3.13 shows a general reduction in the magnitude of the distortions with respect to the statics, but little variation in that magnitude with offset. Note that the phase of the time-distortions is opposite that of the statics, at and near zero offset, and changes gradually with offset, so that the phases match fortuitously beyond about 1.5 km offset. A similar behavior is observed in Figure 3.11. Also observed in Figures 3.11 and 3.13 is a drift in the mean value of the time-distortions toward higher values for the longer offsets, compared to those near zero-offset. Later, we will look more closely into all these.

Finally, in Figure 3.14, the average thickness of the weathering layer has been reduced to $z_w = 10$ m. Only a relatively small reduction in the overall size of the distortions is observed here; the variation (reduction) in the magnitude of the distortions with increasing offset is also rather small; wavefront healing becomes reduced as the

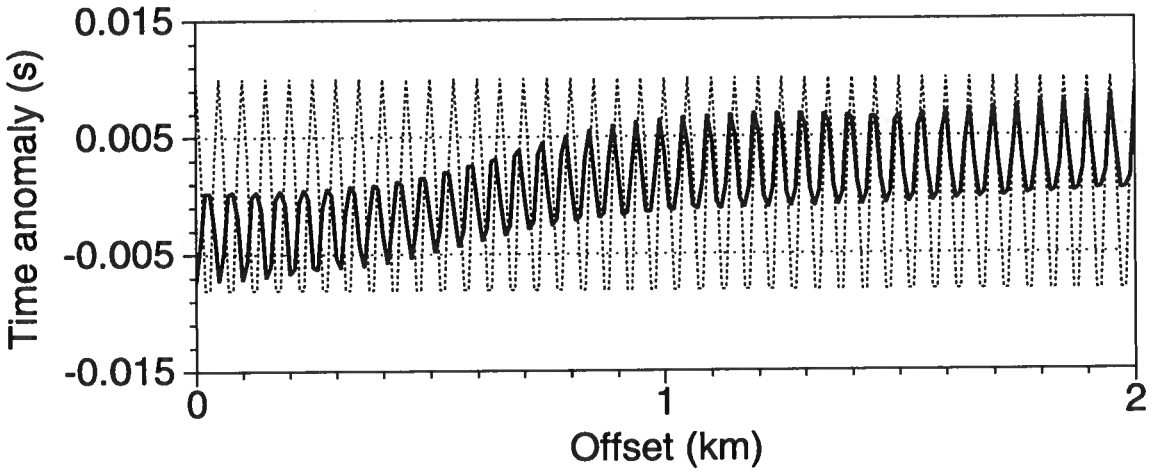

FIG. 3.13. Time-distortions estimated for the data from the 50/50/20 model.

mean thickness of the weathering decreases.

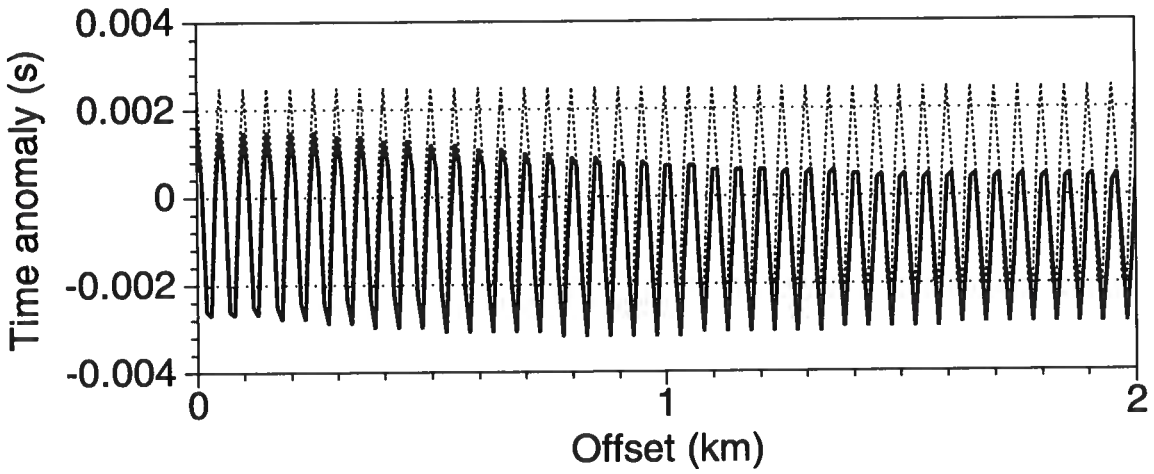

FIG. 3.14. Time-distortions estimated for the data from the 50/10/5 model.

3.4.1 Discussion

Let's summarize what we can say about the character of the reflection-time distortions induced by the presence of the corrugated base of weathering, and the relation to variation in the parameters of the model. First, when the wavelength D of the sinusoid is large compared to the seismic wavelength, the character of the distortions may be understood by ray-theoretical considerations; the departure from surface-consistency increases with increasing offset, but is small in general.

For smaller values of D, close to the seismic wavelength, wave-theoretical phenomena, loosely referred to as "wavefront healing", act to reduce the magnitude of the time-distortions compared to that of the statics. This action increases with increasing mean thickness of the weathering z_w, as well as with increasing source-to-receiver offset. For relatively small values of z_w wavefront healing is largely reduced or essentially nonexistent. Large values of h relative to the size of D give rise to a high level of scattered and diffracted events, which eventually impair meaningful computation of traveltimes.

We observed above that for the larger values of D (e.g., for $D = 400$ m) the mean value of the raw-picked time-lags is pretty close to the vertical shot-static. If we interpret that mean value as indicative of a contribution to the time-distortions associated with the shot, this means that the vertical shot-static is similar to that contribution when D is large.

Consistent with the interpretation just suggested for the mean value of the raw-picked time lags, differences in that mean value, such as those observed in Figures 3.11 and 3.13, can be understood as related to differences in the shot-associated contribution to the time-distortions that can be attributed to departures of ray-theoretical computation from the true behavior of waves. The shot-associated contribution changes as the receiver location changes slowly from zero-offset to the longer offsets giving the appearance of a drift in the time-distortions with offset. We will look further into this later (see Chapter 4), but for now we simply note that variations in that contribution must be related to the sinusoidal variations in the near-surface model. Thus, the drift in the mean value of the time-distortions is most notable when D is small, i.e., when variations in the near surface are rapid. When present, the drift is a long-wavelength feature, suggesting that even if changes exist in the contribution from the shot to the time-distortions, those must vary slowly with offset. In contrast, the shorter-wavelength variations in the time-distortions are related to variations in the contributions from the receiver.

Above, we observed the similar magnitude of the contribution to the time-distortions related to the shot and the vertical shot-static for the case of a relatively large D. Also, for the smaller values of D, the time-distortions have smaller magnitude than do the vertical receiver-statics. This leads us to expect a reduction in the size of the shot-associated contribution relative to the shot static, when D is small. Thus, for the relatively smaller D, the mean value of the raw picks must be smaller than the vertical shot-static. In that case, as observed in Figure 3.10, subtraction of the shot-static from the raw picks yields quantities that, as opposed to the situation for relatively large D, are not zero-mean near zero-offset, but are shifted toward negative values. A similar behavior is observed in Figures 3.13 and 3.14 near zero-offset. For longer offsets the situation is complicated by the ocurrence of drift. We should not, however, expect to get a consistent behavior in Figure 3.11 since, as discussed above, the results shown there are unreliable because of picking problems.

Other features are observed in some of the time-distortion curves, such as the change in phase of the distortions relative to the statics near zero offset. This will be

discussed later, in Chapter 4.

3.5 Issues in practical implementation

Even though finite-difference approximation to the wave-equation provides a convenient and conceptually simple approach to simulation of seismic wave propagation, problems do arise in practical implementations. In this work, I had to deal with issues concerning the boundary condition to be used at the model boundary representing the earth's surface, as well as with defining a suitable and accurate way to represent, in a discretized grid, highly undulating interfaces such as the sinusoidal-shape interface implemented in my tests.

3.5.1 Boundary condition at the earth's surface

As stated earlier, an absorbing-boundary condition was used for all the boundaries in the depth model, in the modeling experiments that make up the core of this thesis. An appropriate question would be that of what would be the implications of using a free-surface condition at the top boundary depicting the earth's surface since, indeed, that seems the more appropriate boundary condition. Conceptually, this should be a better way to honor the physics of the problem, and make the experiments a more realistic simulation.

Tests with free-surface condition I performed a number of tests, similar to those illustrated in the previous sections, but using the free-surface condition. Figure 3.15 illustrates the results of one of these tests, for the 400/25/20 model; this should be compared with Figure 3.2, which features the result for the test with an absorbing-boundary condition.

The shot record on Figure 3.15 is plagued with strong near-surface related multiples not only from the deep reflection but also from the first arrivals and the reflection from the base-of-weathering interface. This strength of multiple energy, much stronger than what is encountered in typical land seismic data, held for all other shot records that I modeled with the free-surface boundary condition. Thus, although the choice of a free-surface condition is believed to be more realistic than the absorbing one, results such as those on Figure 3.15 are unrealistic; such a high level of multiples is rarely seen on land-acquired seismic data, although it can certainly occur in marine data (Yilmaz, 1988).

This suggests that the models I have selected for the near-surface are deficient in some respect. Strong multiples occur because, due to the free-surface condition imposed, the earth's surface boundary becomes a perfect reflector, with a reflection coefficient of -1.0 for waves incident on the boundary from the interior of the model. Those waves, reflected downward into the model, encounter the base-of-weathering interface whose reflection coefficient is a high 0.33, so that a significant amount of energy is reflected back up to the free-surface boundary, and so on, in a guided-wave

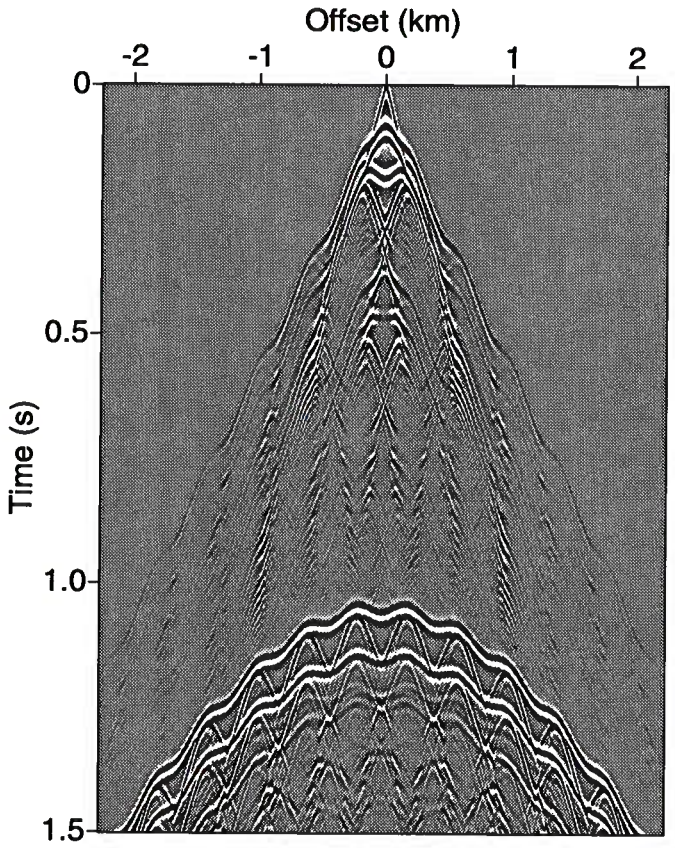

FIG. 3.15. Synthetic shot record generated for the 400/25/20 model, with a free-surface boundary condition along the top boundary of the computational grid.

fashion. It takes several repetitions for the amplitude of these multiple reflections to reduce to negligible levels (simple calculations involving the convolution of the source and receiver reflectivity functions representing this repetitive process show that it is not until the fourth multiple that amplitude becomes less than 10 percent of that of the primary).

On the other hand, as observed in Section 3.3 some surface-related multiples are even present in the data modeled with an absorbing-boundary condition, evidencing imperfections in the performance of the absorbing-boundary. These multiples, however, are much weaker than those present with a free-surface boundary. It is known that the performance of the absorbing-boundary implementation used in this work is dependent on the angle of incidence of the waves on the boundary: it is best for normal and close-to-normal incidence, degrading significantly beyond 30- to 45-degree incidence and considerably for larger angles (Clayton and Engquist, 1977). In situations such as here, where the source is close to the surface, a significant portion of the wavefront incident on the boundary will arrive at relatively large angles at which the performance of the absorbing-boundary is not perfect; this energy will not be totally

attenuated, but instead will be reflected back into the model to some extent, giving rise to the multiples observed in the computed shot records.

Either the depth models or the modeling algorithm used in this work, or most probably both, are just too simplistic to fully address all the details influencing wave propagation in the near-surface. Factors such as anelastic attenuation, more transitional velocity variations (involving smaller reflection coefficients than those in the typical model used here) likely need to be incorporated into the models. Implementing such a detailed modeling scheme of near-surface wave-propagation, goes beyond the scope of this thesis. However, as discussed below (see Section 3.5.2), I explore the implications of including factors such as those just mentioned into the simplistic near-surface models considered in this work. Of concern for the purposes of this research, also, is determining whether the results reached so far are influenced in any way by the introduction of a free-surface, and the occurrence of multiples in levels such as seen in Figure 3.15.

Time-distortions in the free-surface-boundary data I computed the time-distortions induced in the reflection from the deep interface for a number of synthetic shot records generated including the free-surface boundary condition and compared the results with those obtained for data generated using the same velocity model, but an absorbing boundary condition. The presence of multiples disturbed the computation process to some extent, biasing the crosscorrelation and picking process, occasionally yielding faulty or hard-to-interpret results (e.g., cycle skips). These problems were minimized by choosing a narrow correlation window, typically only 100 ms to 150 ms long, aimed to include the primary event of interest, but excluding, as much as possible, undesired events such as multiples and diffractions. This procedure works only because of the synthetic, noise-free nature of the input data; in field-data, due to the presence of noise and the uncertainty on the timing of the events of interest, typically longer correlation-windows are needed. Field data, however, are not so severely troubled as here by multiples or by the diffractions that interfere so constructively because of the sinusoidal near-surface shape.

In many instances the time-distortions estimated for the free-surface-boundary-condition data were similar to their absorbing-boundary counterparts, but differences also existed in a number of cases. Figures 3.16 and 3.17 show one case in which notable differences existed. Figure 3.16 presents the time-distortions estimated for the data from the 50/50/5 model, generated using the free-surface boundary condition. The input shot record for the estimation of the time-distortions in Figure 3.16 was generated, as usual, with a 30-Hz-peak-frequency Ricker wavelet as source signature. Figure 3.17 corresponds to the time-distortions estimated for a shot record also from the 50/50/5 model, but generated with an absorbing-boundary condition; the source signature in the input data was also a 30-Hz-peak-frequency Ricker wavelet.

The differences between Figures 3.16 and 3.17 are immediately apparent: in Figure 3.16 the estimated distortions are very small for small offsets; they grow rapidly to larger values for offsets past about 0.5 km, exhibiting the drift in mean-value

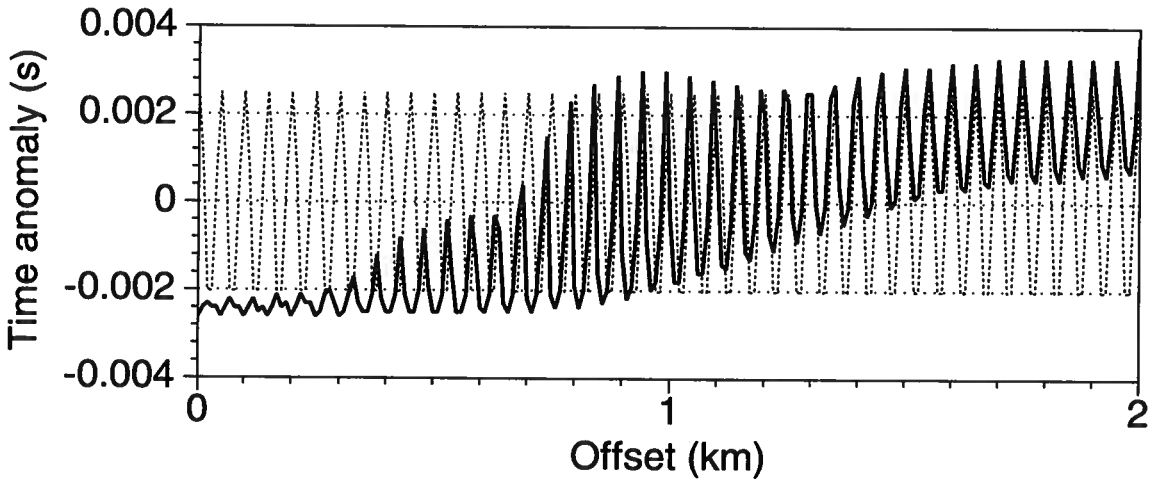

FIG. 3.16. Time-distortions estimated for the data from the 50/50/5 model, generated with a free-surface boundary condition. The source signature was a 30-Hz-peak-frequency Ricker wavelet. Compare with Figure 3.17, which shows the time-distortions estimated for the data from the same model, generated with an absorbing boundary condition.

already mentioned in Section 3.4. In that region, they also become more akin to their absorbing-boundary counterparts in Figure 3.17.

What might be the reason for differences such as those just observed? It is of course related to the choice of boundary condition in the earth's surface, but, what are the implications of that choice for the fundamentals of the wave-propagation phenomena governing the character of the time-distortions? It is unlikely that it is just a matter of interference from the multiples present in the free-surface-boundary case, at least not for long-period multiples (i.e., those multiples whose delay with respect to the primary is larger than the length of the wavelet) since, as explained above, the time-distortions were computed for that case using a narrow window encompassing the primary event of interest.

Examining the wavelets Seeking an answer for those questions, I examined the individual wavelets in shot records differing only in the particular choice of that condition. Figure 3.18 shows the wavelet in data modeled using the free-surface condition, along with its amplitude spectrum. To isolate the action of the boundary condition on the wavelet from that of other factors, such as the shape of the corrugated base-of-weathering, I obtained this wavelet from data generated for a model with a horizontal base-of-weathering. The choice of depth $z_w = 50$ m for the base of weathering minimizes interference of long-period multiples on the shape of the wavelet (for $z_w = 50$ m, the delay of the first multiple from the base-of-weathering relative to the primary is 100 ms, just outside the window used to extract the wavelet). The wavelet

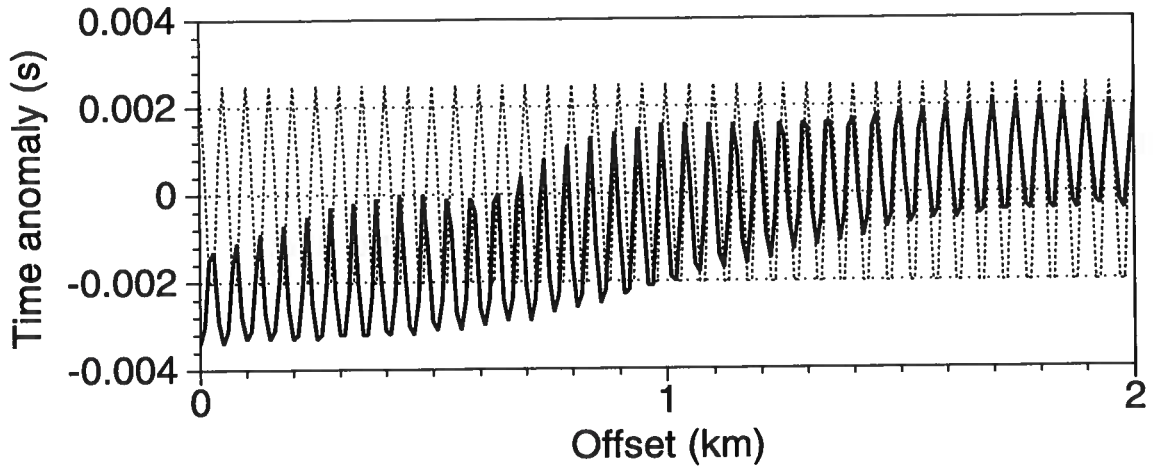

FIG. 3.17. Time-distortions estimated for the data from the 50/50/5 model, generated with an absorbing-boundary condition. The source signature was a 30-Hz-peak-frequency Ricker wavelet.

was obtained by simply extracting the data from the zero-offset trace, in a 100 ms window encompassing the deep interface.

A couple of observations can be made regarding Figure 3.18. First, even though the peak frequency in the input, *source* wavelet was 30 Hz, the peak frequency in the *data* wavelet is quite different, close to 40 Hz. The shape of the wavelet, moreover, is not at all that of a symmetric Ricker-wavelet. So, the wavelet in the data modeled with the free-surface boundary condition is distorted, and its peak frequency is changed from that of the source wavelet.

Figure 3.19 shows the wavelet extracted from data modeled using the absorbing-boundary condition. Although not perfect, the shape of the wavelet is closer to that of the input Ricker-wavelet (see Figure 3.20); the peak-frequency is also close to the 30 Hz of the input. The wavelet in the data modeled with the absorbing-boundary condition is thus pretty much undisturbed, compared to the source wavelet. The minor differences observed presumably are due to interference with very weak surface-related multiples existing because of imperfections in the absorbing-boundary condition, or to imperfections in the finite-difference approximation to wave propagation.

So, a change in the shape and dominant frequency of the wavelet in the data, compared to that in the source signature, is related to the implementation of a free-surface earth's surface boundary. The question is whether or not this would explain the differences observed in the character of the time-distortions in the data with the free-surface condition, compared to those in data with an absorbing boundary. Of course, a change in dominant frequency means a change in the wavelength corresponding to that dominant frequency, or loosely, the "typical" wavelength in the data. Even though I have not fully discussed it so far (see Section 4.1), we have seen in Sections 3.3

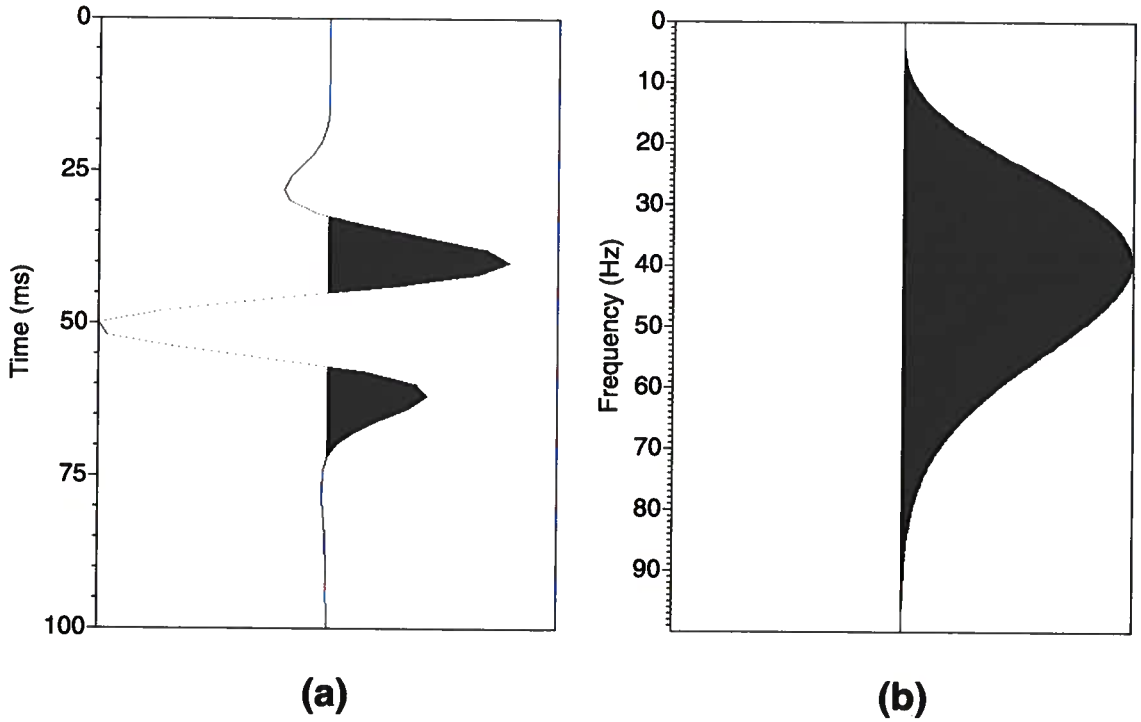

FIG. 3.18. Wavelet in the data modeled using a free-surface boundary condition. The wavelet was extracted from data generated for a model with $z_w = 50$ m and $h = 0$. The source signature was a 30-Hz-peak-frequency Ricker wavelet: (a) the wavelet in time, and (b) its amplitude spectrum.

and 3.4 indications that the character of the time-distortions is greatly influenced by the data wavelength, or rather, the ratio of the seismic wavelength in the near-surface layer, λ_1, to the wavelength of the corrugated base-of-weathering interface, D.

To determine if the change in peak-frequency would explain the above differences in time-distortions, I estimated the time-distortions in data modeled with the absorbing-boundary, but using for the peak-frequency of the source signature the frequency observed in the wavelet from the data with a free-surface boundary (around 38 Hz in Figure 3.18). Figure 3.21 presents the time-distortions computed in this way for data from the 50/50/5 model. Note that, as illustrated in Figure 3.19, we should expect the peak-frequency of the *data* wavelet for this case to be around 38 Hz.

Figure 3.21 reproduces Figure 3.16 remarkably well; the differences are minor. This match suggests that the differences observed between the time-distortions estimated for the data with a free-surface boundary and those estimated for comparable data (i.e., generated for the same depth model), but with an absorbing boundary, all other parameters being the same for both datasets (specifically the peak-frequency in the input wavelet) are due to the fact that the frequency content of the data is not the same in the two cases. Also, this is a prelude to the consistency of the frequency

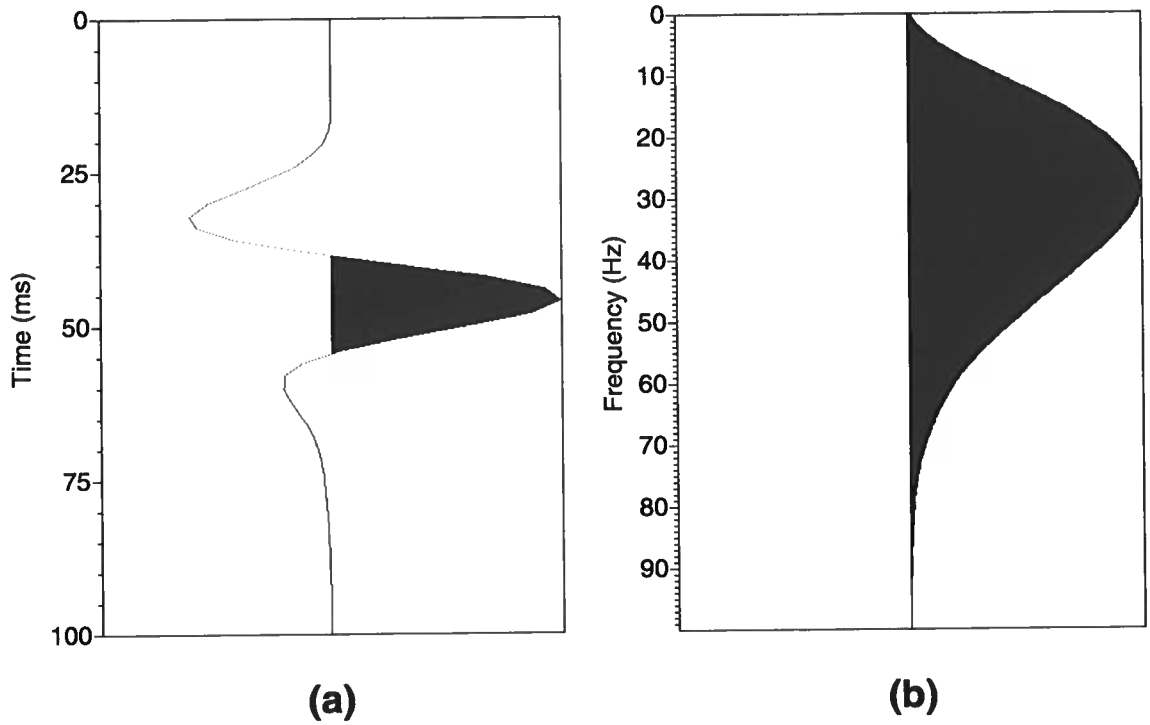

FIG. 3.19. Wavelet in the data modeled using an absorbing-boundary condition. The wavelet was extracted from data generated for a model with $z_w = 50$ m and $h = 0$. The source signature was a 30-Hz-peak-frequency Ricker wavelet: (a) the wavelet in time, and (b) its amplitude spectrum.

dependence of the results that will be seen below (see Section 4.1). When provisions are taken so that the peak-frequency is the same in each of the datasets being compared, the time-distortions are equivalent, regardless of what was the choice of boundary condition in the earth's surface boundary used to generate the data. I found the same sort of match as that between Figures 3.21 and 3.16 in a number of other cases. Note that, as exemplified by Figures 3.18 and 3.19, the shape of the wavelets differs for the data with the two boundary conditions of concern here; I maintained this difference in shape when making the adjustments in peak-frequency and comparisons just discussed. The slight difference in phase does not seem to have a significant influence on the character of the distortions.

The distorting action of source- and receiver-associated ghosts A final issue to address in this subject is the reason for the change in the peak frequency in the data with respect to that in the source signature. As discussed earlier, long-period multiples are removed from the question because they were excluded from the crosscorrelation used to estimate time-distortions in the free-surface boundary case. The change can be attributed to rather short-period ghosts associated with the

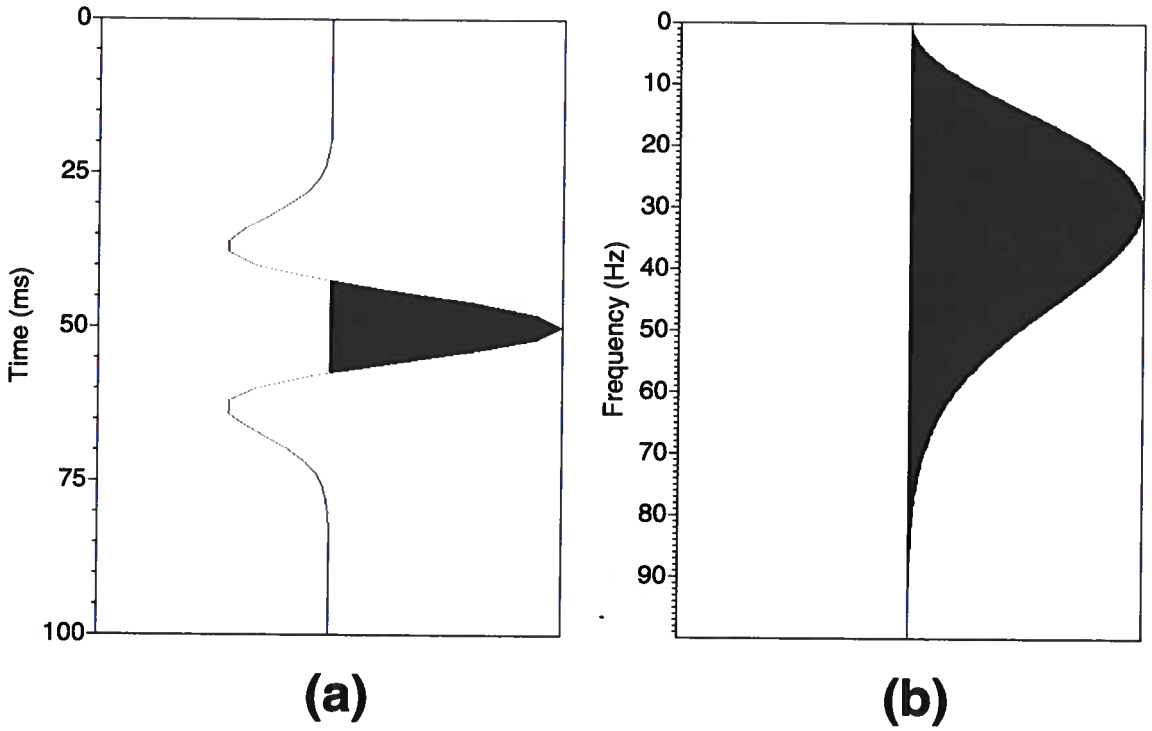

FIG. 3.20. The Ricker-wavelet with a peak-frequency of 30 Hz implemented as the source signature in most of the tests in this thesis: (a) the wavelet in time, and (b) its amplitude spectrum.

source and receiver. A source-ghost is energy generated from a buried seismic source that travels initially upward and is later reflected downward in this case by the earth's surface boundary. The ghost interferes with the down-traveling primary source energy, distorting the shape of the wavelet and its frequency content. A similar phenomenon would occur for a buried receiver — a receiver ghost —, but with downward-traveling energy reflected from the earth's surface interfering with the upward-traveling wave arriving at the receiver.

Buried source and receivers are indeed present in the finite-difference simulations in this thesis. Even though conceptually they are placed at the earth's surface, sources and receivers are actually placed in the second shallowest row of the computational grid. The reason for this has to do with the discrete nature of the calculations involved and the implementation of boundary conditions. For the receivers, it is not desirable to record the wavefield estimated in the topmost row of the grid since it is either distorted by the implementation of an absorbing boundary, or it is plainly zero in the free-surface boundary case. On the other hand, at all boundaries of the grid the length of the finite-difference operator is reduced to three grid-points, the smallest possible for the symmetric operator implemented in the code, (it is normally five points in vertical and horizontal directions, for the fourth-order-in-space operator). Since the

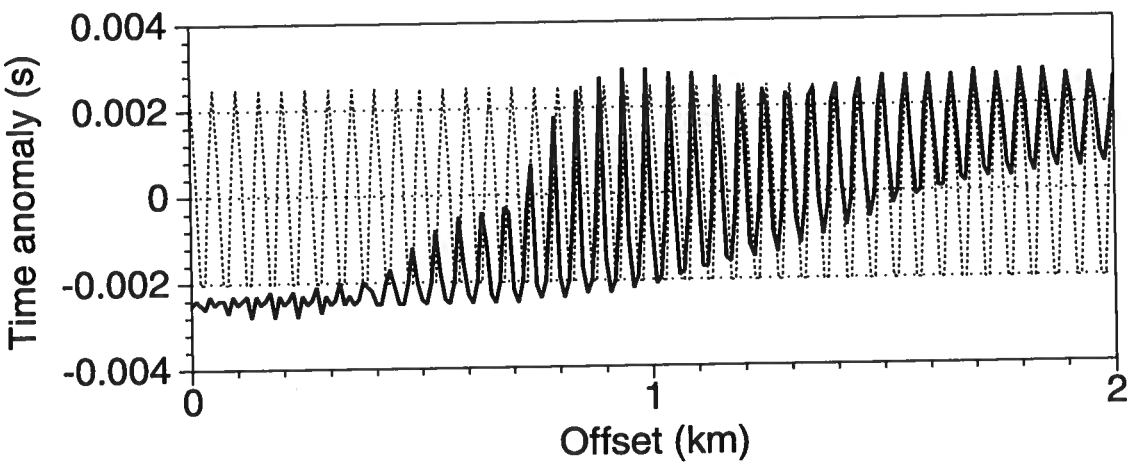

FIG. 3.21. Time-distortions estimated for the data from the 50/50/5 model, generated with an absorbing-boundary condition. In contrast to similar plots presented elsewhere in the thesis, the peak-frequency in the source wavelet was 38 Hz. Compare with Figure 3.16, which was computed for data modeled with a free-surface boundary condition, and a source peak-frequency of 30 Hz.

source must be placed in the center of the symmetric operator, this leaves the second inner position from the boundary as the outermost possible choice for location of the source. For the top, earth's-surface-boundary, this is the second-shallowest position.

For the finite-difference modeling here, source and receivers were placed at a depth $z_s = z_r = 3.75$ m. The frequency response of the ghost operator for this case is schematically depicted in Figure 3.22. This operator is simplistically estimated using a vertical path to calculate the time delay of the ghost with respect to the primary: $\tau = 2z_s/V_1 = 2z_r/V_1$. Non-vertical paths would be required to describe the ghosts for nonzero-offset data. The frequency response of the ghost operator has a maximum at around 67 Hz, and a notch at about 133 Hz. The convolution of this operator with a Ricker wavelet, would shift the peak frequency of the output toward larger values than that in the input, as long as the peak frequency of the source wavelet is less than or equal to the maximum-response frequency of 67 Hz.

I convolved the 30-Hz Ricker wavelet with the time-domain representation of the ghost operator to obtain the distorted wavelet shown in Figure 3.23, which should be compared with Figure 3.18. The distorted wavelet-shape and the frequency spectra in the two plots, although not identical, are quite similar; this similarity holds as well for the peak-frequency in the spectra.

Based on these considerations, we should expect that as a result of the ghosting just described, a 30-Hz peak-frequency wavelet would be present in the data generated using a free-surface boundary at the earth's surface and a 25-Hz peak-frequency source signature. The time-distortions estimated earlier for data featuring a 30-Hz

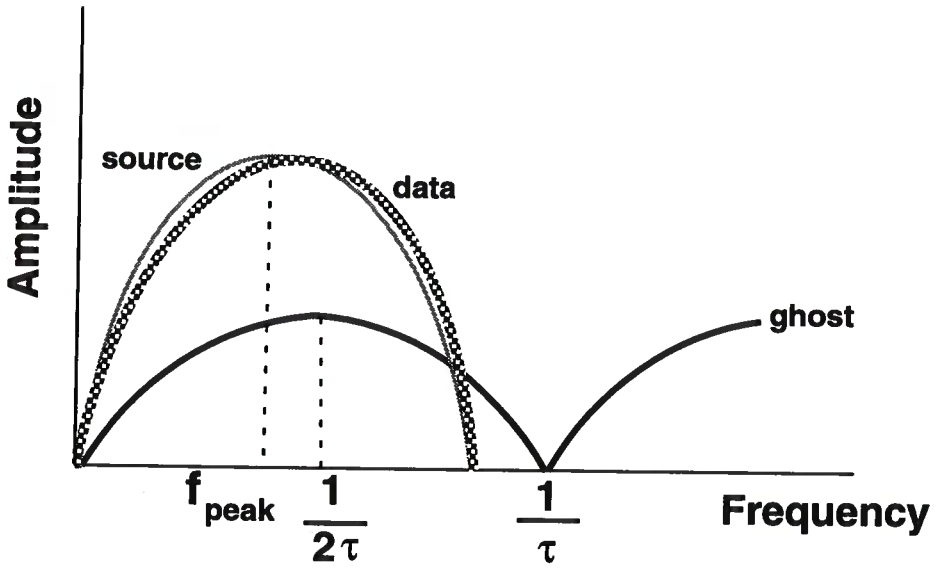

FIG. 3.22. The action of a short-period ghost operator on a source-signature wavelet featuring a peak frequency that is smaller than the maximum-response frequency of the ghost spectrum. Convolution with the ghost operator yields multiplication of the frequency spectra, schematically depicted here. That multiplication will shift the peak frequency of the output (data) spectrum to a higher value than that in the input.

peak-frequency wavelet (the data generated with an absorbing boundary) should be comparable to those estimated from data generated using the free-surface condition and a 25-Hz peak-frequency source signature. Figure 3.24 shows such estimated time-distortions, again for the 50/50/5 model. Quite nicely, the distortions in Figure 3.24 closely match those in Figure 3.17.

The choice of a boundary condition It is clear from the previous discussion that the results obtained from the finite-difference tests, of concern for the subject of this study, are basically the same regardless of the choice between a free- or absorbing-boundary condition at the earth's surface boundary of the computational grid. In other words, the character of the time-distortions induced by the presence of the sinusoidal-shape interface is not influenced directly by the type of boundary-condition, but by the frequency of the data, or rather, the ratio of the wavelength in the data with respect to the wavelength of variations in the base-of-weathering interface. If the distortions are characterized in terms of that ratio, little need exists to refer to the choice of boundary condition. Of course, the character of the wavefield is highly dependent, in general, on the choice of boundary condition. Such differences in the wavefield, however, do not influence the character of the time-distortions for the *primary* event of interest,

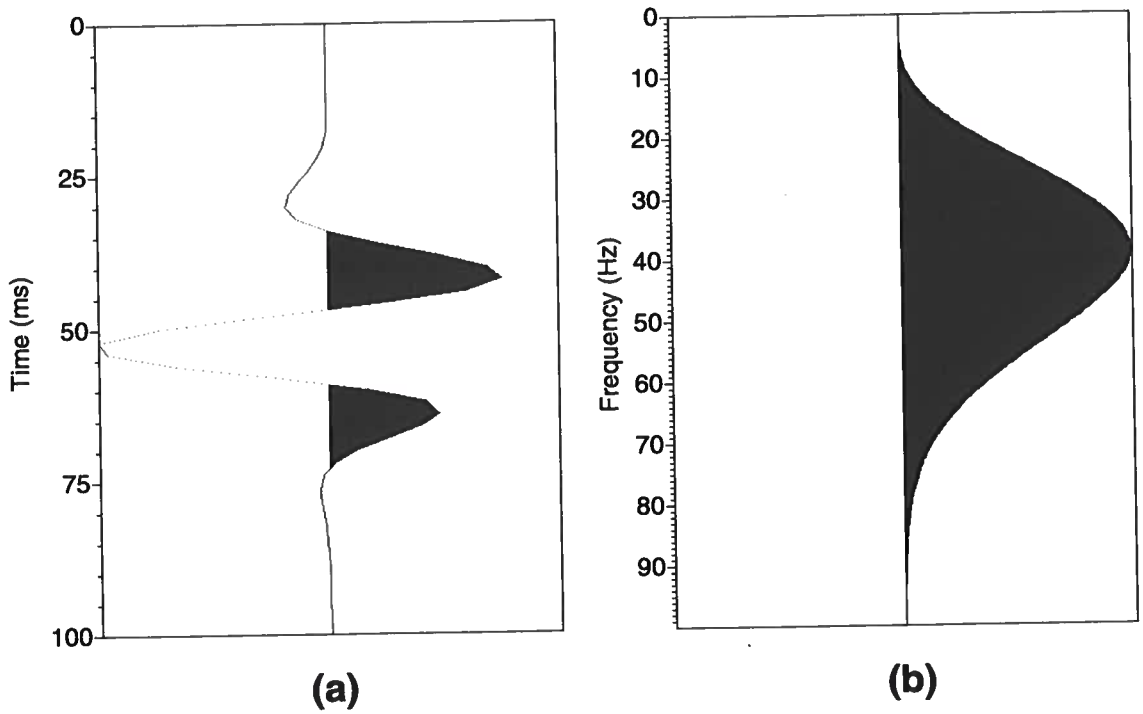

FIG. 3.23. A 30-Hz Ricker-wavelet convolved with the ghost operator corresponding to a 3.75 source- and receiver-depth: (a) the wavelet in time, and (b) its amplitude spectrum. Notice the distortion in the wavelet shape and the shift in peak frequency to about 38 Hz.

the key quantities analyzed in this study of surface consistency.

Having said that, the choice of a boundary condition becomes a matter of convenience. Choosing an absorbing boundary is convenient because the small level of multiples present in that case gives rise to less noisy, more interpretable data; as discussed earlier, the estimation of time-distortions also benefits from the noise-free character of the data.

3.5.2 Incorporation of additional factors in the model

Even though the essentials of the estimation and character of the time-distortions are independent of the choice of boundary condition at the earth's surface in the sense discussed in the previous section, the unrealistic level of multiples present in data generated with the implementation of a free-surface condition in the typical models in this work, and the related potential limitations of these models, as well as those of the modeling algorithms, still remain unresolved issues. Next, I discuss the results of some attempts to examine the possible influence of factors that are likely to be found in real situations but were not considered in the tests that make the core of the work of the thesis.

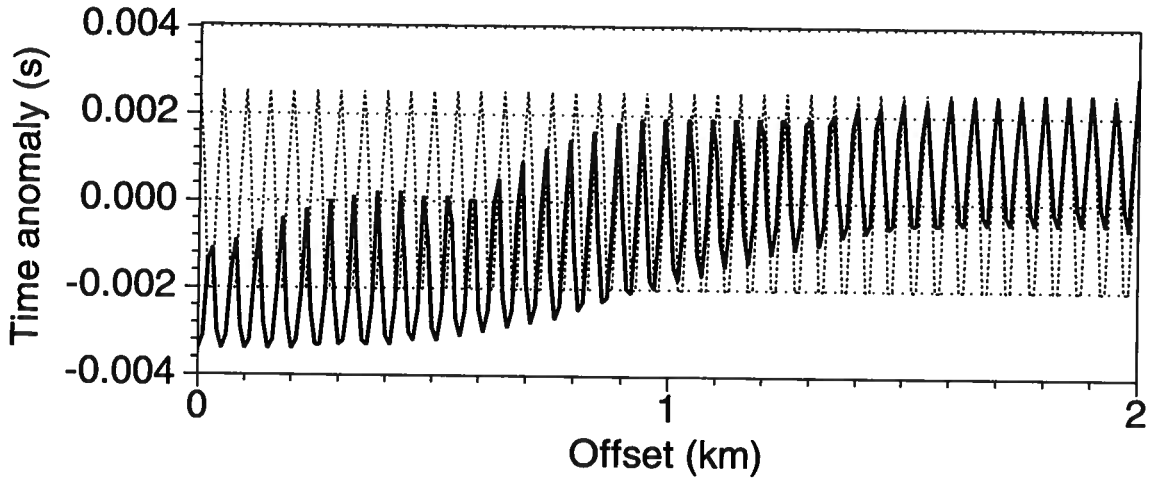

FIG. 3.24. Time-distortions estimated for the data from the 50/50/5 model, generated with a free-surface boundary condition. The peak-frequency in the source wavelet was 25 Hz. Compare with Figure 3.17, which portrays the distortions estimated for data from the same model, generated with an absorbing-boundary condition and a 30-Hz source signature.

Taking attenuation in the near-surface into account Unfortunately, a code to allow attenuation to be considered in a fully 2D-variant earth model such as those of interest in this work was not available to me. The reflectivity modeling code of Gouveia (1996), however, allows attenuation to be considered in layered-earth models; it also allows the choice of a free-surface boundary condition. Attenuation in that code is simulated using a constant-Q type of model (White, 1983). I tested the influence of the magnitude of attenuation on the weathering layer, determined by the choice of values for the attenuation parameter Q, on the amplitude of the free-surface-related multiples. In order to test a layered velocity model bearing some relation to the 2-D sinusoidal base-of-weathering interface models of interest in this work, I chose a model such as that in Figure 1.1, but with a horizontal base of weathering; i.e., the model used was the reference model for the estimation of time-distortions, as described in Section 3.4.

Figure 3.25 presents the results from one of these tests, where the magnitude of Q was chosen to be the extremely low value of 10. Notice that, even for such a low Q-value, the amplitude of the multiples is quite large, for both the deep reflection and the first breaks. The reason, simply, is that the reverberations do not travel sufficient distance in the near-surface to experience significant attenuation. I found that a value of Q as low as 5 was necessary to obtain synthetic shot records in which the amplitude of multiples was reduced to what might be a realistic level for land data (assuming that a realistic situation in this case would be to have at most a significant first multiple, but much weaker later multiple arrivals). In practice, such low Q-values can be found in the near-surface, but mostly at very shallow depths, in the order of a couple of

meters (Rice et al., 1991). Q is found to increase in magnitude for larger depths, so that the mean value for a depth of several tens of meters, such as the situation portrayed in the tests in this thesis, should be much larger.

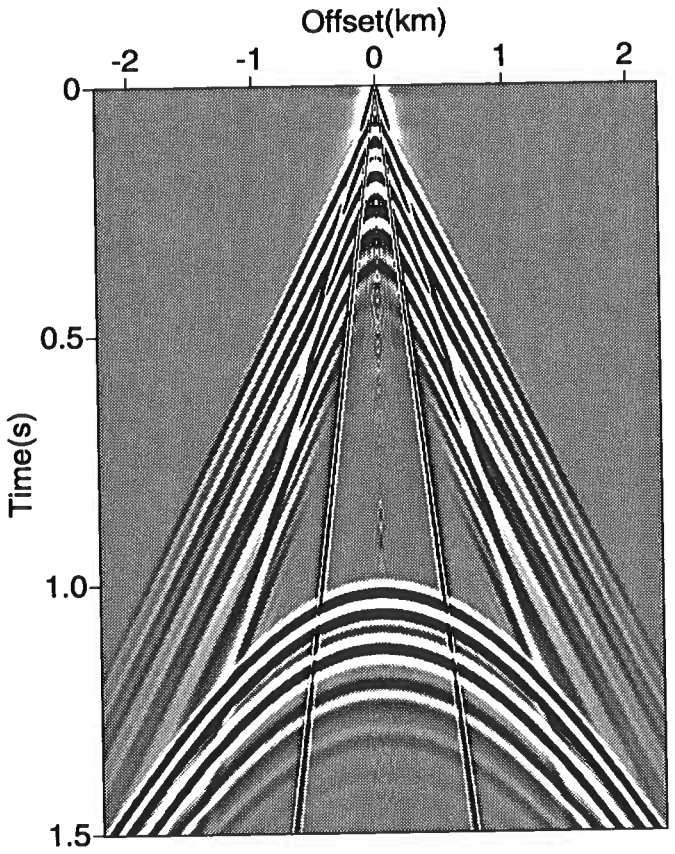

FIG. 3.25. Synthetic shot record generated by reflectivity-modeling, including attenuation. The depth model consists of a flat, horizontal base of weathering at 50-m depth, and a deep reflector. A free-surface condition is implemented at the earth's surface boundary. The value of Q for the weathering layer is 10.

Therefore, including attenuation in our model of propagation of waves in the near-surface does not by itself yield more realistic levels of the relative strength of multiple energy arising from the presence of a free surface.

A smaller velocity contrast? I also did some tests to understand the implications of having a milder velocity contrast at the base-of-weathering interface, compared to that in the tests presented in Section 3.3. Specifically, I modified the depth model of Figure 1.1 to include a transition between the 1000 m/s velocity in the weathering layer and the 2000 m/s velocity in the subweathering: in the modified model the velocity immediately below the base of the weathering is 1500 m/s and

increases linearly at a rate of 2.5 m/s/m, within a 200-m thick transition zone, up to the 2000 m/s value; all other details in the model are unchanged with respect to those in Figure 1.1. The modified model might describe a situation in which the contrast between the weathering and sub-weathering results from the presence of the water table but is not as sharp as that in the more simplistic model in Figure 1.1.

Figure 3.26 shows the results obtained in tests with the modified velocity model. Because of the reduced velocity contrast at the base-of-weathering, the amplitude of the multiples has decreased to a considerable extent, compared to that with a free-surface condition, such as that in Figure 3.15. The first breaks and associated events are much stronger than those in Figure 3.15, and of a different character, exhibiting increased strength and duration in time with increasing offset.

It is commonly understood that most of the strong first arrivals seen in land seismic data are refracted waves ("diving waves") related to likely transitional velocity variation in the near-surface. In the presence of a positive velocity gradient with depth, these waves are continuously refracted along a curved path and thus turn back up to the surface rather than travel as pure head waves along the boundary. Since the diving waves are formed by a larger part of the incident wavefront than are pure head waves, they carry more energy thus resulting in stronger arrivals (Tsvankin, 1995). This difference in strength is exemplified here by the difference between the strong first arrivals related to the transitional-velocity near-surface in Figure 3.26 and the weaker first-arrivals in Figure 3.15 due to head waves originated along the base of the weathering in the simpler, constant-velocity sub-weathering of the model in Figure 1.1.

The reduced velocity contrast in the transitional-velocity near-surface model yields a reduction in the relative size of the time-distortions, as can also be observed in Figure 3.26 (compare the size of the oscillations in the primary deep reflection with those in the corresponding event in Figure 3.2). A postulated transitional variation in velocity in the near-surface would contribute to an explanation of the relatively-low level of surface-generated multiples commonly observed in land data, but fails to account for the occurrence, common as well, of near-surface-induced time-distortions of significant amplitude.

3.5.3 Interface representation

The accurate representation of dipping or curved boundaries, such as the sinusoidal boundary proposed for the modeling studies in this thesis, is a challenge for finite-differences methods (Fornberg, 1988; Muir et al., 1992). Straightforward discretization of the velocity model yields a "stair stepped"-like representation of steep interfaces that generates artificial, unwanted diffractions arising from the sharp features (vertical steps) thus created, as illustrated in Figure 3.27. I have found such problems when computing time-distortions in models implemented with such a representation. The severity of the problems increases as the wavelength D decreases (the curvature of the sinusoid increases). Similarly, we can expect difficulty in characterizing the shape of the base of the weathering when the amplitude h of the sinusoidal

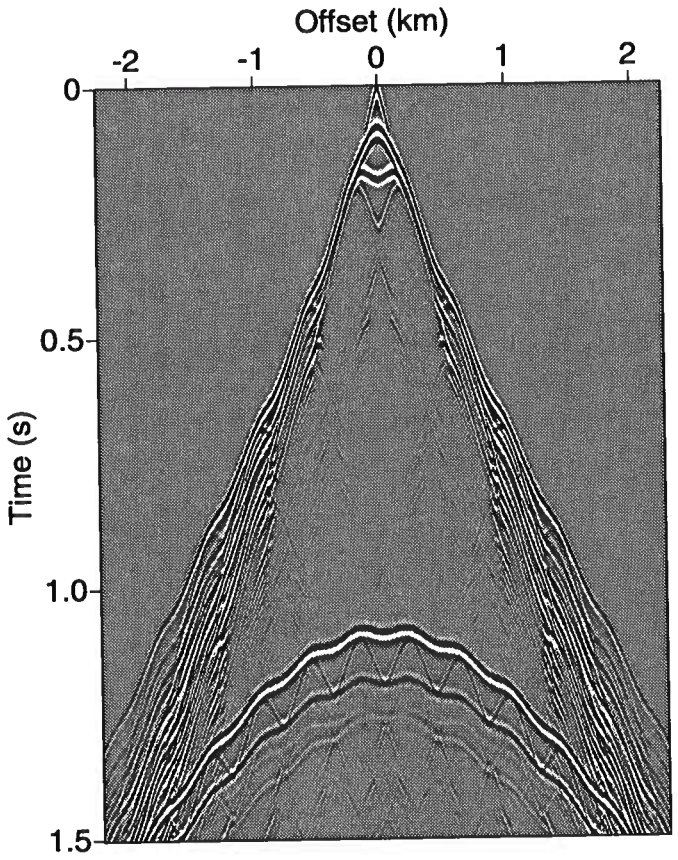

FIG. 3.26. Synthetic shot record generated for a model with a deep reflector such as in Figure 1.1, but with a transitional velocity variation at the base of the weathering; other near-surface parameters are $D = 400$ m, $z_w = 25$ m and $h = 20$ m.

base of the weathering becomes small relative to the step-size of the computational grid.

Since these problems arise because the grid-step size is too coarse to accurately represent rapid variations in the shape of the interface, they should be alleviated by a reduction in the size of that parameter; specifically, I tested reducing the grid-step size in the vertical direction, aiming to address the problem by reducing the vertical size of the "stair-steps." I found that a grid-step size as small as 1.0 m in the vertical direction should be used in order to avoid these problems. This, however, is a costly solution: the computational size of the problem increases by a factor of 6.25 (an increase by a factor of 2.5 in the number of cells and of time steps) compared to that for the already-fine, computationally-speaking, 2.5-m step size.

For any grid size, straightforward discretization of a velocity model containing interfaces is imperfect whenever the true position of the interface is not exactly in the middle of two grid points, since it will be represented on the computational grid as being positioned at the middle (see Figure 3.28). As a result, traveltimes are wrong, in

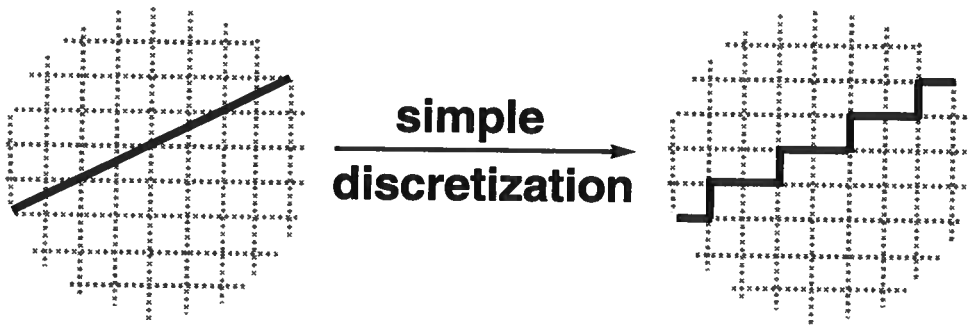

FIG. 3.27. Simple discretization of a velocity model containing steep or curved interfaces yields an imperfect, stair-step-like representation of those interfaces.

addition to the potential for generating diffractions. I addressed this shortcoming by assigning to every grid cell containing a segment of the interface, a velocity calculated from a weighted average of the slownesses above and below the interface; the weights were the relative vertical distances from the interface to the neighboring grid points above and below (see Figure 3.28). This is a correct solution for vertical traveltimes, and is considered acceptable for propagation in other directions (Muir et al., 1992). This scheme allowed me to use the 2.5-m vertical and horizontal step-size grid with results comparable to those obtained with the 1.0 m vertical and 2.5 m horizontal step-sizes grid, but at significantly lower computational effort.

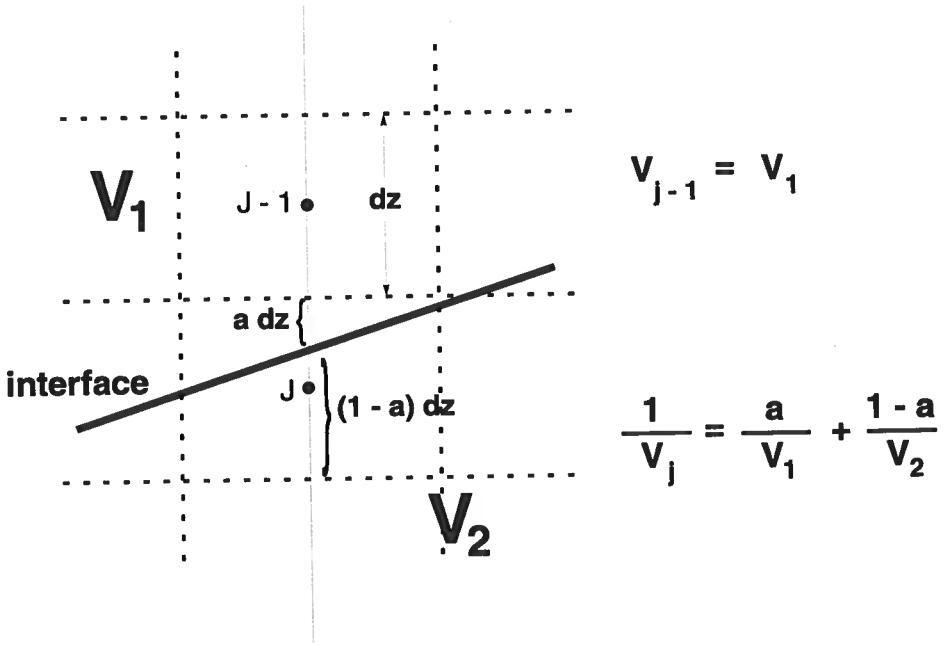

FIG. 3.28. Method employed to represent the curved interface of the models in this work. If the interface location is not exactly in the middle of the grid points $j-1$ and j here, simple discretization would assign $V_{j-1} = V_1$ and $V_j = V_2$, effectively positioning the boundary in the middle of the $j-1$-th and j-th grid points. Vertical traveltimes are more accurately preserved if a weighted slowness-averaging procedure is implemented as shown.

Chapter 4

THE CHARACTER OF THE TIME-DISTORTIONS AND THE DEPARTURE FROM SURFACE-CONSISTENCY

Having obtained reflection-time distortions for a number of experiments involving variation in the near-surface parameters, the goal now is to develop an understanding of the relationship between the character of the distortions, the departure from surface-consistency and those parameters. Here, I use the familiar concept of Fresnel zone to state in more precise terms what earlier I have referred to as "wavefront healing."

In the second part of this chapter, I use the comparison between the wave-theoretic time anomalies and those expected under the assumption of surface consistency to quantify the extent of departure from that assumption. I then study the dependence of that departure on variations in the model parameters and discuss implications for the validity of the surface-consistency assumption.

4.1 The relationship between the character of the time-distortions and the subsurface parameters

4.1.1 The concept of Fresnel zone

We have observed in Chapter 3 variations in the relative size of the wave-theoretical reflection-time distortions for variations in the subsurface parameters. For example, we saw that when the wavelength D of the sinusoidal base-of-weathering interface was reduced to values close to the size of the seismic wavelength, the magnitude of the distortions decreased compared to that of the distortions associated with much larger wavelengths of the sinusoidal interface, all other parameters being unchanged. Moreover, we also saw indications that other parameters, such as the mean depth of the base of the weathering z_w, had an influence on the relative size of the estimated time-distortions.

By Huygens' principle, a sizable portion of a reflector contributes to a reflection as seen in a seismic trace, the size of which is usually estimated using the concept of *Fresnel zone* (Sheriff, 1980; Berkhout, 1984). The Fresnel zone is defined as the portion of a reflector from which reflected energy can reach a receiver within sufficiently short time after the first arrival of the reflection that contributions from this zone are considered to add constructively to produce the reflection. The maximum delay-time is usually set as a fraction of the period of the seismic waves: common choices are half a period (Sheriff, 1980) and a quarter of a period (Berkhout, 1984).

The generalization of the concept of Fresnel zone is that of *Fresnel volume* (Cerveny and Soares, 1992). As illustrated in Figure 4.1, the Fresnel volume for a given

event, such as the reflection from the deep interface in the modeling experiments in this thesis, is defined as the locus of points such that the sum of traveltimes from the point to the source and from the point to the receiver is within some delay time of the traveltime from the source to the receiver for the event of interest, so that contributions scattered from these points interfere constructively. Cerveny and Soares (1992) use one-half of a period in their formulation.

In a homogeneous medium, the shape of the Fresnel volume is that of an ellipsoid, whose foci are coincident with the source and receiver locations (Cerveny and Soares, 1992). Wave propagation can be thought of as a spatial convolutional process that smears information from a finite portion of the medium to a point receiver on the surface. The Fresnel volume is an estimate of the region of the medium effectively contributing in that process.

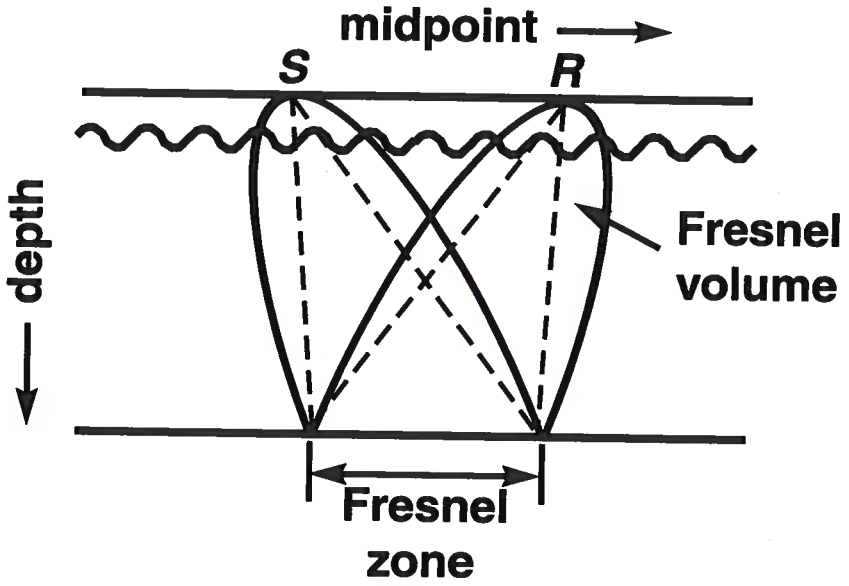

FIG. 4.1. Schematic picture of the Fresnel volume for the reflection from the deep interface in the typical tests of this thesis. Waves traveling within the limits of the Fresnel volume will contribute to a single arrival of the reflection. The intersection of an interface and the Fresnel volume determines the Fresnel zone for that interface. One can then refer to a separate Fresnel zone in the deep interface and another in the base of the weathering as well.

As illustrated in Figure 4.1, we can think of a Fresnel zone on an interface as the intersection of the interface with the Fresnel volume for the event of interest. In particular, the Fresnel zone on the base-of-weathering interface for the deep reflection in the tests in this thesis represents the portion of that interface that contributes to the reflection, and hence to the character and magnitude of the observed time-distortions.

Therefore, I estimate the width of that "contributing portion" of the reflector by taking advantage of the concept of Fresnel zone, following the procedure illustrated in Figure 4.2; note that I used a quarter-wavelength criterion in that estimation. I found that the expression developed using this choice helps in understanding the behavior of the time-distortions, as seen in Section 4.1.2 below. Contributions from terms proportional to quadratic and larger powers of the seismic wavelength are neglected in the estimation of the size of the Fresnel zone for reflectors whose depth is large compared to that wavelength (Sheriff, 1980). For the models in this work, in which the seismic wavelength is not small relative to the average thickness of the weathering layer, the width F of the contributing zone, as depicted in Figure 4.2, is given by

$$F = \frac{0.25\sqrt{\lambda_1\,(\lambda_1+16Z)\,(\lambda_1+16Z-8z_w)\,(\lambda_1+8z_w)}}{\lambda_1+8Z}\,, \tag{4.1}$$

where $\lambda_1 = V_1/f$ is the seismic wavelength in the weathered layer, f is dominant frequency, Z is the depth of the reflector whose reflection contains the time-distortions, and z_w is the mean depth of the weathering interface.

The contributions to the composite output from different points along the extent of the contributing zone are not equally weighted. They should be relatively larger for the central portion of the zone, compared to the contribution from the outer portion (Berkhout, 1984; Snieder and Lomax, 1996), because a larger relative number of raypaths satisfying the quarter-wavelength criterion pass through that central region. Therefore, we should expect the effective size of that zone to be smaller than that predicted by equation (4.1), increasingly so for near-field situations (e.g., for small z_w) in which seismic amplitude varies inversely with the square of the distance from the source, which would act to further downweight contributions from the outer portion of a zone of width as estimated with equation (4.1).

The size of the contributing zone is frequency-dependent, being larger as frequency decreases; in what follows I use the peak frequency in the source-signature wavelet as an estimate of the dominant frequency in the data. The discussion in Section 3.5.1 supports this choice for the data generated using the absorbing-boundary condition for the earth's surface boundary.

4.1.2 The dependence of the amplitude of the anomaly on the size of the contributing zone

As discussed above, a simple and convenient way to view the complexity of seismic-wave propagation is to assume, in accordance with Huygens' principle, that it effectively takes place within the bounds of a contributing zone for the interface of interest. If variations exist within the medium, such as those in the sinusoidal near-surface model, one would expect that the ratio of the size of the contributing zone to the wavelength of those variations plays a role in influencing wave-propagation phenomena. Thus, the time-distortions of interest here should be influenced by the length along the corrugated boundary over which Huygens secondary sources contribute to a given

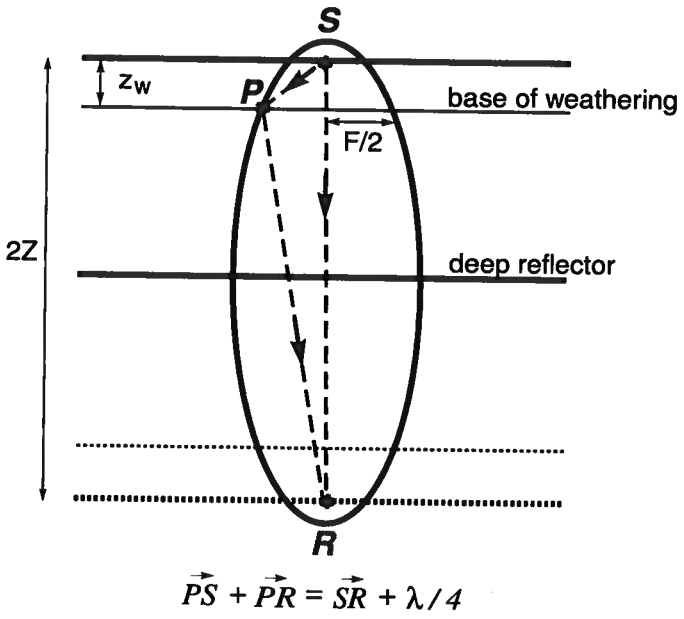

FIG. 4.2. Geometry used to define the width of the portion of the base-of-weathering interface contributing to a reflection arrival, using the concept of Fresnel zone, for a coincident-source-and-receiver situation. The receiver is shown as the image of the source with respect to the deep interface. The sum of the traveltimes from a point P on the edge of the zone to the source-location S and to the receiver-location R has to exceed the time of the direct arrival from S to R by a quarter of a period; for a constant-velocity medium this condition is equivalent to the geometrical relation shown, which in turn leads to equation (4.1).

frequency component in the observed reflection. For example, if a significant portion of one wavelength of the corrugated boundary contributes, we expect an averaging of arrival times for contributions from along the boundary.

I studied the reduction in amplitude of the time-distortions in a number of tests involving variations in the model parameters D, h and z_w; for each test, variation in the dominant frequency in the data provided sampling of a range of values of the width F of the contributing zone. In every case, I computed the relative size of the time-distortions with respect to the size of the corresponding statics in a region near zero-offset, as a function of the ratio F/D, with F evaluated by equation (4.1).

Let's study first the implications of variations in D. Figure 4.3 presents the results for variations in D from 400 m to 50 m, with a fixed $D/h = 20$. Here and in Figures 4.4 and 4.5, below, the thick-line portion of the curves highlights the results for the range of frequencies between a low-frequency threshold of 10 Hz and a high-frequency threshold at 50 Hz. The results in these figures are not reliable for frequencies above about 50 Hz (i.e., small F/D) because of the presence of numerical dispersion in the finite-difference-generated data.

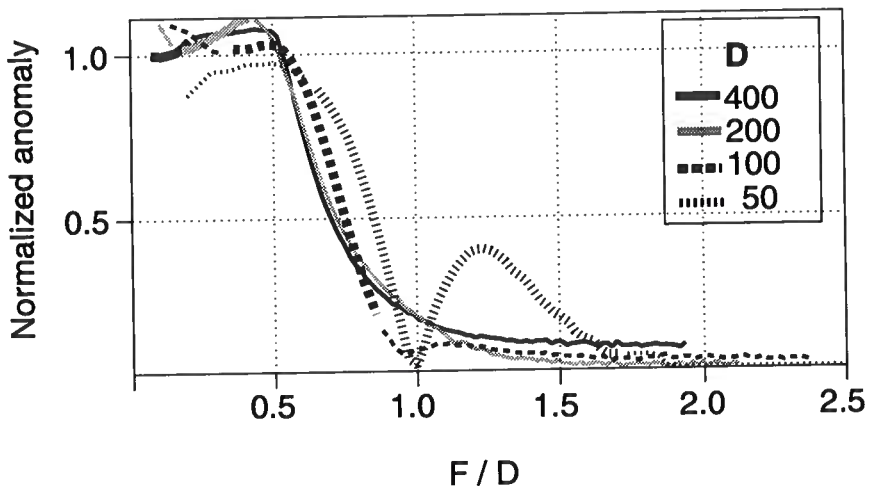

FIG. 4.3. Ratio of the amplitude of the time-distortions to the corresponding vertical statics as a function of the ratio of the contributing-zone size F to the wavelength D of the base of the weathering. The thick-line portion of each curve represents the values for the frequency range from 10 to 50 Hz common in field data; this portion is very small in the curves for $D = 400$ m and $D = 200$ m, restricted to low values of the ratio F/D. That convention is followed in Figures 4.4 and 4.5 as well. Note that F/D increases with decreasing frequency. Each curve was computed for a different value of D, keeping $D/h = 20$ and $z_w = 25$ m. The amplitude of the distortions was estimated from the peak-to-trough values measured in a 1.0-km-wide window centered around zero offset.

Figure 4.3 shows a marked high-cut behavior in the ratio of the amplitude of the time-distortions relative to the size of the vertical static, as a function of the ratio F/D. Differences between the curves in Figure 4.3 indicate that the problem is not linear as a function of D. Those differences, however, are small for some of the curves indicating that for a range of values of D the nonlinearity is not significant. The largest departure is observed for the smaller values of D (e.g., the curve for $D = 50$ m). This curve does not follow the general trend of an increased reduction in the size of the time-distortions with increasing values of F/D, but shows a "bounce back" to a cycle of increase and subsequent decrease in the size of the distortions with increasing offset, after having reached a minimum near $F/D = 1.0$. A discussion of this characteristic is given in the next section.

The "high-cut" behavior seen here is an expression of what I earlier referred to as "wavefront-healing". An increase in the ratio F/D gives rise to a reduction in the size of the time-distortions, provided that F/D is high enough (i.e, larger than about 0.5, in Figure 4.3). As the wavelength D of variations in the thickness of the near-surface layer becomes small relative to the size of the contributing zone, the seismic waves become less sensitive to the presence of those variations. In this argument, wavefront

healing should be stronger for the smaller values of D (i.e., all other parameters unchanged, F/D increases with decreasing D), as we indeed observed in Section 3.4. For the larger values of D (e.g., $D = 400$ m and $D = 200$ m), on the other hand, values of F/D large enough to cause a reduction in the size of the time-distortions are reached for frequencies that are smaller than those commonly found in exploration seismology (i.e., in the thin-line portion of the curves in Figure 4.3).

Let's now examine implications of variations in the thickness of the weathering z_w. Figure 4.4 shows the results of another suite of experiments featuring variation in this parameter. In contrast to Figure 4.3, the curves for different values of z_w here do not parallel each other so closely, although similarities exist in the general trend for some of the curves. Time-distortions behave in a highly nonlinear fashion as a function of z_w; the nonlinearity is higher for the larger values of z_w (e.g., the curve for $z_w = 100$ m exhibits the largest departure from the other curves in Figure 4.4). Again, a general trend of reduction in the relative size of the time anomalies with increasing values of F/D is observed; in this case, however, several of the curves exhibit the "bouncing-back" in the magnitude of the distortions past $F/D = 1.0$ observed in Figure 4.3 for the $D = 50$ m-curve. Differences in the details in this feature in the curves for which it occurs, constitute a large part of the observed departure between the curves in Figure 4.4.

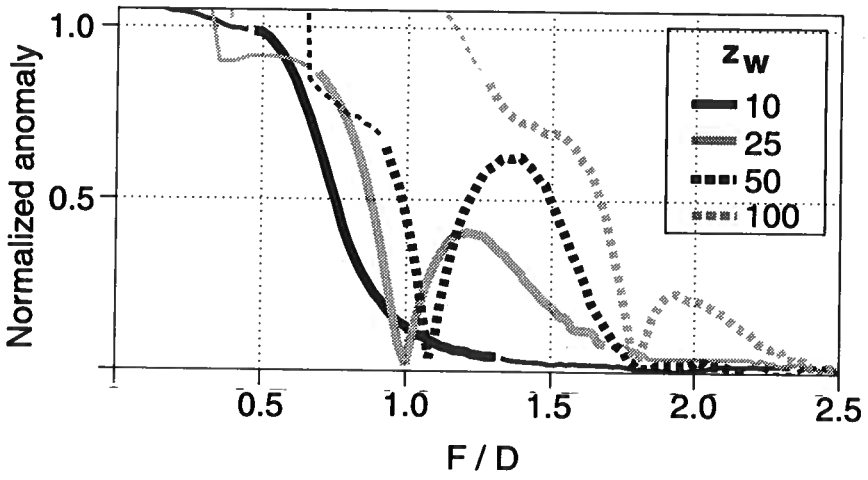

FIG. 4.4. Ratio of the amplitude of the time-distortions to the corresponding vertical statics as a function of the ratio F/D for tests where $D = 50$ m, $h = 5$ m and z_w takes on several values ranging from 10 m to 100 m, as shown. Again, the size of the distortions was estimated from peak-to-trough values near zero offset. The thick portion of each curve represents the values for the frequency range from 10 to 50 Hz.

Finally, Figure 4.5 shows the results for variation in h. The magnitude of the time-distortions depends approximately in a linear fashion on the height h of the sinusoid, for low values of h; for relatively large values of h, scattering from the

corrugated interface becomes important, and the problem turns into a highly nonlinear one. The results in Figure 4.5 suggest that $h/D \leq 0.1$ might be a criterion for what we could call small h. In Figures 4.4 and 4.5, the thick-line portion of the curves pertaining to the range of frequencies considered of interest here is in general within a range of relative magnitude of the time-distortions smaller than 1.0, even when a regrowth in the magnitude of the distortions (i.e., the bounce-back already mentioned) is observed. Also in Figures 4.4 and 4.5, some of the curves (e.g., those for $z_w = 50$ m and $z_w = 100$ m in Figure 4.4) exhibit an anomalous behavior for very high frequencies. These faulty results occur because of the presence of numerical dispersion in the modeled shot-record data.

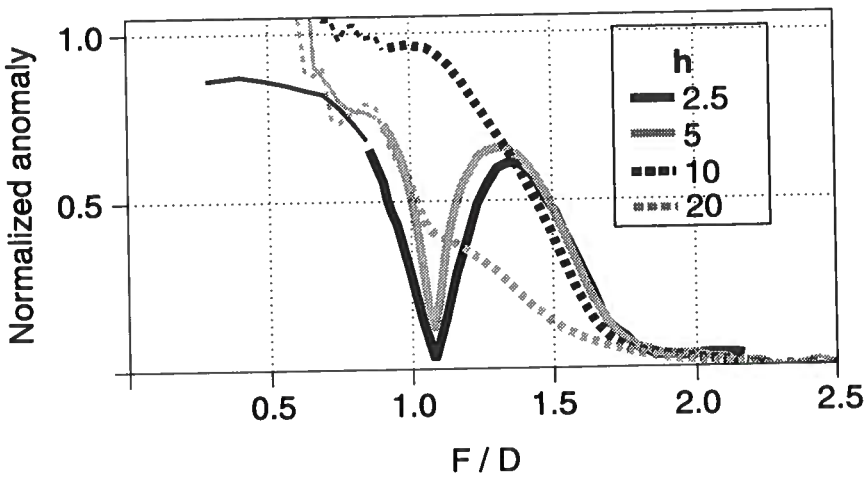

FIG. 4.5. Ratio of the amplitude of the time-distortions to the corresponding vertical statics as a function of the ratio F/D for tests featuring variation in the magnitude of the height of the sinusoidal shape of the base-of-weathering. Here $D = 50$ m, $z_w = 50$ m and h ranges from 2.5 m to 10 m. The thick portion of each curve represents the values for the frequency range from 10 to 50 Hz. The amplitude of the distortions was estimated from peak-to-trough values measured near zero offset.

The dependence of the size of the time-distortions on variations in the parameters of the near-surface, as indicated by the results just examined, is highly nonlinear, as we should expect. We gain insight into the problem, however, by studying the connection with variations of the ratio F/D. When that ratio increases, either by an increase in λ_1 or z_w or a reduction in D, wave-theoretical phenomena are increasingly more important. The size of the distortions decreases with increasing F/D, for values of F/D approximately between 0 and 1.0; past around $F/D = 1.0$ (or F/D around 1.8 for the curve for $z_w = 100$ m in Figure 4.4) in some cases a cycle of regrowth and subsequent decrease in the magnitude of the distortions with increasing F/D is observed. These and other related issues are discussed next.

4.1.3 Discussion

The results obtained in the previous section can be understood in relation to the distinction made earlier between ray- and wave-theoretical modeling of wave propagation. For sufficiently small values of F with respect to D, λ_1 would also be small with respect to D, and we are in the high-frequency domain of validity of ray theory (Figures 4.3 through 4.5 suggest that $F/D < 0.5$ would be an adequate rule-of-thumb for defining what is a sufficiently small value of F compared to D). For the near-zero-offset region used to estimate the amplitude of the distortions in Figures 4.3 through 4.5, wave propagation would be mostly vertical. If wave propagation can be validly conceived of as vertical-ray propagation, as discussed previously, the near-surface-induced time-distortions can be estimated as simple statics, hence the match observed between these quantities (i.e., a ratio of the size of the wave-theoretical distortions to the statics close to 1.0), especially in Figure 4.3.

Since wave propagation involves contributions from a finite portion of the medium, the time-distortions of interest in this work should be some sort of average of those individual contributions from every point on the anomalous sinusoidal-shape interface, over the length of the contributing zone (Vasco et al., 1995; Snieder and Lomax, 1996). As the size of the contributing zone increases, this averaging would yield a smoothing of the observed time-distortions compared to the individual contribution of a tiny piece of the interface in the center of the zone (i.e., the ray-theoretical distortion, which is the same as the static for zero-offset). As a result, when the wavelength D of the base of the weathering is small compared with the size F of the region contributing to the recorded wavefield, the seismic waves little perceive the presence of lateral variations in the near-surface layer.

As previously noted, viewing wave propagation as being spatially limited to the bounds of a contributing region is a simplification of a complex process involving the whole medium; moreover, the quantitative estimation of the size of such a region is by no means exact and subject to the choice of a defining criterion. Therefore the use of an estimated value for F here is qualitative and aimed at gaining insight into the behavior of the time-distortions observed in the data. Having said that, let's move on with study of that behavior.

The size of the contributing zone will be relatively smaller as z_w decreases; moreover, we have already noticed that equation (4.1) overestimates the size of the zone for low z_w, due to near-field-associated downweighting of contributions from outer portions of a zone of width F. The smaller the size of the contributing zone, the less intense is the smoothing of the time-distortions due to averaging along the length of that zone. This means that, for a given wavelength of near-surface variation, D, and seismic frequency, we should not expect so severe a decrease in the magnitude of the time-distortions for situations in which the thickness of the weathering layer is small. Combee (1994; 1995) has shown that the size of wave-theoretical time-distortions of relatively small wavelength is not reduced much for situations in which the thickness of the weathering layer approaches zero. Taner et al. (1988) discuss a similar depend-

ence on the thickness of the weathering for the amplitude of time-distortions observed in refraction (first-break) arrivals. They notice that the short-wavelength components of the distortions originate from the shallowest portions of the near-surface.

The reduction in the amplitude of time-distortions associated with arriving waves occurs because of the oscillatory nature of the interface shape. For contributing zone larger than some threshold value (close to $F = D/2$, as suggested above), significant contributions to the time-distortions of opposite sign contribute to the averaging process, thereby lowering the magnitude of the average distortions. When the width of the contributing zone is close to D, the average should yield small time-distortion values (e.g., the mean value of a sine function over a period is zero), as seen in most of the curves in Figures 4.3 through 4.5.

Consistent with this picture of the time-distortions as an average of sinusoidally-varying contributions, one would expect the time-distortions to grow in magnitude past $F/D = 1.0$ reducing to low values again for $F/D = 2.0$, and so on. This feature, which I earlier referred to as a "bounce-back" of the relative size of the distortions past $F/D = 1.0$, is observed in some, but not all, of the curves in Figures 4.3 through 4.5.

The averaging process is not uniformly weighted. In particular, some outer portions of the contributing zone contribute relatively less to the wavefield than does the central portion (Sheriff, 1991; Snieder and Lomax, 1996). Moreover, as discussed earlier, the contribution from the outer portion of the zone should be particularly downweighted in the near-field situation, e.g, when z_w is small. If that is the case, one should expect that contributions from the outer portions of the contributing zone decrease as F becomes larger relative to the mean depth z_w of the interface.

Following along these lines, the absence of the bounce-back or regrowth in the size of the distortions past $F/D = 1.0$ could be interpreted as indicative of a relative smaller weighting of the contribution of the outer portion of the contributing zone. In other words, the absence of the regrowth past $F/D = 1.0$ would indicate that the effective value of F is reduced so that portions of the sinusoid beyond the first cycle contribute significantly less to the average time-distortion, relative to those portions within the first cycle. If this is indeed the case, from the near-field argument above one should expect the absence of the regrowth in situations in which the ratio F/z_w is relatively large. In fact, we observe in Figure 4.3 that the regrowth is present only for the curve with $D = 50$ m, the case with the smallest relative value of F/z_w (if F/D is not much larger than 1.0, F is similar to D and since z_w is fixed here, F/z_w is smallest if D is smallest). In Figure 4.4 the only case in which the regrowth is absent is that for the smallest value of z_w, and hence the largest relative value of the ratio. This dependence of the shape of these curves on F/z_w is further evidence of the nonlinearity of the problem of reflection time-distortions.

If, roughly, the observed time-distortions result from averaging the contribution of points along the sinusoidal base-of-weathering, then we should have a net distortion with *negative* amplitude for values of F/D approximately between 1.0 and 2.0 (i.e., the mean value of a sinusoidal function of wavelength D is of negative amplitude for

an averaging length between D and $2D$). This is the reason for the change in phase of the time-distortions relative to the statics observed, specially near zero-offset, in some of the distortion curves in Section 3.4 (see Figures 3.11 and 3.13). For instance, the estimated width of the contributing zone F using equation (4.1) is 60 m (slightly larger than the corresponding $D = 50$ m) for the model corresponding to Figure 3.13.

So, the "regrowth" in the size of the time-distortions which also occurs for values of F/D roughly between 1.0 and 2.0 corresponds to a second cycle of variation in the average, with net values of the distortions that are of negative amplitude. Curves such as those in Section 4.1.2 show the absolute value of the amplitude of time-distortions; thus, they are "rectified" versions of the variation from positive to negative amplitude. Moreover, examination of time-distortion curves for the experiment with $z_w = 100$ m in Figure 4.4 reveals that the regrowth observed there past around $F/D = 1.8$ corresponds to a second bounce in the averaging, since the polarity of the time-distortions changes from negative to positive as that regrowth occurs. The inconsistency in the value of F/D at which the regrowth occurs (i.e., the fact that it is not at $F/D = 2.0$, as expected) is indicative of the imperfect and qualitative nature of our understanding of the phenomena concerning the time-distortions. The first bounce, which should occur for values of F/D between about 1.0 and 1.8, is not observed; results in this region are untrustworthy largely because they arise from relatively high frequencies for which dispersion occurs in the modeled shot-record data, as discussed above.

In Section 3.4.1, the drift in the mean value of the distortions from near zero-offset to the longer offsets was explained as the result of variations in the contribution to the time-distortions from near the shot. We can see now how those variations can occur: the shot-associated contributing zone samples a slightly different region of the sinusoid as the receiver location changes from zero-offset to the longer offsets (see Figure 4.1). In the common-shot configuration used for the tests in this work, the portion of the contributing zone associated with the shot changes more slowly with offset than does that associated with the receiver. Therefore, the shot-related drift is a relatively long-wavelength feature while the shorter-wavelength variations in the time-distortions are related to variations in the contribution from the receivers, as was also observed in Section 3.4.1.

The wave-theoretical results presented in the previous section and discussed here indicate that we should not find significant near-surface-induced time anomalies of a relatively small lateral wavelength in field seismic data unless the thickness of the weathering is small. If they indeed are observed, they may be some sort of noise not associated with near-surface anomalies or may have a very shallow origin. Below, however, we shall find that the reduced time-distortions associated with increased z_w does not necessarily imply better quality of the surface-consistency assumption.

4.2 The departure from surface-consistency

Having discussed the character of the wave-theoretical time-distortions, let us now focus on study of the extent and implications of the departure of the distortions

from those predicted under the assumption of surface-consistency.

Even though it is an interesting phenomenon, the reduction in size of the wave-theoretic time anomalies for relatively small values of D does not exemplify a shortcoming of the assumption of surface consistency. As illustrated by the examples of surface-consistent statics corresponding to the time-distortions in Section 3.4, for the sinusoidal interface, surface-consistency implies a repetition of the sinusoidal pattern for all offsets. Surface-consistency assumes a single magnitude for the statics, regardless of the offset. In what follows I will refer to half the peak-to-trough height of the laterally-invariant sinusoidal-shape curve as the magnitude of the statics.

Departure from surface-consistency is then associated with a pattern of time-distortions that varies with offset. Any departure from a strict repetition in the anomaly pattern with offset poses a problem for the assumption of surface-consistency. This type of departure is commonly present to varying extents in the wave-theoretical distortions, as exemplified by Figures 3.9 through 3.14.

Quantifying the extent of departure of the wave-theoretic time-distortions from surface-consistency requires the definition of a reference time-distortion pattern. The difference between the measured time-distortions and the reference distortion pattern would indicate the amount of departure from surface-consistency for the time-distortions considered.

The reference distortions should be an estimate of what the computed surface-consistent statics would be if data contaminated with the wave-theoretical time-distortions of interest here were input to a static-corrections estimation procedure. In conventional statics-estimation, static corrections are computed by an inversion procedure, fitting the time-distortions present in the input data in some way. The surface-consistent statics portrayed in Section 3.4, which were not estimated from the time-distortions but instead consider simple vertical-ray propagation in the near-surface model, are a poor estimate for that reference in many cases. Specifically for relatively low values of D, those statics poorly fit the data, because of the reduction in relative size of the wave-theoretic anomalies already discussed. Thus, for example, the difference between the solid and dashed lines in Figure 3.10 is not the appropriate measure we are looking for.

4.2.1 Estimating statics from a single shot-record

In common practice, static corrections are estimated by an inversion procedure applied to CMP gathers of data from an entire seismic line. The data from a single shot gather, available from the finite-difference tests, is clearly too limited to allow any sort of statics estimation as is conventionally done.

On the other hand, the repeated finite-difference modeling of lines of survey data for sinusoidal-weathering models characterized by differing wavelengths D would be inordinately costly, in fact totally impractical. I therefore resort to making educated guesses as to what the estimated statics would be for the simple sinusoidal variations in the near-surface studied here. Hopefully, the simplicity of the sinusoidal model will

allow the formulation of plausible assumptions.

Conventionally, static corrections are estimated for every trace in the data, as the sum of surface-consistent components associated uniquely with each individual shot and receiver location; the traces in a common-shot gather will share a single value for the shot-static and will differ in the receiver-static. Therefore, in dealing with common-shot data we are concerned specifically with receiver statics, and the comparison between those and the time-distortions in the data. Moreover, with data from only a single shot, we cannot even guess as to the nature of the shot statics. I will make the assumption that receiver- and shot-statics are independent of one another, so that receiver statics can be explored without concern for the potential influence of shot-associated contributions. This assumption would hold, in particular, if the contribution to the time-distortions associated with the shot was a single static time-shift whose occurrence could be easily recognized and removed. We already saw in Section 4.1.3 that it is not always the case since variations in the contribution from the shot (manifested as the drift in the mean value of the distortions with offset) indeed exist. Below, I implement a procedure to minimize the influence of those contributions.

If shot-recorded data data generated for a sinusoidal-near-surface model and, as a result, contaminated with time-distortions such as those observed in Section 3.4, were input to a conventional statics-estimation procedure, then static corrections would be computed by an inversion procedure, fitting those time-distortions in some way. If we assume that the data are recorded with a spreadlength X_{max}, then the data recorded at any given receiver position consist of traces from sources whose offset ranges from 0 to X_{max}. Therefore, the time-distortions present in the input data in that range of offsets will contribute to the estimation of a static correction.

Because of the variation with offset in the time-distortions, we should expect the estimated static corrections to depend on X_{max}. For example, considering input data showing distortions such as observed in Figure 3.9, we should expect that the magnitude of the estimated static correction will be different if the range of offsets goes, for example, from 0 to 1.0 km ($X_{max} = 1.0$ km) as opposed to a range that goes up to a larger value such as 2.0 km ($X_{max} = 2.0$ km). Moreover, it seems reasonable to assume that the magnitude of the estimated static correction is *larger* for $X_{max} = 2.0$ than that for $X_{max} = 1.0$ since the magnitude of the time-distortions in Figure 3.9 *increases* with increasing offset. The added range of offsets between 1.0 and 2.0 km will thus supply contributions of larger magnitude to the hypothetical statics computation. If the time-distortions in the data were such as those in Figure 3.10 we should rather expect the magnitude of the estimated static corrections to *decrease* with increasing spreadlength X_{max}, corresponding to the observed reduction in the magnitude of the distortions with increasing offset.

The computation, for each value of X_{max}, of a *single* magnitude for the static correction from contributions that change with offset, such as the time-distortions of interest here, should involve some sort of averaging of those contributions by the inversion procedure. I postulate that an appropriate guess for that magnitude is the

root-mean-square average of the magnitude of the wave-theoretical time-distortions over the offset range from 0 to the spreadlength X_{max}. Then the assumed shape of the surface-consistent receiver statics would be that of a laterally-invariant, somewhat sinusoidal pattern with magnitude given by this average.

4.2.2 Quantifying the departure from surface-consistency

The contributions to errors in the assumption Presuming the pertinence of the above postulate gives us a way of estimating the surface-consistent static corrections corresponding to the time-distortions of interest in this work. Those estimated surface-consistent statics provide a reference for establishing the errors in the surface-consistency assumption. Specifically, errors in residual-statics estimation due to the departure from the surface-consistency assumption will be given by the difference between the wave-theoretical time-distortions and that reference distortion pattern, e.g. the difference between the solid- and dashed-line curves of Figure 4.6, which shows curves for the 50/25/2.5 experiment and a spreadlength $X_{max} = 2.0$ km.

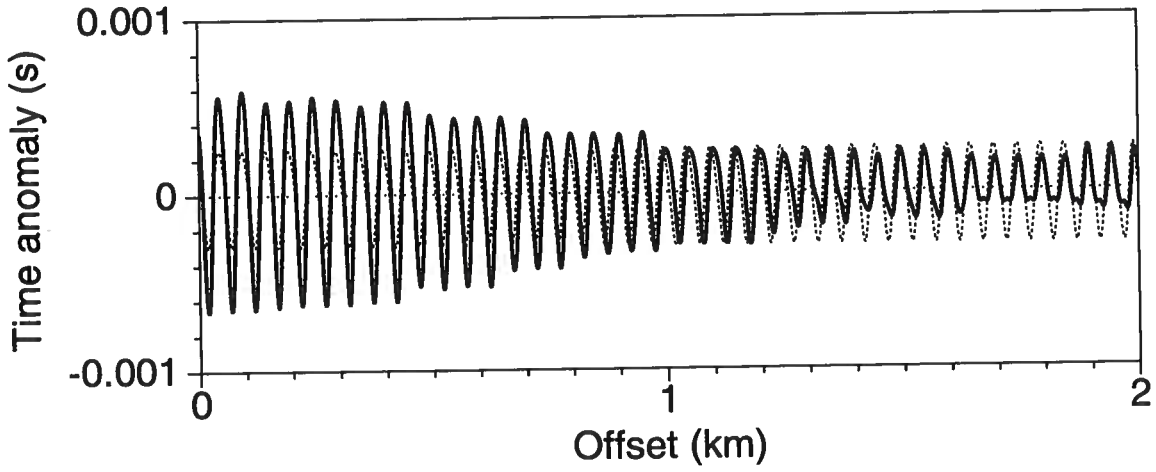

FIG. 4.6. Dashed curve: assumed shape of the surface-consistent receiver statics, for the spreadlength $X_{max} = 2.0$ km in the 50/25/2.5 model. Solid curve: the wave-theoretical time-distortions, slightly modified from those in Figure 3.10, as described in the text. Half the peak-to-trough height of the dashed-curve is equivalent to the rms average of the magnitude of the time-distortions between the offsets 0 and 2.0 km, whose estimation is also described in the text. The repetition with offset of the somewhat sinusoidal pattern is the desired behavior for surface-consistency in the sinusoidal near-surface model.

The solid curve in Figure 4.6 was obtained by subtracting the mean value (i.e., the DC component) and a long-wavelength trend (drift with wavelength larger than 1.0 km) from the time-distortions estimated for the 50/25/2.5 experiment, the solid

curve shown in Figure 3.10. Time-distortions modified in this way are the input data for the estimation of errors associated with the departure from surface-consistency for this particular experiment, and for all other experiments presented below. In the case of Figure 4.6 the difference between the original and modified quantities is approximately a constant time-shift; the preconditioning procedure does not modify the short-wavelength components, which are of most interest here.

The subtraction of these long-wavelength components is convenient for isolating the shorter-wavelength contributions to the time-distortions associated with the sinusoidal variations in the near-surface, which are of the greatest interest in this study. Besides, this operation removes the (long-wavelength) drift in the mean value of the time-distortions which, as discussed in Section 4.1.3, is a signature of variations in the shot-associated contribution. Removing this contribution preconditions the data in such a way that they better comply with the assumption of independence between the receiver- and shot-associated contributions to the time-distortions. As a further justification, the subtraction of the long-wavelength components parallels to some extent what is done in practice by performing NMO-correction prior to the estimation of residual-static corrections.

The reference dashed-line curve in Figure 4.6 exhibits the repetition with offset of the somewhat sinusoidal pattern that we have associated earlier with surface-consistency in the sinusoidal near-surface model. The magnitude of the sinusoid (i.e., half its peak-to-trough amplitude) is made equal to the rms average of the magnitude of the modified time-distortions, computed over the range of offsets from 0 km to $X_{max} = 2.0$ km. The difference between the solid and dashed curves of Figure 4.6, shown in Figure 4.7, represents estimated contributions to errors in the surface-consistency assumption for the 50/25/2.5 experiment and $X_{max} = 2.0$ km.

A similar procedure to that just described was repeated for other experiments whose results are shown later for all values of the spreadlength X_{max} in the range from 0 km to 2.25 km. Let's examine another example of the computations, this time for the 400/25/20 model and a spreadlength of 2.0 km. Figure 4.8 presents the time-distortions along with the estimated surface-consistent reference quantities. Here, the modifications introduced in the time-distortions by the preconditioning procedure are minor, and the separation between the time-distortion and reference curves is small, even for the relatively large spreadlength considered here. Consistent with this observation, the relative magnitude of the contributions to the error shown by the difference curve presented in Figure 4.9 is small; this arises from the small variations with offset present in the time-distortions for this model.

Assigning a magnitude to the overall error A surface-consistent correction applied to data featuring wave-theoretical time-distortions will be imperfect if the time-distortions are not truly surface-consistent. The difference between the modified time-distortions and the surface-consistent statics represents an error incurred due to that imperfection. Predicting the magnitude of the surface-consistent statics as postulated in Section 4.2.1 allows for such differences to be computed for different models and

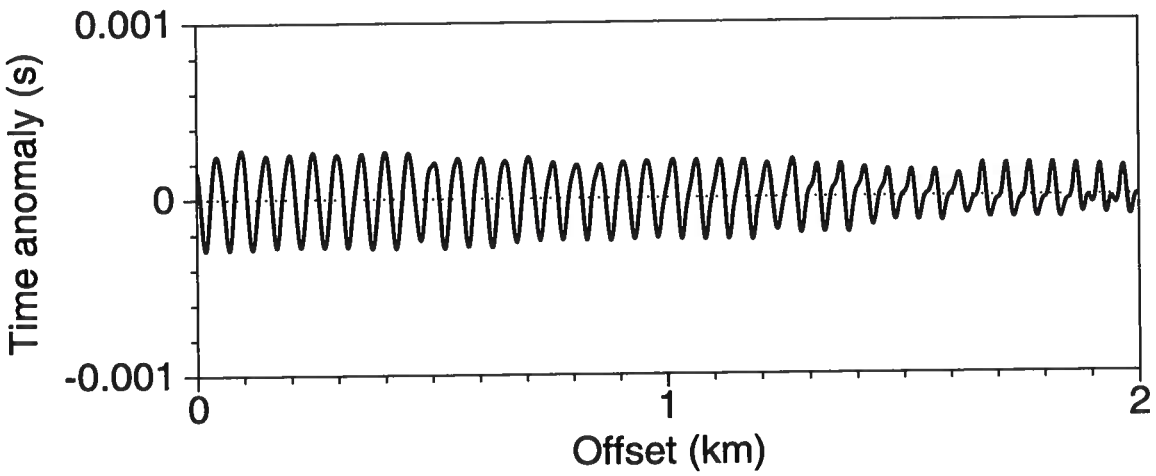

FIG. 4.7. Difference between the modified time-distortions and the estimated surface-consistent reference curve shown in Figure 4.6. The differences here represent contributions to errors in the surface-consistency assumption for the 50/25/2.5 model and a spreadlength of 2.0 km.

a number of values of the spreadlength X_{max}, as exemplified in Figures 4.6 and 4.7 for the 50/25/2.5 model and a spreadlength of 2.0 km, or Figures 4.8 and 4.9 for the 400/25/20 model and a spreadlength also of 2.0 km.

The rms-average of the differences (such as in Figures 4.7 and 4.9) over the length of the spread provides an overall measure of the departure of the time-distortions from those that would be estimated under the assumption of surface-consistency. Repetition of this averaging operation for all possible individual values of X_{max} yields the variation, as a function of spreadlength, in the magnitude of the errors due to the assumption of surface-consistency. Figure 4.10 presents the result of such a computation, in this case contrasting the results for the 400/25/20 and 50/25/2.5 models.

In Figure 4.10, the values for the error in the surface-consistency assumption computed by the averaging procedure just described are presented as a fraction of the magnitude (i.e., half of the peak-to-trough amplitude) of the time-distortions near zero-offset. I call these errors "relative rms errors." For example, the error values for the curve corresponding to the 50/25/2.5-model in Figure 4.10 are rms errors normalized by the magnitude, near zero-offset, of the time-distortions shown in solid line in Figure 3.10. The spreadlength values along the abscissa have been normalized by the depth Z of the deep interface whose reflection contains the time-distortions.

The results in Figure 4.10 indicate that the errors incurred if correcting for wave-theoretic time-distortions with surface-consistent statics are considerably larger for the 50/25/2.5-model experiment than those for the 400/25/20 model. Examination of the time-distortion curves in Figures 3.10 and 3.9 reveals a larger variation with offset in the magnitude and phase of the time-distortions in the former, compared

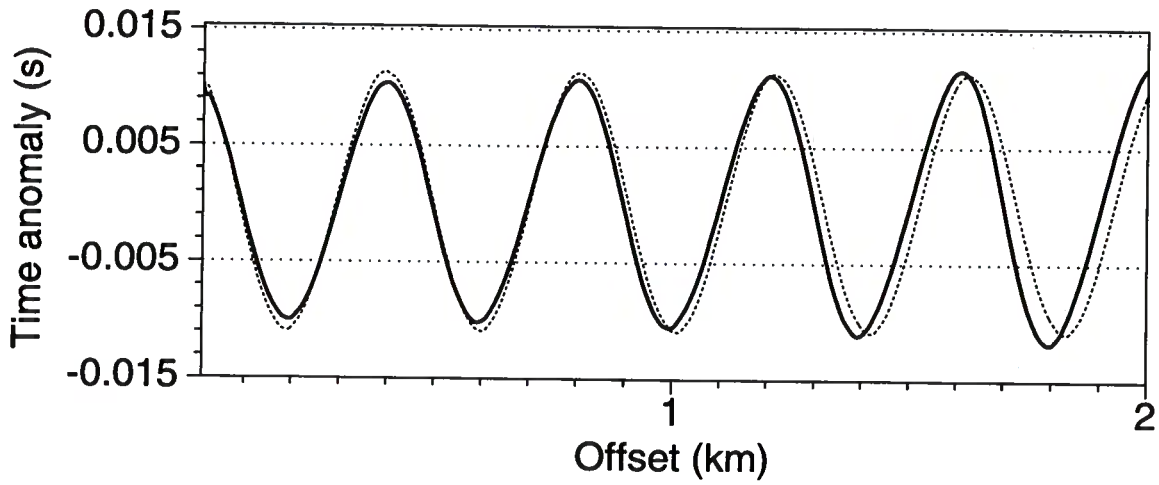

FIG. 4.8. Same as Figure 4.6 except that here the anomaly is for the 400/25/20 model.

with a mild variation in the latter case. Thus, computations such as those presented in Figure 4.10 summarize information on the magnitude of the errors associated with the surface-consistency assumption.

4.2.3 Relationship between the extent of departure and the near-surface parameters

I computed error-estimation curves such as those in Figure 4.10 for a number of experiments involving variation in the near-surface parameters. The results of those computations are presented in this section in Figures 4.11 through 4.15; a discussion on those results is the subject of next section.

Figure 4.11 presents the results for models with differing wavelength of the sinusoidal base-of-weathering interface D. Note that even the largest value of D considered here ($D = 400$ m) is still short-wavelength in the sense of Wiggins et al. (1976), in that D is small compared to the spreadlength X_{max}, assuming that, as is usual in common practice, the spreadlength is chosen of a magnitude comparable to the depth of the reflector of interest (i.e., $X_{max} \approx 1000$ m or $D/X_{max} \approx 0.4$, which is relatively small). On the other hand, the smallest $D = 50$ m would be sampled at Nyquist wavenumber by a (quite common) 25-m receiver group interval. The magnitude of the errors for the larger values of D ($D = 400$ m and $D = 200$ m) is relatively small, increasing notably as D is reduced to 100 m, mainly for relatively large spreadlength values, which are probably not common in practice (i.e., those with $X_{max}/Z > 1.0$). The errors are largest when D is further reduced to 50 m, reaching relatively large values even in the $X_{max}/Z < 1.0$ range.

Normalization of the errors relative to the magnitude of the time-distortions, as in Figures 4.10 and 4.11, gives information on how large are those errors compared

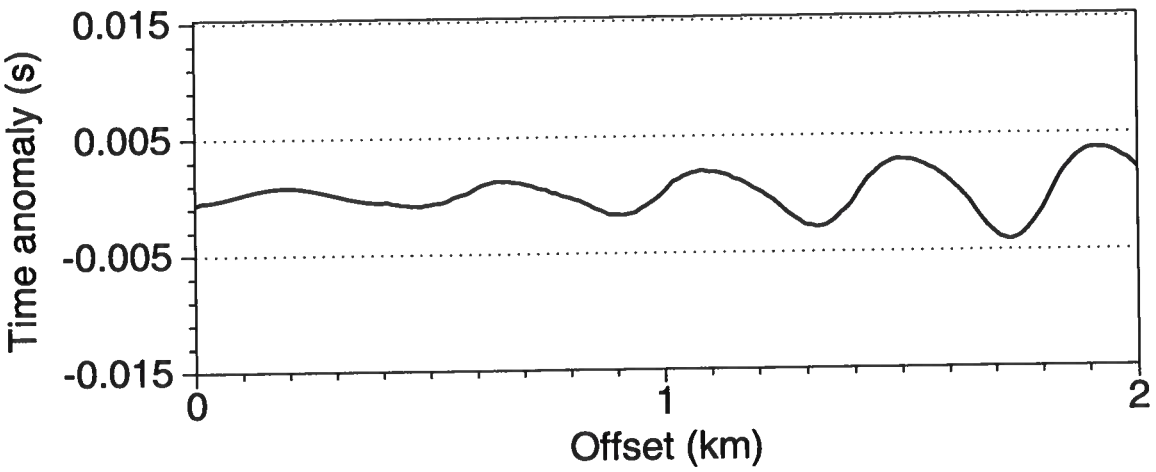

FIG. 4.9. The difference between the modified time-distortions and the estimated surface-consistent reference quantities in Figure 4.8. The differences here represent contributions to errors in the surface-consistency assumption for the 400/25/20 model and a spreadlength of 2.0 km.

to the size of the time-distortions present in the data, thus indicating to what extent a surface-consistent static correction fails to cure the problem of the time-distortions. For example, the curve for $D = 100$ m in Figure 4.11 shows a relative error of around 0.2 for $X_{max}/Z = 1.0$ (again, spreadlengths such that $X_{max}/Z > 1.0$ are not so often found in practice); this indicates that 20% of the time-distortion problem is not solved by a surface-consistent static correction, or equivalently, that 80% of the problem has been solved. Quite likely such an incurred error is considered small in most cases, so we can say that the quality of the surface-consistency assumption for such models is pretty good. The situation is much better for larger values of D (e.g., $D = 400$ m and $D = 200$ m), but for $D = 50$ m the relative error is large, close to 50%. This means surface-consistency solves only half the time-distortion problem in that case. As observed in the discussion concerning Figure 4.10, larger variation with offset in the magnitude and phase of the time-distortions occurs for smaller D, thus giving rise to a large departure from the laterally invariant behavior we associate with surface-consistency, and yielding large error values such as those for $D = 50$ m in Figure 4.11. The variations in the magnitude of the distortions are due to wavefront healing while those in the phase of the distortions are related to changes in the departure from vertical of the raypaths within the weathering layer.

Since, due to wavefront healing, the magnitude of the time-distortions is relatively small for the smaller values of D, the above interpretation of the error results in Figure 4.11 might be pessimistic; i.e., the error for $D = 50$ m in Figure 4.11 is large relative to a quantity that is relatively small (i.e., the time-distortion problem is relatively small). For small D, it may be appropriate to consider a normalization of the errors relative to the magnitude (i.e., half the peak-to-trough amplitude) of the

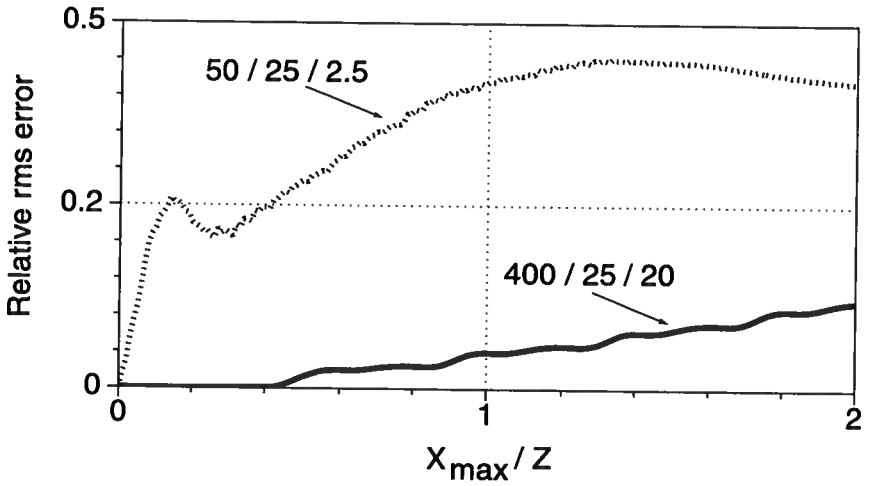

FIG. 4.10. A measure of the errors incurred by using the surface-consistency assumption to estimate corrections for the wave-theoretical time-distortions, for the models 400/25/20 and 50/25/2.5. For a range of values of the spreadlength X_{max}, the error has been computed as the rms-average of differences such as those illustrated in Figures 4.7 and 4.9. The time-distortion values have been normalized by half the peak-to-trough amplitude of the time-distortion near zero-offset.

statics computed assuming vertical-ray propagation through the near-surface velocity model, rather than a normalization relative to the magnitude of the time-distortions.

Such a normalization has been done in Figure 4.12, for the models presented in Figure 4.11 (note that in Figure 4.12 and similar figures presented below, I have labeled the errors normalized in this way as "static-normalized rms errors"). For example, the error values for the curve corresponding to the 50/25/2.5-model in Figure 4.12 have been normalized by half the peak-to-trough amplitude of the *vertical* statics shown in dotted line in Figure 3.10.

Since the time-distortions near zero-offset and the statics are of similar magnitude for the larger values of D, the corresponding curves (i.e., those for $D = 100$ m and larger) are similar in Figures 4.12 and 4.11. The situation is different, however, for the curve for $D = 50$ m, since in that case the magnitude of the statics is much larger than that of the time-distortions, because of wavefront healing. As a result, the relative errors for $D = 50$ m portrayed in Figure 4.12 are much reduced relative to those in Figure 4.11 and are generally smaller than those for $D = 100$ m. This contrasts with the situation for the relative errors shown in Figure 4.11, which are largest for $D = 50$ m.

For situations in which wavefront-healing causes a reduction in the magnitude of the time-distortions, normalization of the errors relative to the statics indicates how large are those errors compared to what, hypothetically, would be the size of the time-distortion problem in the absence of wave-theoretical wavefront healing. Because

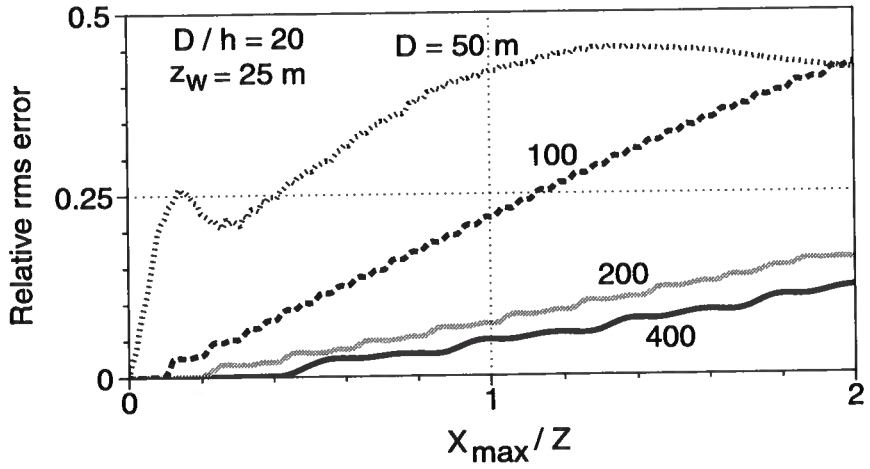

FIG. 4.11. Estimates of the relative error in the surface-consistency assumption as a function of spreadlength for experiments with values of D ranging from 400 m to 50 m, keeping $D/h = 20$ and $z_w = 25$ m. As in Figure 4.10, the values of the spreadlength X_{max} have been normalized by the depth Z of the deep interface, and the time-anomaly values have been normalized by half the peak-to-trough amplitude of the time-distortions near zero-offset.

of wavefront-healing, even if the size of the rms errors relative to the magnitude of the time-distortions is large, the time-distortions, and hence the errors, are small relative to the vertical statics. They are also small relative to the time-distortions (and the errors) that occur for larger values of D. For our purposes of quantifying the severity of shortcomings in the surface-consistency assumption, this implies that we are interpreting as large, errors that in some other sense might be regarded as less severe. For the example at hand, that of the model for $D = 50$ m in Figures 4.11 and 4.12, the error in the surface-consistency assumption is regarded as large compared to the magnitude of the time-distortions present effectively in the data. At the same time, such an error is relatively less severe when compared to the size of the problem in the absence of wavefront-healing and also compared to the relative size of the problem for other models in which wavefront-healing is of lesser importance.

Figure 4.13 shows the error estimates for models with a relatively small $D = 50$ m, and variations in the thickness-of-weathering z_w from 10 m to 100 m; h has been kept fixed at a value of 5 m. Here, the errors have been normalized relative to the magnitude of the time-distortions near zero-offset. The relative magnitude of the errors increases with increasing z_w for values of X_{max} approximately within $X_{max}/Z < 1.2$; for larger values of X_{max}, the magnitude of the errors reduces somewhat for the larger compared to intermediate values of z_w ($z_w = 100$ m compared to $z_w = 50$ m). The magnitude of the errors is larger in general in Figure 4.13 than in Figure 4.11. Errors of a relative magnitude approaching 1.0, as observed for some of the models in Figure 4.13, mean that static corrections under the assumption of surface-consistency fail completely to

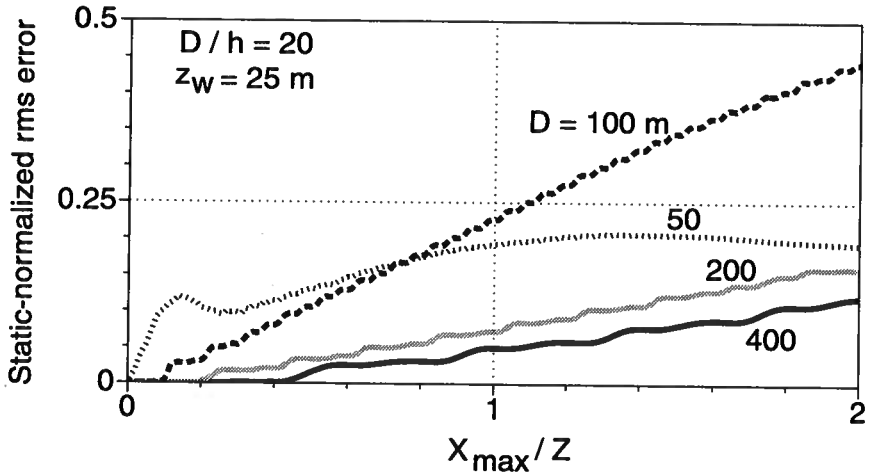

FIG. 4.12. Estimates of the relative error in the surface-consistency assumption as a function of spreadlength for experiments with values of D ranging from 400 m to 50 m, keeping $D/h = 20$ and $z_w = 25$ m. In contrast to Figure 4.11, the time-anomaly values have been normalized here by half the peak-to-trough amplitude of the vertical statics.

solve the problem of time-distortions present in the data.

Figure 4.14 shows the errors for the same models as in Figure 4.13, this time with normalization relative to the magnitude of the corresponding vertical statics. Since wavefront healing is present in the time-distortions in all the models considered here ($D = 50$ m in all cases), the time-distortions are in general smaller than the statics. As a result, the numerical values of the relative errors in Figure 4.14 are smaller in general than those in Figure 4.13.

Note that the relative magnitude of the errors is similar in Figures 4.13 and 4.14 for the model with $z_w = 10$ m, since, as previously discussed, the reduction in size of the time-distortions is small in that case. That reduction is larger for the model with $z_w = 25$ m, so that the relative errors, which are larger for $z_w = 25$ m in Figure 4.13, become smaller than those for $z_w = 10$ m in Figure 4.14. The reduction in the relative magnitude of the error is somewhat larger for $z_w = 100$ m compared to $z_w = 50$ m from Figure 4.13 to Figure 4.14 since, as also observed previously, wavefront healing is stronger for the larger $z_w = 100$ m.

Finally, the results of experiments involving variation in the value of the velocity in the weathering layer V_1 are presented in Figure 4.15, where the error values are normalized relative to the magnitude of the time-distortions. Here, V_1 takes values between 1000 m/s and 3000 m/s, with other parameters set at $D = 100$ m, $z_w = 25$ m, $h = 10$ m and $V_2 = 2000$ m/s. In Figure 4.15, a moderate increase in the velocity in the weathering layer V_1 from 1000 m/s to 1500 m/s leads to an increase in the estimated error. This trend, however, is reversed for a large increase in the magnitude of V_1. Surprisingly, the error for $V_1 = 3000$ m/s decreases relative to that for the smaller

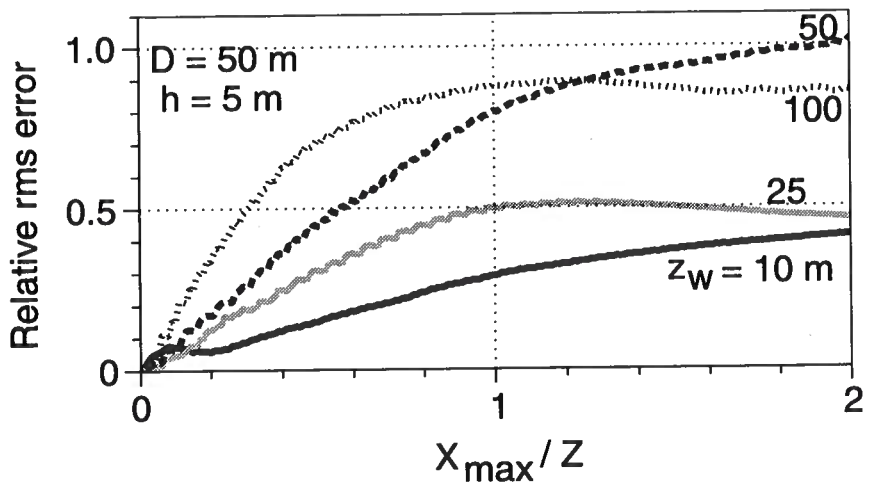

FIG. 4.13. A collection of error curves for experiments with differing values of z_w from 10 m to 100 m, with fixed $D = 50$ m and $h = 5$ m. The errors have been normalized relative to the magnitude of the time-distortions near zero-offset.

$V_1 = 1500$ m/s at about $X_{max}/Z = 0.8$ and beyond, though it is still slightly larger than that for $V_1 = 1000$ m/s.

Again, Figure 4.16 presents the results for the experiments with variation in V_1, this time with normalization relative to the magnitude of the statics. Figures 4.15 and 4.16 are similar in character and in the range of numerical values, since in general the reduction in the time-distortions is small for the models considered here. That reduction, however, is relatively larger for $V_1 = 3000$ m/s giving rise to some reduction in the relative magnitude of the errors from Figure 4.15 to 4.16. A slight reduction also occurs for $V_1 = 1500$ m/s.

4.2.4 Discussion

With only a few exceptions, the general trend in the results obtained in this section is for the magnitude of the errors to increase as X_{max} increases; consistent with experience, the quality of the surface-consistency assumption deteriorates with increasing spreadlength.

The range of variations considered for the ratio X_{max}/Z in Figures 4.11 through 4.16 is somewhat wide. For common data-acquisition practice it is probably more typical to have X_{max}/Z no larger than around 1.0. For $X_{max}/Z \leq 1.0$ notice that, for the larger values of D (e.g, $D = 400$ m and $D = 200$ m) in Figure 4.11, for which wave-theoretic wavefront healing does not reduce the magnitude of the time-distortions (for common frequencies), the relative error is not larger than around 0.15. For such models, we can say that shortcomings in the surface-consistency assumption introduce errors of a magnitude no larger than about 15% of the magnitude of the time distortions present in the data. In other words, the reduction in the time-distortion

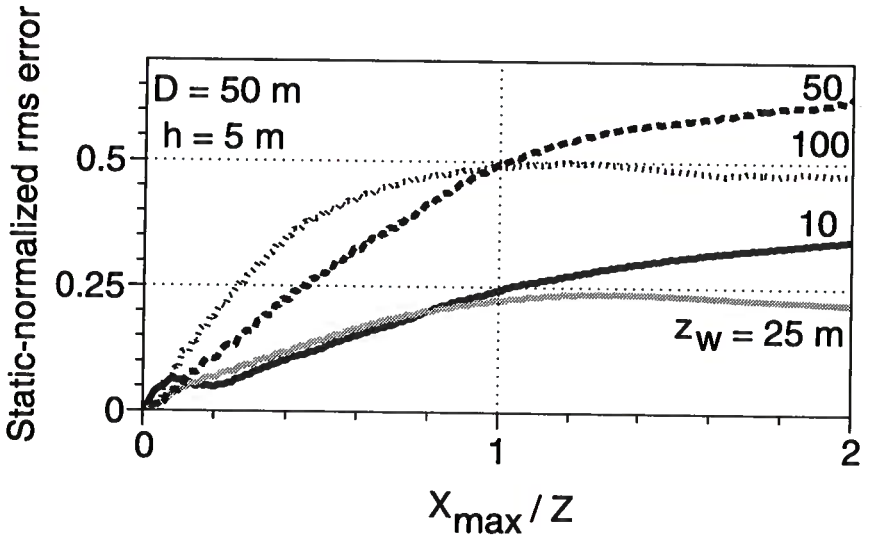

FIG. 4.14. Error curves for the same models as in Figure 4.13, but with normalization relative to the magnitude of the corresponding vertical statics.

problem is about seven-fold when residual statics are estimated under the assumption of surface-consistency. The quality of the surface-consistency assumption in those models is pretty good.

On the other hand, for some other models the magnitude of the errors is large, even in the $X_{max}/Z \leq 1$ range, as observed in Figure 4.13 in which values of the relative error as large as around 0.9 are observed for the larger values of z_w. Such a value for the relative error means that the imperfections of a surface-consistent static correction are about as large as the time-distortions themselves. That is, the time-distortion problem *is not corrected under the assumption of surface-consistency.* Fortunately, wavefront healing reduces the magnitude of the time-distortion problem itself when z_w is large. That is, although static correction is poor for cases of thick weathering, the need for static correction is also reduced where the weathering is thick. Figure 4.14 nevertheless gives the largest errors relative to the vertical static for the larger values of z_w.

To understand the reasons for the increase in the magnitude of the errors for the larger values of z_w, it is convenient to examine the corresponding time-distortions. Figure 4.17 presents the time-distortions for the 50/100/5 model, corresponding to the curve for $z_w = 100$ m in Figure 4.13; the time-distortions for the 50/50/5 model, corresponding to $z_w = 50$ m in Figure 4.13, are those previously presented in Figure 3.17.

The variations in the peak-to-trough size of the time-distortion curves in Figures 3.17 and 4.17 do not seem to be large compared to some others we have observed and for which the estimated errors are relatively small. Observe, however, that in both curves the phase of the time-distortions changes notably with offset. The polar-

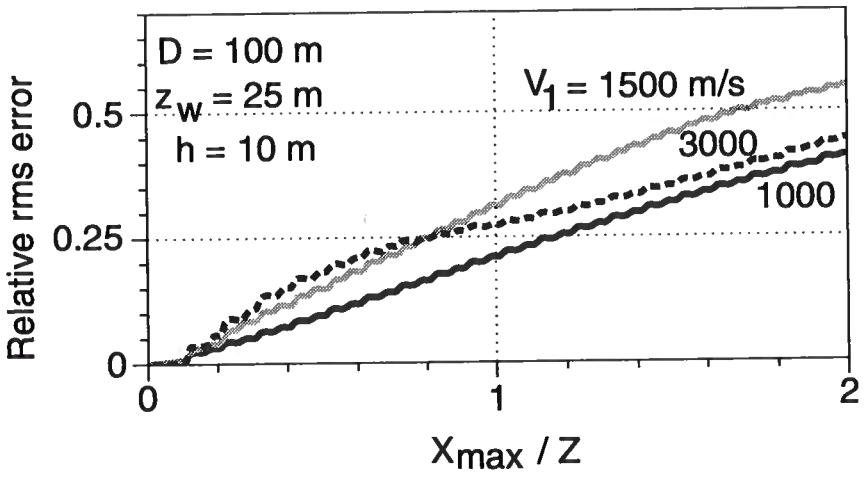

FIG. 4.15. Errors associated with the surface-consistency assumption for models with differing velocity in the weathering layer V_1. The subweathering velocity $V_2 = 2000$ m/s in all cases. The error values are normalized relative to the magnitude of the time-distortions near zero-offset.

ity is opposite that of the vertical statics near zero-offset while for the longer offsets the phases match pretty well. The variations in the phase of the time-distortions are essentially a ray-theoretical phenomena. Because of Snell's law, raypaths in the near-surface not only depart from vertical, but also change from one offset to another; i.e., the amount of departure from the vertical changes with offset. The variation is determined by factors such as the thickness of the weathering z_w, the velocity contrast V_1/V_2 and the shape of the base-of-weathering. For example, one should expect more rapid variation in the phase of the distortions with offset as z_w increases because of the increased length of the slant raypath. That is the reason for the larger variations observed in the phase of the time-distortions in Figure 4.17 (for which $z_w = 100$ m) compared to that in Figure 3.17, in which z_w is a smaller 50 m.

Consistent with the postulated repetitive character (with offset) for surface-consistent statics in the sinusoidal model, the phase and magnitude of the reference curve used in the estimation of the error in surface-consistency are invariant with offset. Thus, variations with offset in the phase or magnitude of the time-distortions represent a departure from surface-consistency that contributes to the estimated error. Significant variations in the phase of the time-distortions are responsible for the large errors for the larger-z_w values ($z_w = 50$ m and $z_w = 100$ m) in Figures 4.13 and 4.14. Those variations are large for the shorter offsets in Figure 4.17 giving rise to a rapid increase in the magnitude of the error in the small-X_{max} range in Figures 4.13 and 4.14. It can be shown from simple geometrical considerations, involving ray bending in the near-surface due to Snell's law, that not only the variations in the phase of the time-distortions increase as the thickness of the weathering increases, but also that, for any thickness of weathering, the largest rate of increase occurs for the shorter offsets

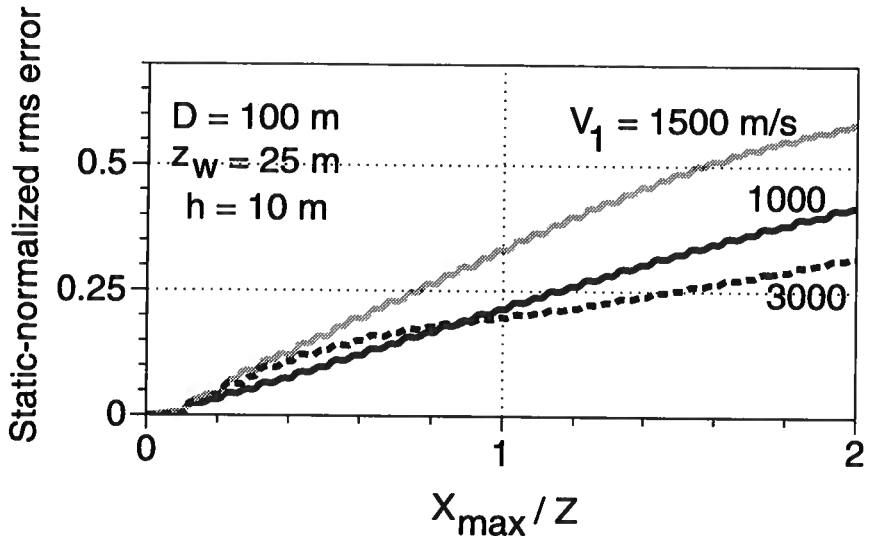

FIG. 4.16. Errors associated with the surface-consistency assumption for models with differing velocity in the weathering layer V_1. The subweathering velocity $V_2 = 2000$ m/s in all cases. The error values are normalized relative to the magnitude of the vertical statics.

(e.g., as observed in Figure 4.17 most of the increase in those variations occurs for the short offsets). For the longer offsets in Figure 4.17, the variations in the phase of the time-distortions are small, giving rise to small change in the computed error in the large-X_{max} range. The variations with offset in the phase of the time-distortions in Figure 3.17 are less rapid but more steady compared to those for the time distortions in Figure 4.17. That's why the curve for $z_w = 50$ m in Figures 4.13 and 4.14 grows continuously with increasing X_{max}/Z as opposed to that for $z_w = 100$ m, which reaches a fairly stable level as the variations in the phase of the time-distortions are small.

Thus, the slant-path character of wave propagation in the weathering influences the character of the time-distortions for both long- and short-wavelength anomalies. For larger D, the influence is mostly on a moderate increase of the magnitude of the distortions, with increasing offset. For smaller D, the major influence is in the increase in variations in the phase of the distortions with increasing thickness of the weathering; as that thickness increases, most of the change in the phase of the distortions occurs for the short offsets.

For the smaller values of z_w, for which the reduction in the magnitude of the distortions is considerably less severe, the relative rms errors are small since the variation in the magnitude of the time-distortions with offset is also small (see for example Figure 3.14) and the phase error associated with departure of slant paths from vertical in the weathering layer is relatively small for thinner weathering layer. Figure 4.13 shows a relative error of about 0.3 for $X_{max}/Z = 1$; this is about half to one third of

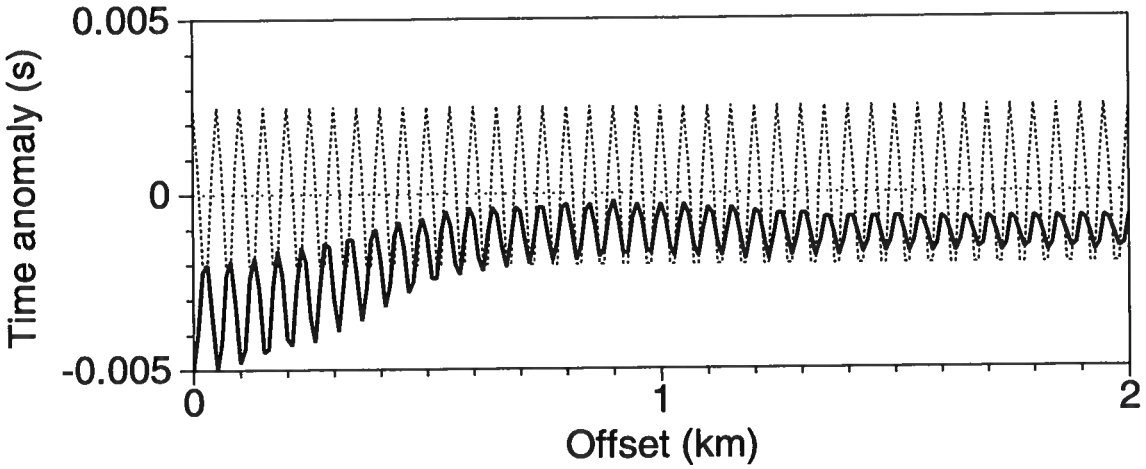

FIG. 4.17. Time-distortions estimated for the data from the 50/100/5 model.

the error for the larger values of z_w, as just discussed. Perhaps this is an acceptable value for the error, in terms of compliance with the surface-consistency assumption. A value of 0.3 for the error can be interpreted as a three-fold improvement in the solution of the problem of time-distortions, or equivalently, a reduction in 70% of the magnitude of that problem.

So, for the smaller values of the wavelength of the near-surface sinusoidal anomaly D, the variation with offset of the time-distortions conforms pretty well to the assumption of surface consistency for the thin-weathering case even though the mollifying action of wavefront healing is limited. For large z_w, the departure from surface consistency is large, corresponding to large variations with offset in the magnitude and, notably, the phase of the time-distortions; the variations in the phase are due to departure from vertical raypaths in the weathering layer.

Regarding the ratio of the velocity of the weathering layer to that in the subweathering (V_1/V_2), the conventional wisdom is that we should expect more severe shortcoming in the assumption of surface-consistency as the velocity of the weathering-layer increases relative to that in the subweathering. Expectedly, the higher the ratio V_1/V_2, the larger the increase in the magnitude of the time-distortions with increasing offset, due to increased departure from the vertical of the raypaths in the weathering. A larger error in the surface-consistency assumption would result from time-distortions whose magnitude further increases as V_1/V_2 increases.

We certainly observe an increase in the magnitude of the errors in Figures 4.15 and 4.16 for $V_1 = 1500$ m/s relative to those for $V_1 = 1000$ m/s. However, the magnitude of the errors decreases when V_1 is further increased to 3000 m/s, relative to those for $V_1 = 1500$ m/s, in the region $X_{max}/Z > 0.8$ in Figure 4.15. That reduction is even larger in Figure 4.16 in which the relative errors for $V_1 = 3000$ m/s are smallest in the same region $X_{max}/Z > 0.8$. As previously mentioned, the greater reduction in

the relative errors for $V_1 = 3000$ m/s compared to that for the smaller values of V_1 evidences a larger wavefront-healing-associated reduction in the magnitude of the time-distortions for that larger value of V_1, which can be attributed to the larger seismic wavelength in the higher-velocity weathering layer.

As observed in Figure 4.18, the behavior of the time-distortions is quite opposite to that expected. We do not see there an increase in the magnitude of the distortions with increasing offsets, but rather a (mild) reduction in the size of the time-distortions on the longer offsets, while on the short offsets the time-distortions match the statics pretty well. This behavior of the time-distortions is rather indicative of the occurrence of wavefront-healing.

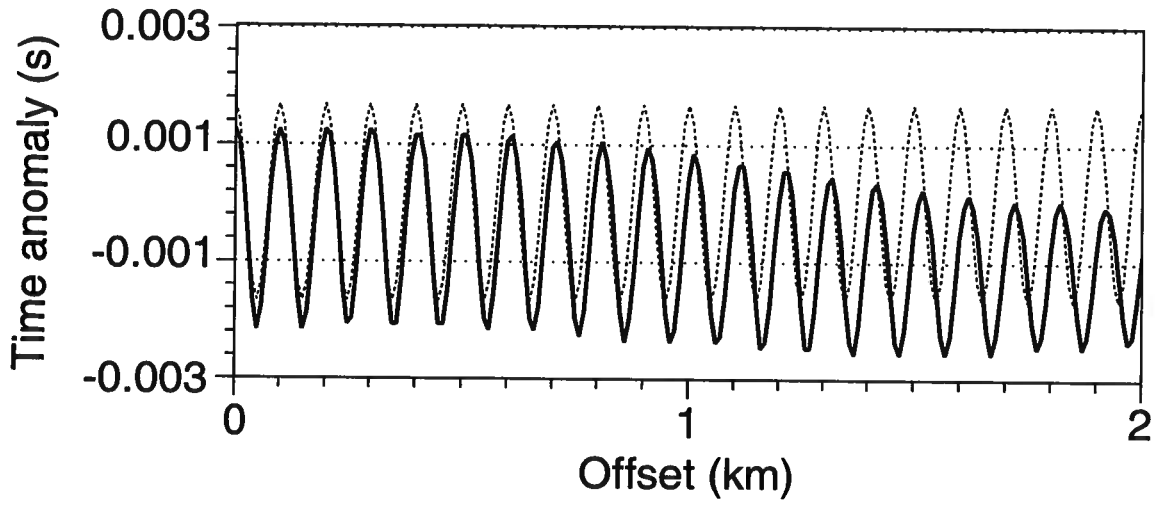

FIG. 4.18. Time-distortions for the data from the 100/25/10 model, for a velocity in the weathering layer $V_1 = 1500$ m/s. Here and in Figure 4.19 the raw time-distortions are shown; i.e., the preconditioning procedure described in Section 4.2.2 has not been applied.

Note that as the velocity increases there is an increase in the magnitude of the seismic wavelength λ_1 and, most importantly, of the width of the contributing zone F. This means that wave-theoretical factors (e.g., wavefront healing) become increasingly important as V_1 increases, and it is those, and not the ray-theoretical departure from the vertical, that give rise to the variations of the time-distortions in Figure 4.18 and to the errors seen for $V_1 = 1500$ m/s in Figures 4.15 and 4.16.

As V_1 is further increased to 3000 m/s (i.e., higher than the subweathering velocity), the increased ray bending remains a factor influencing the character of the time-distortions, as evidenced by the growth in the size of the distortions in Figure 4.19 with increasing offset. This, however, is balanced by an overall reduction in size, relative to the vertical statics (i.e., even though the size of the distortions increases with offset, for all offsets the distortions are smaller than the vertical statics)

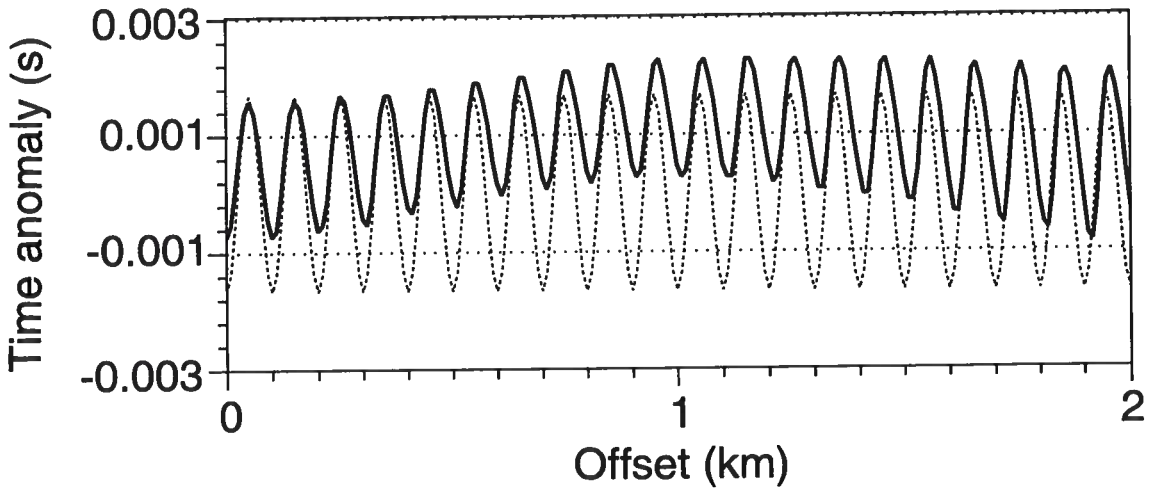

FIG. 4.19. Time-distortions for the data from the 100/25/10 model, and a velocity in the weathering layer $V_1 = 3000$ m/s. Note the long-wavelength drift in the mean value of the distortions, as well as the increase in the magnitude of the distortions, with increasing offset.

due to increased wavefront healing, which becomes increasingly important as V_1 and thus λ_1 increases.

The balance between ray bending and wavefront healing gives an overall mild increase in the size of the distortions with increasing offset, resulting in errors in Figure 4.15 that are not as large as might have been anticipated.

Chapter 5

THE INFLUENCE OF VARYING REFLECTOR DIP

So far, the earth models considered in this thesis have contained a deep horizontal interface whose reflection is contaminated with time-distortions induced by propagation through the sinusoidal weathering layer. In this chapter, I explore the implications of dip in the reflector for the character of the time-distortions and the departure from surface-consistency.

For that purpose, the model of Figure 1.1 is modified here to the dipping-reflector model of Figure 5.1. The depth of the dipping reflector in the middle of the model (i.e., under the zero-offset position in Figure 5.1) has been kept at 1000 m; it has been set to 200 m and 1800 m at the left- and right-side boundaries of the model, respectively. Thus, the dip to the reflector is of about 19.6 degrees.

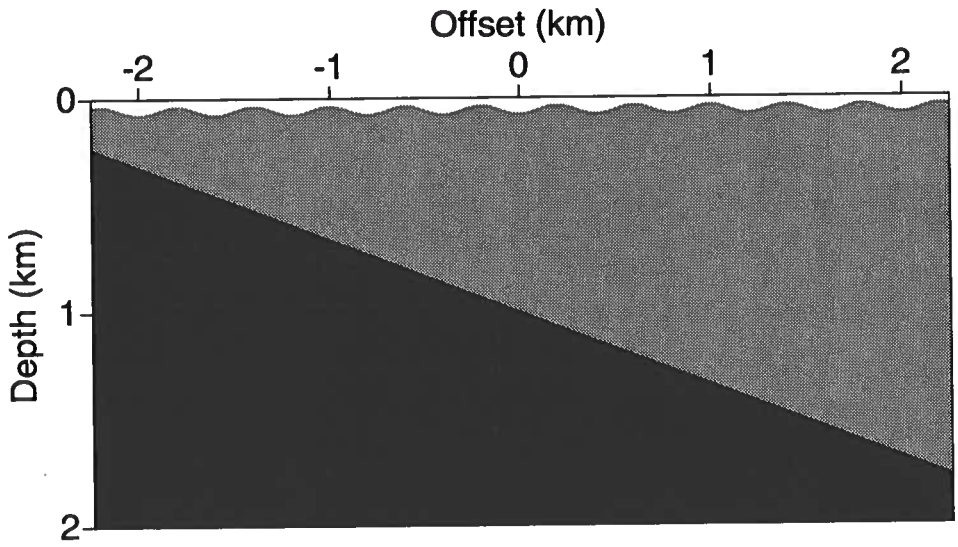

FIG. 5.1. Schematic depth section for a model including a sinusoidal base-of-weathering such as that in the model of Figure 1.1, but modified to consider a dipping reflector.

Figure 5.2 shows a shot record generated for the dipping-reflector model, in this case for the 400/25/20 near-surface. In general, the data for the dipping reflector model are similar to their horizontal-reflector counterpart, with the only major difference in the expected asymmetric shape in the moveout of the deep reflection due to the reflector dip (compare Figure 5.2 and Figure 3.2). Because of the dip in the reflector, for a

given absolute value of source-to-receiver offset the reflection arrival-time is larger in the downdip side than on the updip side of the spread. In order to record the reflection at all offsets on the downdip side, the recording time has been increased here, relative to that for the horizontal-reflector case, to 1.8 s.

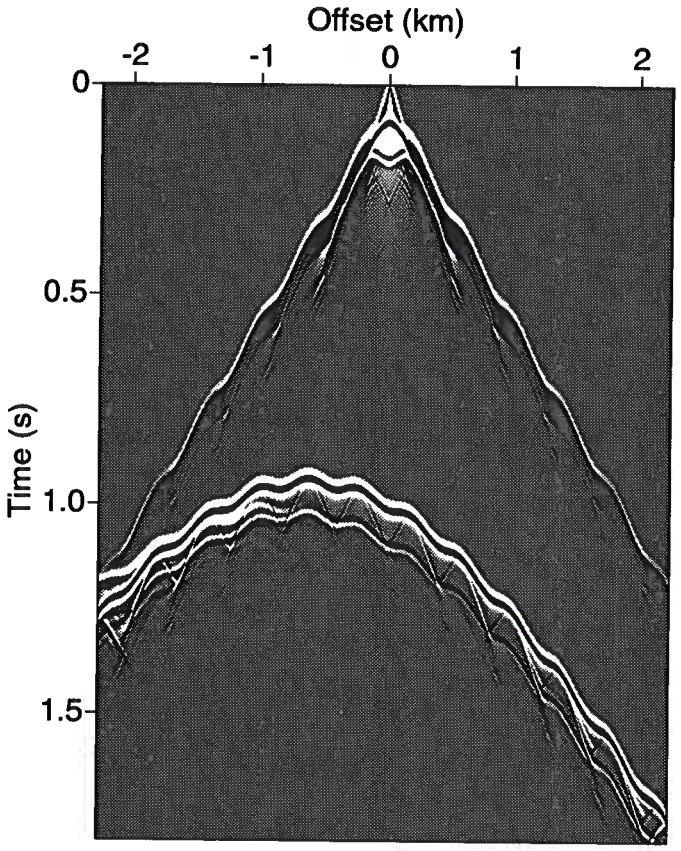

FIG. 5.2. Data generated for the dipping-reflector model with 400/25/20 near-surface parameters. Maximum recording time is 1.8 s.

5.1 Implications for the time-distortions

Time-distortions were estimated for data from the dipping-reflector model, for a number of variations in the near-surface model parameters. Figure 5.3 shows the time-distortions for the data from the 400/25/20 model in Figure 5.2. Notice that since the situation is no longer symmetric with respect to zero-offset, the horizontal scale in Figure 5.3 has been changed relative to that in previous time-distortions plots to include negative and positive offsets. For reference, Figure 5.4 shows the time-distortions for the 400/25/20 horizontal-reflector model including negative and positive offsets, at the same horizontal scale as in Figure 5.3.

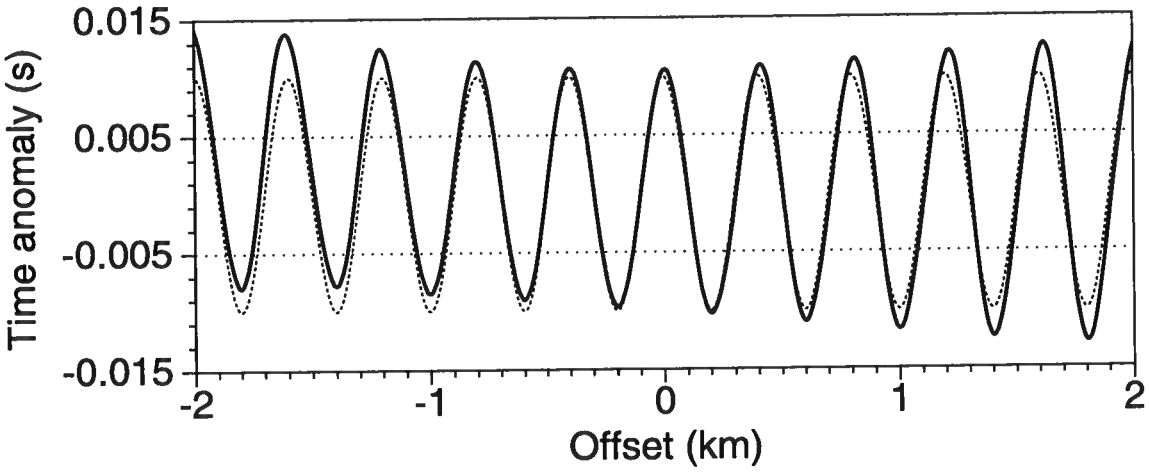

FIG. 5.3. Solid line: time-distortions estimated for data from the dipping-reflector model and 400/25/20 near-surface parameters. Anomalies for positive as well as negative offset are shown since the model is not symmetric with offset; i.e., the horizontal scale has changed with respect to that in similar plots for the horizontal-reflector model. Dashed line: the corresponding surface-consistent statics, computed as vertical traveltimes through the near-surface velocity model.

Comparing Figures 5.3 and 5.4, the size of the time-distortions is larger for the dipping-reflector data on the downdip (i.e., the positive offsets) side of the spread, compared to the size of the distortions for the horizontal reflector. The behavior is the opposite in the updip (negative offsets) side of the spread. This is due simply to the departure from the vertical of the raypaths in the near-surface. Because of the reflector dip, this departure is increased on the downdip side of the spread, while the incidence angle is closer to the vertical on the updip side, compared to the situation for a horizontal reflector. We have already seen that ray-theoretical considerations are dominant for the character of the time-distortions for the larger values of D, as is the case here.

Figure 5.5 shows the time-distortions estimated for the data from the dipping reflector and the 50/25/2.5 near-surface. Again, Figure 5.6 shows the horizontal-reflector counterpart at a comparable scale.

Similar to the horizontal-reflector case, wavefront-healing is seen to be present in the reduction in the amplitude of the time-distortions in Figure 5.5; in this case, a larger reduction in the amplitude of the distortions is observed on the positive offsets compared to the negative side of the spread, with the exception of the larger-magnitude negative offsets (say, from -2.0 km to -1.5 km) where the magnitude of the time-distortions becomes pretty small.

Due to the presence of the dipping reflector, time-distortions are no longer symmetric with respect to zero-offset, as was the case for the horizontal-reflector situation.

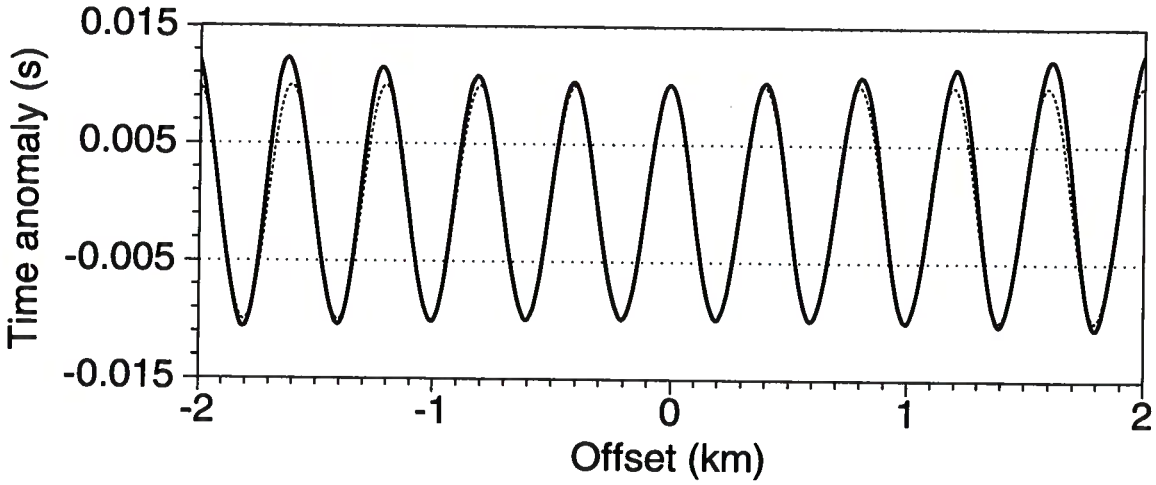

FIG. 5.4. Time-distortions for the data from the 400/25/20 horizontal-reflector model, as in Figure 3.9, presented at the same scale as in Figure 5.3.

Rather, as illustrated by comparison between Figures 5.3 and 5.4 and between Figures 5.5 and 5.6, the pattern is shifted to being somewhat symmetric about offsets at which the paths in the weathering are near vertical (which, for the model in Figure 5.1, are relatively short negative offsets).

5.2 Implications for the departure from surface-consistency

Just as for the horizontal reflector, a measure of the error incurred by the surface-consistency assumption can be obtained from the difference between the time distortions present in the data and those expected under that assumption. Our earlier observations about the nature of surface-consistent statics in the sinusoidal model still hold true; i.e., surface-consistency in the time-distortions is always to be related to a repetition with offset in the near-sinusoidal pattern. Thus, error calculations can be performed again by quantifying the difference between the time-distortions present in the data and the laterally invariant quantities estimated from the time-distortions, as described in Chapter 4.

I performed several such calculations, for experiments involving variation in the model parameters, paralleling what was done in Chapter 4 for a horizontal reflector. Figure 5.7, for example, presents the results for models involving variation in D.

The results in Figure 5.7 are similar to those for the horizontal reflector in Figure 4.11, with the only notable exception of the curves for $D = 50$ m, for which the error is somewhat larger in the dipping-reflector case. Error estimates for the dipping reflector are similar to those for a horizontal reflector in a number of other experiments I performed (whose results are not shown here) paralleling those in Chapter 4. Note that the error calculations for the dipping-reflector case, such as those shown in Figure 5.7, are performed assuming, as is common for land-acquired data, a sym-

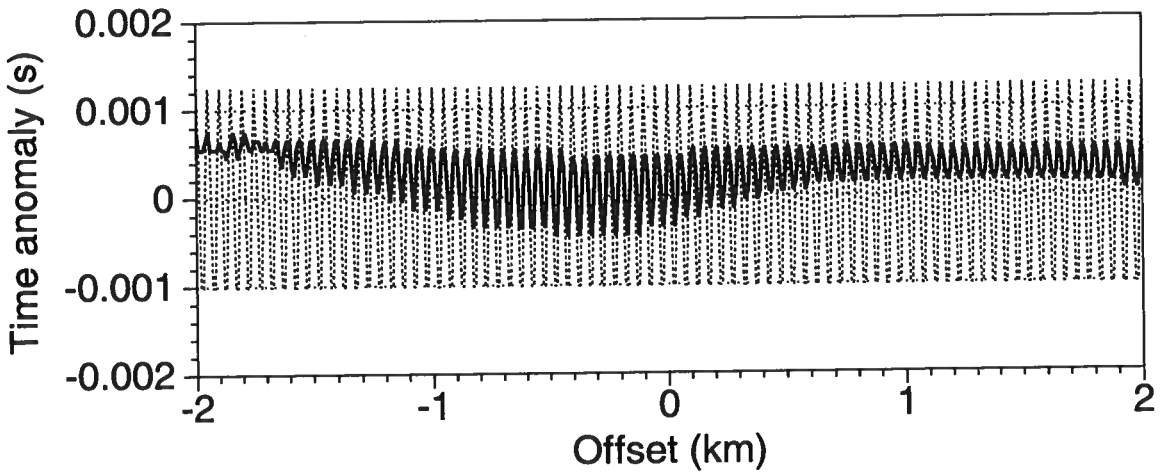

FIG. 5.5. Solid line: time-distortions estimated for data from the dipping-reflector model and the 50/25/2.5 near-surface parameters. Dashed line: corresponding surface-consistent statics.

metric split spread. That is, the computations for a given value of the spreadlength X_{max} include data from all the existing positive and negative offsets (i.e., downdip and updip sides of the spread) in the range from $-X_{max}$ to X_{max}. This is also the case for the horizontal-reflector situation in which there is symmetry with respect to zero-offset.

As mentioned above, the time-distortions for the dipping-reflector data differ from those for a horizontal reflector, and the character of the differences changes from the updip to the downdip side of the spread; in fact, they are pretty much opposite to one another. Specifically, when ray-theoretical factors dominate the character of the distortions, increased departure from the vertical for the raypath in the near-surface occurs for the positive (downdip) offsets. On the contrary, less departure from the vertical is present for the negative (updip) offsets. Moreover, when wave-theoretical aspects dominate, the reduction in magnitude of the time-distortions is more severe on the downdip side, since (for given D and λ_1) the size F of the contributing-zone increases with increase in the incidence angle, relative to the situation for a horizontal reflector. On the updip side, that reduction is smaller since the magnitude of F reduces relative to the horizontal-reflector case.

Since the differences between the time-distortions for the dipping- and horizontal-reflector case are somewhat opposite in character for the negative compared to the positive offsets, the contributions in the error computations approximately balance, explaining the similarity in the results in Figures 5.7 and 4.11. If large relative differences occur arising from the data from one side of the spread, those are compensated by smaller differences on the other side. That would not be the case if only one side of the spread were used in the computations. In fact, I performed a number of error computations for data for the dipping-reflector model, including only information

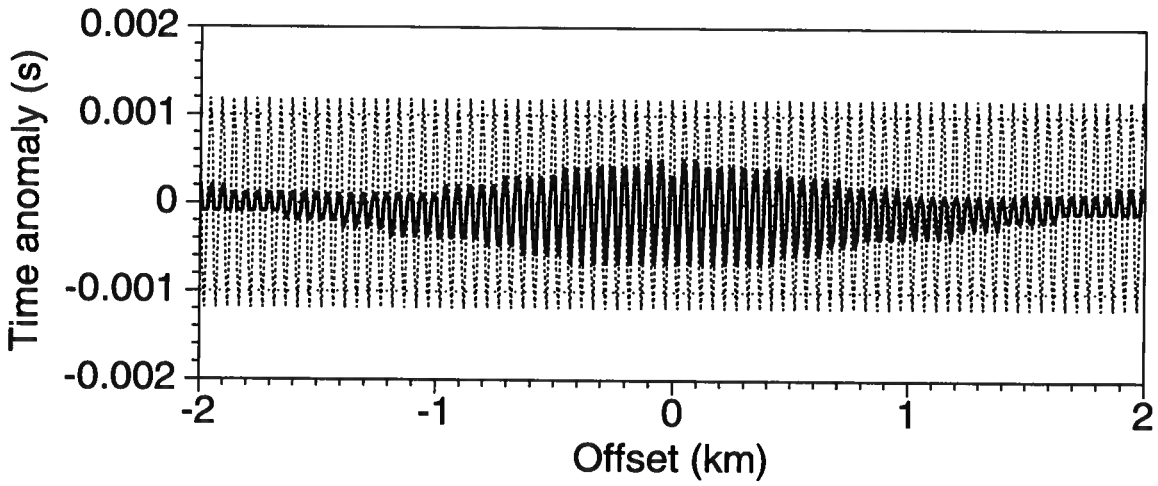

FIG. 5.6. Time-distortions for the data from the 50/25/2.5 horizontal-reflector model, as in Figure 3.10, shown at the same scale as in Figure 5.5.

from one side of the spread (positive or negative offsets), and compared the results with the error computations for the horizontal-reflector case (which, because of the symmetry relative to zero-offset, are the same whether one or both sides of the spread are included).

I observed large differences in some cases, between the one-sided and two-sided computations. For example, because of the increased magnitude of the time-distortions in the downdip side of the spread for the larger values of D, the estimated error is larger when information from only that side of the spread is included. For the smaller values of D, in some cases the variations with offset in the time-distortions are relatively small on the downdip side of the spread (see Figure 5.5, for example) so that the estimated errors are smaller when information from only that side of the spread is included. Computations including only one side of the spread are representative of end-on acquisition, which is not usual in land, but almost universal in marine seismics (where "static" problems are generally less severe).

We might regard the dip of the reflector considered here (about 20 degrees) as being rather moderate, hopefully representative (within the limitations of the simplistic model used throughout this work) of situations likely to be found in practice. Further complications could arise if larger dips are present. It seems reasonable, however, to expect that the balance observed here in the character of the time-distortions for the dipping-reflector, and in the differences with the distortions for a horizontal reflector, will continue to occur, at least for some range of values of the reflector dip.

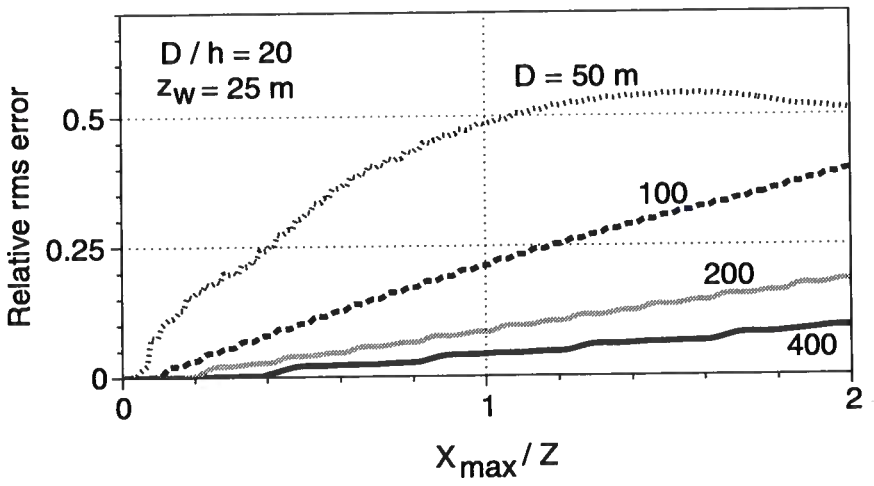

FIG. 5.7. Estimates of the error in the surface-consistency assumption as a function of spreadlength for experiments involving variation in D, in the time-distortions in data for the dipping-reflector model. The error values are relative to the magnitude of the time-distortions near zero-offset. Compare with results for a horizontal reflector in Figure 4.11.

5.3 The error due to the time-invariance assumption

Since the time-distortions are different for the horizontal- and dipping-reflector, similarly the static corrections, which are estimated from those time-distortions present in the data, must depend on reflector dip. This has implications in practice since, under the assumption of surface-consistency, the corrections estimated and applied to the data are time-invariant, not reflector-dependent. Commonly in practice, corrections are estimated from a window in the data encompassing the reflections of interest, so that the corrections are best suited to those reflections. Thus, an error would be incurred in applying those corrections to other reflections, for which they might not be appropriate.

I examined the implications of using corrections suited for a particular reflection to correct for the time-distortions present in a different reflection, for the simplistic models used in this work. Hopefully this would give us some insight as to the magnitude of the errors incurred in practice because of the time-invariant nature of static corrections. Specifically, I quantified the difference between the time-distortions present in data from the dipping-reflector model and the surface-consistent receiver statics expectedly estimated for comparable data (i.e., for a model with the same near-surface parameters as the dipping-reflector model) for the horizontal-reflector case. To quantify the difference I followed the same procedure used in Chapter 4 to estimate the departure from surface consistency as a difference between the time distortions and the reference statics. For the statics corresponding to the time-distortions present in the horizontal-reflector data, I used those previously estimated from the distortions,

also in Chapter 4, as a reference to quantify the departure from surface-consistency.

Figure 5.8 illustrates the details of the computations suggested. The solid-line curve shows the modified time-distortions in data from the dipping-reflector model (for the 400/25/20 near-surface parameters) obtained from those previously shown in Figure 5.3, by correcting for long-wavelength drift as explained in Section 4.2.2. The dashed-line curve shows the estimated surface-consistent statics, computed from the time-distortions for data from the horizontal-reflector model (and the 400/25/20 near-surface parameters as well). Thus, the statics are those already estimated for the horizontal-reflector model, also in Section 4.2.2; i.e., those shown in dashed-line in Figure 4.8. For ease of reference, Figure 4.8 has been repeated here, as Figure 5.9, including negative and positive offsets, at the same scale of Figure 5.8.

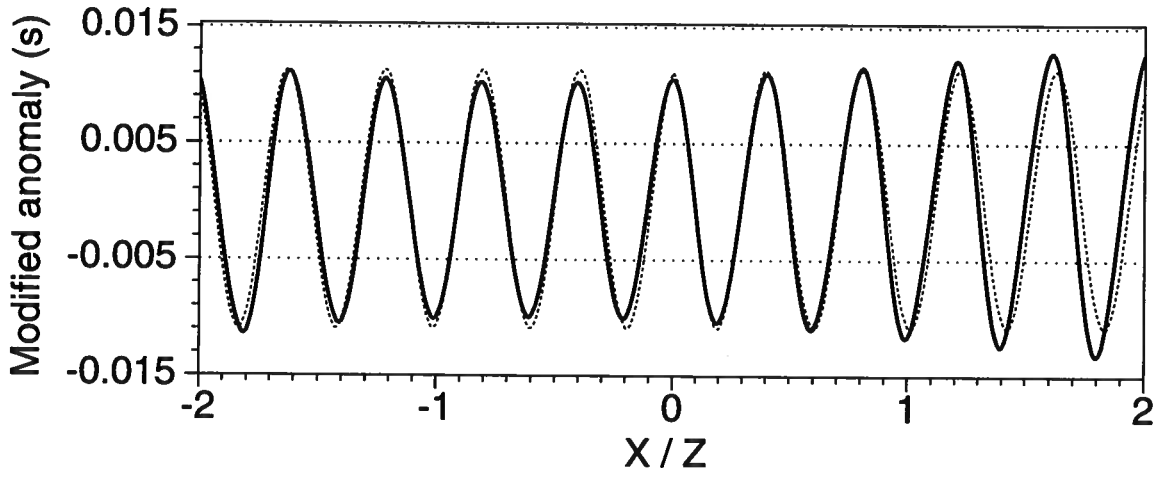

FIG. 5.8. Dashed curve: assumed shape of the surface-consistent receiver statics, for the spreadlength $X_{max} = 2.0$ km in data for the 400/25/20 model and a *horizontal* reflector. These are the quantities shown in dashed line in Figure 4.8, but shown here for both negative and positive offsets. Solid curve: time-distortions in the data for the 400/25/20 model and a reflector dipping at about 20 degrees, modified by removing the long-wavelength drift, as discussed in Chapter 4. The dashed-line quantities related to the horizontal reflector, are symmetric with respect to zero-offset; the solid-line time distortions are not symmetric.

Similar to what was done in Chapter 4, the difference between the modified time-distortions and the statics in Figure 5.8 represents contributions to errors, this time related to the choice of static corrections that are not optimally suited to the data from the reflection of interest. The rms-average of the difference over the length of the spread (including both negative and positive offsets) provides an overall measure of the error for the given value of X_{max}. Repetition of the averaging operation for all the possible values of X_{max} yields the variation, as a function of spreadlength, in the magnitude of the error.

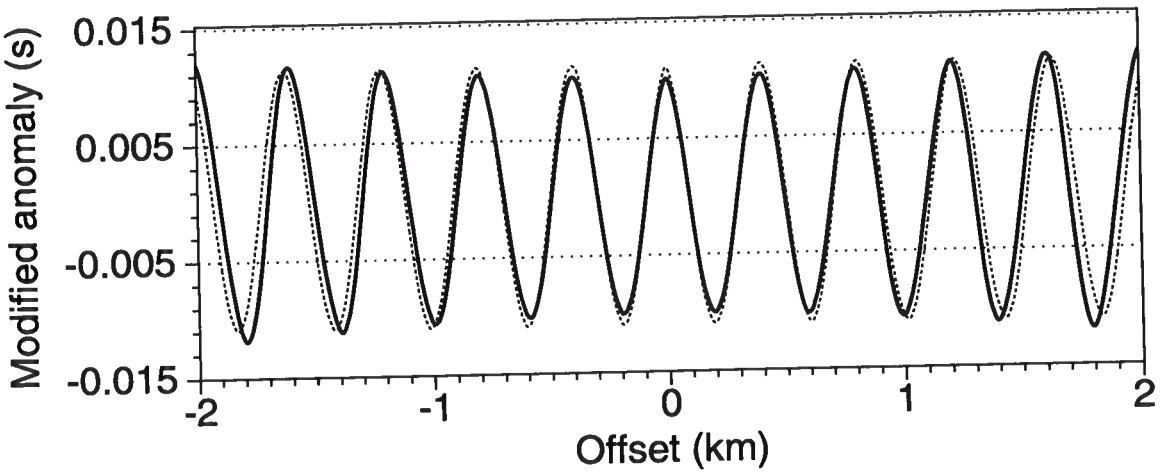

FIG. 5.9. Same as Figure 4.8, but shown here for negative and positive offsets. Solid curve: the modified time-distortions in the data for a horizontal reflector and the 400/25/20 near-surface. Dashed curve: the assumed shape of the surface-consistent receiver statics.

As for previous error-estimation efforts in this thesis, I performed computations such as those just described, for a number of variations in the near-surface parameters. Figure 5.10 shows the results for models involving variation in the value of D. The behavior of the errors in Figure 5.10 is different from that in similar figures discussed previously. In the curve for $D = 50$ m, contrary to most of the curves we have seen so far, the errors decrease with increasing offset, though they are of a relatively large magnitude at all values of X_{max}/Z. Also opposite to the errors related to imperfections in the surface-consistency assumption, the errors in all cases here are non-zero even for small values of the spreadlength (i.e., around $X_{max}/Z = 0$).

As seen in Figure 5.8, the reference curve in the error computation in Figure 5.10 (the "wrong" statics, derived from the time-distortions in the horizontal-reflector data) is shifted in phase relative to the time-distortions; also, the amplitudes of the two curves do not necessarily match near zero-offset. Because of this approximate shift, the time-distortions are somewhat out-of-phase relative to the reference at zero-offset, and the phase difference is more significant as the value of D decreases (i.e., whatever the shift, it will be a relatively larger fraction of a wavelength in the approximately sinusoidal time-distortion curves, as that wavelength is smaller). That is the reason for the large values observed for the errors in Figure 5.10 for the smaller $D = 50$ m. Interestingly, then, for the shortest-wavelength variation in the weathering, it actually *helps* the surface-consistency assumption to use longer spreadlength. Even for larger D, the quality of the surface-consistency assumption does not degrade severely with increasing spreadlength.

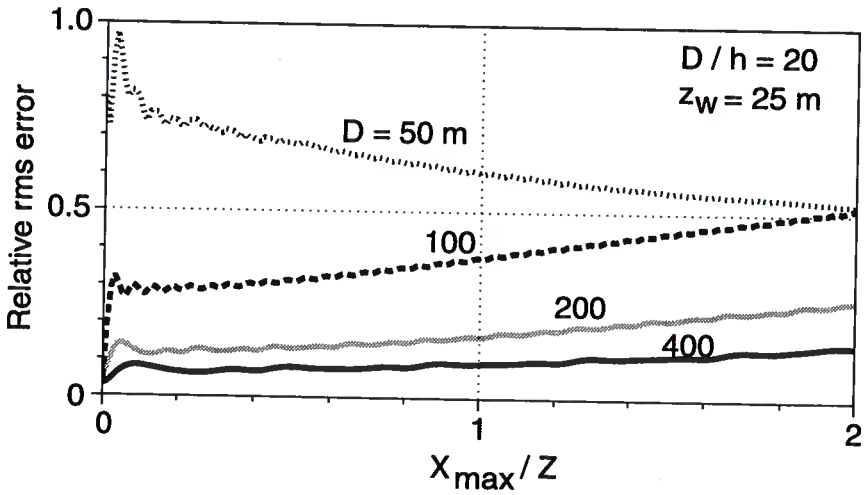

FIG. 5.10. Estimates of the error incurred by correcting for the time-distortions in the data for the dipping-reflector model using surface-consistent static corrections derived from data for the horizontal-reflector model, for experiments involving variation in D.

Chapter 6

CONCLUSIONS

Using measurements of reflection time computed from finite-difference modeling in earth models with a sinusoidal base of weathering, I have studied in this thesis the character of time-distortions in reflections from depth, as well as the departure from those that would be predicted under the assumption of surface-consistency. I have also characterized the dependence of those phenomena on the near-surface parameters. Albeit simple, the subsurface models considered are meant to address the essentials of the problem of residual-statics estimation. As a result, I make predictions of the severity of shortcomings in the surface-consistency assumption in residual-statics estimation as a function of parameters of the subsurface. Next I highlight the results of this work.

6.1 The character of wave-theoretic time-anomalies

We have seen notable variations in the character of the time-distortions for changes in the wavelength of variations in the near-surface and the thickness of the weathering. Wavefront healing, resulting from the fact that a finite portion of the medium contributes to a given seismic arrival, acts to reduce the amplitude of the time-distortions for short-wavelength anomalies, i.e., anomalies of a wavelength comparable to the size of the dominant seismic wavelength, except where the weathering is thin, also compared to the dominant seismic wavelength.

For the larger-wavelength anomalies, again compared to the dominant seismic wavelength, the distortions increase in amplitude with increasing offset due to the departure of the raypaths from the vertical. In all cases, the wavelength of variation of the time-distortions approximates that of the variations in the subsurface model.

6.2 Issues concerning the character of the time anomalies

Even though it constitutes a simplification of a complex phenomenon involving the whole medium, viewing wave-propagation as a spatial process that averages information from a finite region in the medium into a given arrival at the receiver helps in understanding qualitatively the character of the time-distortions and its relation to the medium parameters. The size of that region along the base-of-weathering interface has been estimated using the familiar concept of Fresnel zone. The approximation used is coarse. The effective contributing zone can be smaller than the estimated size due to a relative reduction in the contribution of the outer portions of the zone. This reduction is most notable in near-field conditions, i.e, if the weathering is thin.

Consistent with the picture of a spatial-averaging process, the character of the time-distortions is basically governed by the ratio of the contributing zone to the wavelength of variations in the shape of the base of the weathering. When that ratio is small, i.e., when the variations in the near-surface are of a relatively large wavelength, the mixing takes place along a relatively small zone and is of a lesser importance; in this case, ray-theoretical considerations help explain the observed behavior of the distortions.

Wave-theoretical aspects are of greater influence for short-wavelength anomalies: when the variations in the near-surface are of a small wavelength compared to the size of the contributing zone, the spatial smoothing associated with wave propagation is important in determining the character of the distortions. If the weathering is thin, since the effective size of the contributing zone is relatively small, the ratio of the width of that zone to the wavelength of the near-surface variations can be relatively small even for small values of that wavelength. Thus, wave-theoretical aspects (and hence the associated reduction in the size of the anomalies) are less important, for the character of the time-distortions, in the thin-weathering case. Conversely, the size of the contributing zone increases with increasing depth of the weathering, so that wave-theoretical aspects are increasingly important as the depth of the weathering increases.

The presence of reflector dip adds one more factor to consider. Because of dip, the angle of incidence of reflection arrivals changes relative to that for a horizontal reflector, increasing for the downdip side of the spread, and decreasing on the updip side. Thus, when ray-theoretical aspects dominate the character of the time-distortions, the distortions are larger, because of the increased ray-bending, on the downdip side of the spread, compared to the distortions on the updip side. When wave-theoretical aspects are more important, a larger reduction in the magnitude of the distortions occurs on the downdip side, since the size F of the contributing-zone increases because of the increase in the incidence angle, relative to the situation for a horizontal reflector.

6.3 The quality of the surface-consistency assumption for residual statics

I have found that the assumption works best for relatively long-wavelength anomalies (compared to the size of the contributing zone), in a weathering that is thin compared to the dominant seismic wavelength. In such situations, the error in correcting for the time distortions present in the data with a surface-consistent static correction can reach around 15% of the magnitude of those distortions. Viewed differently, residual statics estimated under the assumption of surface-consistency cure 85% of the time-distortion problem, or improve it by a factor of seven-fold. That is probably good in most cases. For the longer-wavelength anomalies, departure from surface-consistency is mostly associated with the departure of raypaths from the vertical, which gets larger with increasing source-to-receiver offset.

A large departure from surface-consistency, associated with wave-theoretical phenomena, occurs for short-wavelength anomalies when the weathering is thick (the dif-

ference between the time-distortions and reference curve as a result of the departure of slant paths from vertical causes larger phase errors for the shorter-wavelength anomalies). There, the magnitude of the errors in the correction for the time-distortions, due to imperfections in the surface-consistency assumption, can be as large as the magnitude of the time-distortions themselves. That is, the correction with surface-consistent residual statics will be of no benefit at all. However, it is in those cases that the reduction in the size of the distortions attributable to wavefront healing is larger, i.e., the magnitude of the anomalies involved is relatively small. This limits the shortcomings in the quality of the assumption for the thick-weathering situation. Short-wavelength anomalies, on the other hand, conform pretty well to the assumption of surface-consistency when the weathering is thin. The error in the surface-consistent static correction can be around 30%, or a three-fold improvement in the solution to the time-distortion problem, in that case.

These conclusions about the quality of the surface-consistency assumption are drawn for the restricted, but quite usual, range of spreadlengths not larger than the depth of the reflector of interest. The quality of the assumption deteriorates as the spreadlength X_{max} increases.

The results here contrast with those of Wiggins et al. (1976) for the quality of residual-static corrections computed as the solution to a general linear inverse problem, which is founded upon the assumption of surface-consistency. Their conclusions, however, are not necessarily inconsistent with those of this thesis since completely different issues are addressed in each case. They found that the quality of the solution is better for short-wavelength anomalies, or equivalently, for large spreadlength. We have found here a larger departure from surface-consistency for the smaller D (and intermediate to large z_w) and for the larger X_{max}. Remember, however, that even the largest $D = 400$ m considered here is still short-wavelength in the sense of Wiggins et al. (1976), and the shortest $D = 50$ m is very short, since it would be sampled at Nyquist wavenumber by a common 25-m receiver group interval.

Most of the tests conducted in this work, and thereby the results reached, address the vastly common situation of a weathering layer featuring an average velocity smaller than the underlying subweathering. In some situations, reflection-time distortion problems result from a weathering layer whose velocity is anomalously high (e.g., permafrost areas). For the shortest-wavelength anomalies of interest for residual-statics problems, wavefront healing for the relatively longer seismic wavelengths associated with the higher velocities limits the influence of ray-bending, yielding variations in the time-distortions that conform better with the assumption of surface-consistency than may have been previously supposed.

Where the subsurface has reflectors with dip, the departure from surface-consistency in the time-distortions is similar to that for a horizontally-layered subsurface when a symmetric split-spread configuration is used. Such an acquisition geometry is the most common for land seismic surveys, for which near-surface-induced time-distortions typically are of great concern.

When both dipping and horizontal reflectors are present, errors are incurred

when correcting for the time-distortions in the data from the dipping reflector with static corrections derived from the distortions in data for the horizontal reflector. The errors in general are larger — though not severely larger — than those incurred when using the proper corrections derived from the distortions present in the data from the dipping reflector. Moreover, the errors are significant even for small values of the spreadlength X_{max}, as opposed to the situation for errors attributed to failures in the surface-consistency assumption. For the smaller wavelengths of variation in the near-surface, the errors decrease with increasing spreadlength.

6.4 The estimation of time-distortions

Even for the synthetic shot-records used in this work, the estimation of time-distortions is far from being a trivial operation. Several events present in the data act like noise and bias computed estimates of reflection times. A particularly annoying feature associated with the sinusoidal-shape boundary is the presence, in many cases, of diffraction events contaminating the primary reflection arrivals of interest. In some cases constructive interference makes these features so strong that identification of proper arrival times is difficult (see Figures 3.11 and 3.12).

Multiples are another example of events that impair the estimation of time-distortions. Particularly strong multiples occur when a free-surface boundary condition is implemented in the model boundary representing the earth's surface. In many tests, time-distortions just could not be determined in a reliable way when such strong multiples were present: the crosscorrelation-and-picking procedure yielded faulty, hard-to-interpret results.

I overcame those difficulties, at least partially, in some cases by using a narrow crosscorrelation-window encompassing primarily the reflection event of interest, and in others by using a narrow picking-window around the zero-lag of the crosscorrelation. These strategies work reasonably well because of the synthetic, noise-free nature of the data. When dealing with field data, time-distortions are estimated by using relatively long crosscorrelation-windows, encompassing several reflections. This procedure generally makes the estimation more robust by increasing redundancy and signal-to-noise ratio, but it also tends to smear the information from the different reflections into a single global estimate. Nevertheless, field data likely do not suffer from such strong contamination of time-distortions by multiples and diffractions as do the synthetic shot records generated for such simple models as here.

6.5 Issues concerning finite-difference modeling

Even though finite-difference methods provide a much desired full-waveform solution of the wave equation, their implementation is not straightforward, more so when attempting to model wave propagation in the near-surface.

First, finite-difference methods are costly; the wavefield for the whole medium has to be updated recursively, in small steps in space and time. For study of not just

one but many different models involving variations in the near-surface parameters, going beyond generating just a single shot for every individual model would be highly impractical and could not be done in this work. In essence, a wide scope in choices for variations in the near-surface parameters and in honoring wave-theoretical aspects was achieved here at the expense of having no redundancy (i.e., a single shot-record) in the amount of generated synthetic data. Hopefully, for the repetitive sinusoidal symmetry of the models considered this limitation in the amount of available data is not significant.

Even with the fine grid-step size imposed by accuracy requirements on the discretization of the wave equation, the representation of steep, contorted interfaces such as those in the sinusoidal base-of-weathering interface in this study, demands extra care in the discretization of the velocity-depth model. Accurate representation of regions near interfaces was achieved here by a simple procedure involving a weighted averaging of the slownesses in the neighborhood of the interface, as described in Section 3.5.3.

Finally, the choice of a boundary condition for representing the earth's surface boundary of the model proved to be an important matter in this study. The data obtained with a free-surface boundary condition were considered unsatisfactory, containing an unrealistically high level of surface-associated multiples. This is simply one example of our present inability to accurately model wave-propagation in the near-surface, as discussed in next chapter. Also, I showed that specifically for the time-distortions of interest in the study, the primary effect of the choice of a free-surface boundary condition arises through a change of the dominant frequency in the data in the presence of surface-related source- and receiver-ghosts. When this change in frequency is taken into account in data generated with an absorbing-boundary condition, the reflection time-distortions, are basically identical (see Section 3.5.1) to those generated under the free-surface assumption.

Chapter 7

OPEN QUESTIONS AND SUGGESTIONS FOR FUTURE WORK

I refer here to some issues related to the subject of this research that were either not considered or not fully resolved in the work already done. I also give some thoughts on what could be some issues to consider in further work in this subject.

7.1 Realistic modeling of near-surface wave propagation

Attempting to model wave-propagation in the near-surface in a more accurate way was beyond the scope of the work reported in this thesis; moreover, to my knowledge such more-accurate modeling is still a largely unsolved matter. Our knowledge of the near-surface is still quite imperfect, both in the formulation of a proper model of wave propagation and in the definition and estimation of relevant physical properties.

In that respect this work is fairly simplistic, both in the sort of velocity-depth models considered and in the approach and model adopted to simulate wave propagation. As discussed above, the choice of simple near-surface models was dictated by the expectation that general relationships could be established between the results of the modeling studies and a few model parameters. I believe that it has been the case here. As to the model adopted for wave propagation in the near-surface, I used the acoustic wave equation with no wave attenuation as a first approximation, maintaining simplicity while addressing at least some of the wave-theoretical issues concerning the character of near-surface-associated reflection-time distortions.

In some situations, specifically when attempting to include a free-surface condition in the model boundary representing the earth's surface, the modeling scheme implemented here was probably too limited to yield realistic results, e.g., an unrealistically-high level of surface-associated multiples present in the generated data. I performed further tests intended to simulate more realistic conditions in at least a couple of ways, as described in Section 3.5.2.

These tests did not yield more realistic results in terms of the relative strength of multiple energy arising from the presence of a free surface. For the tests including attenuation, I found that the magnitude of the attenuation coefficient Q had to be reduced to unusually low values to obtain synthetic shot records in which the amplitude of multiples was reduced to what might be a realistic level for land data. Similarly, although the test with a transition in velocity at the base of the weathering resulted in weaker multiples, it also led to a reduction in the relative size of the time-distortions, just because of the reduced velocity-contrast.

There is an apparent contradiction here. A mild velocity-contrast between weathering and subweathering might explain the relatively low level of multiples observed

in field data but then how do we account for sizable time-distortions often observed as well? The reason for this apparent contradiction must lie in the already-acknowledged simplistic nature of the models considered. Probably a more realistic representation of the near-surface should reconcile mild vertical variations with stronger lateral variations. Whether this is possible in a plausible way and what would be the results in terms of the character of the generated data are open questions.

Again, by using the acoustic wave equation to model wave propagation in the near-surface I could, as a first approximation, allow for the inclusion in the simulation of time-distortion problems of some of the wave-theoretical aspects of interest for this research. One could think of several ways in which the modeling algorithm can be made more general and sophisticated; a major question still would be whether those implementations are more realistic.

First, a 3D model of wave propagation could be considered. This would imply a major increase in the computational and data-handling magnitude of the problem, but would also provide increasing accuracy in the simulation. Some of the features identified in the 2D results in this work as interfering diffractions or dispersion events might in fact be the "tails" following the main pulse of the events, that are known to develop in 2D wave propagation. The "tail" corresponds to the contributions from portions of the source located outside of the plane, arising because that source is assumed implicitly as an infinitely-long line perpendicular to that plane.

Some other wave-propagation aspects could be more accurately addressed by an elastic model of that propagation. For example, attenuation and partitioning of energy at interfaces into compressional and shear waves could give rise to a reduced level of surface-associated multiples when a free-surface condition is implemented. A better implementation of the free-surface condition itself should result from the possibility of independently setting the proper conditions for stress and displacement values. Some other near-surface-associated phenomena such as ground roll would be generated. I believe that the influence of those phenomena on the main issues related to the time-distortion problem will be of a second order relative to those already taken into account in the simple models considered in this work. For example, attenuation should be important mainly in determining the frequency content in the data; that has been made in a great extent here simply by choosing for the source signature in the finite-difference simulation a wavelet with a frequency content similar to that commonly found in field data. On the other hand, the presence of phenomena such as ground roll or converted P-S reflections will certainly involve additional problems for the measurement of time-distortions.

Moreover, a potentially more realistic modeling scheme for near-surface associated phenomena could result from integrating all the factors mentioned in a single formulation. An attempt at generality magnifies the problem of building a forward-modeling algorithm. The implementation of a finite-difference 3D elastic code is a large computational problem, but is certainly feasible, as is being done in some other research work in this department. If factors like attenuation are considered, development of visco-acoustic or visco-elastic codes not only increases the computational size

of the problem but, most important, is near the edge of current research; including anisotropy or other complications is even beyond that. Also, a more general formulation increases largely the number of parameters required to describe the medium, making it more difficult to characterize the influence of individual parameters on problems of interest.

It is not clear whether or not the implementation of modeling algorithms along the lines just described would result in a more realistic representation of physical properties and wave propagation in the near-surface. One can even wonder whether conventional wave equations, and their extensions including phenomena such as those just discussed, are the proper way to describe wave propagation in such heterogeneous conditions as presumably exist in the near-surface (a major problem is our lack of knowledge on what those conditions are really like, which is related to the lack of resolution of our measurements, because seismic exploration is generally focused on deeper targets rather than on the shallow near-surface layers). The wave equation itself might be inadequate to describe near-surface situations, involving distances ranging from a fraction of the length of a seismic wavelength to a few times that length, if the variations in the medium are large within a length-scale smaller than the length of the seismic wavelength.

7.2 The rough interface problem

Simulation of wave propagation in situations involving a reflecting interface whose shape is rough (e.g., h is large relative to D, in the sinusoidal model case) and at least approximately periodic, is a subject of considerable interest in acoustics and electromagnetics. One could wonder to what extent solutions to the problem developed in those disciplines apply to situations of interest in exploration seismology.

Such solutions commonly refer to the portion of the wavefield reflected from the interface, while in time-distortion problems we are primarily interested in the influence of the presence of irregularities on the interface upon the waves transmitted through the interface to and from deeper reflectors. Study of the influence of such irregularities on the amplitude of the waves reflected from the interface might be of interest for AVO and related fields.

A large portion of the developments in the study of reflections from rough-shaped interfaces, mainly in electromagnetics, addresses situations in which the wavelength D of the periodic shape is small, of a length comparable to the wavelength λ_1 of the incident wavefield. A typical example is that of the diffraction-grating problem. Results from the study of such problems could probably be of help in further understanding the character of features such as the diffraction events observed in some of the data generated in this work, (in particular for larger values of the aspect ratio h/D). We simplistically identified those events as noise for the purposes of studying reflection-time distortions.

7.3 Consideration of additional factors

A number of factors not considered in this work might have significance for the character of reflection-time distortions and the quality of the surface-consistency assumption, and might be of interest in further work on the subject.

Commonly-used source and receiver arrays are one such a factor. Arrays are designed to filter out events whose seismic wavelengths along the recording surface are relatively short, roughly comparable to the length of the array or shorter. Thus, events such as low-velocity surface waves or high-frequency reflections arriving at non-vertical incidence are attenuated by the action of arrays. It is not so clear, however, what is the action of arrays on the *timing* of such or other events. Combee (1994, 1995) points out that spatial averaging of the wavefield by the action of arrays can be detrimental to the resolution of near-surface anomalies and thus to the performance of methods aimed at correcting for the action of those anomalies on the timing and wavelet shape of reflection events. Indeed, variations, within the length of the array, in the time-distortions arising from such anomalies will be averaged by the action of the array so that the time-distortions in the recorded data will be a smoothed version of those originally present in the wavefield. Since they are averaged, those intra-array variations in the time-distortions cannot be discriminated and hence corrected-for, from the information in the output data. This averaging, or stacking, of the uncorrected distortions will hurt the higher-frequency components in the data. Commonly, the length of the arrays is relatively short, and intra-array variations of concern would be of even shorter wavelength. Such variations must arise from the shallowest portions of the near-surface since wavefront-healing, which is the determining factor for the magnitude of such short-wavelength anomalies, becomes important as the depth of the anomalies increase. In general, we can view the averaging action of the array over the time distortions as similar, though surely not identical, to the wave-theoretical averaging over the length of the contributing zone discussed in Chapter 4.

Time-distortions in land seismic data also arise from variations in elevation on the recording surface. One could think of using a sinusoidal model of that surface, similar to that considered for the near-surface here, to explore the implications of variations in surface topography for the character of wave-theoretical time-distortions. Wavefront healing should not be an issue for time-distortions related to surface topography since in that situation reflection-time distortions arise from variations at the receivers themselves, and not from distant features such as the base-of-weathering interface in the models considered in this thesis (colloquially, there is no "room" for healing to act in this situation, or equivalently, the size of the contributing zone is very small). Time-distortions related to surface topography are generally addressed by using field-static corrections derived from surface elevation information. Problems arise, however, not only because of the potential limitations of the static approach (i.e., the assumptions of surface-consistency and time-invariance might be in error) but also if information on surface-elevation (and very-near-surface information) is not available in fine spatial detail.

Non-sinusoidal variations in the shape of the base of the weathering have been considered in some work by Ed Jenner, a fellow graduate student in the CSM Geophysics Department. He performed a spectral analysis of the time-distortions in synthetic shot records obtained for a model with spatially filtered pseudo-random variations in the shape of the interface at the base of a constant-velocity weathering layer. The shape of the statics computed for his model are shown in Figure 7.1, along with the time distortions he found in synthetic data generated for the model, using finite-difference and ray-tracing algorithms.

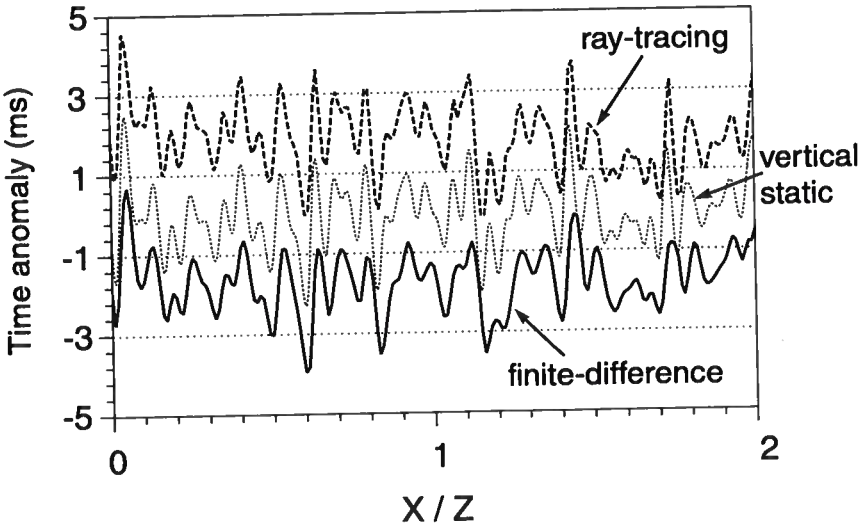

FIG. 7.1. Time-distortions and vertical statics for a model with spatially filtered pseudo-random variations in the shape of the base of a constant-velocity weathering. The statics were computed as vertical traveltimes through the near-surface velocity model so that the shape of the base-of-weathering interface is a scaled version of the shape of the statics. Also shown are the time-distortions found in data generated with finite-difference and ray-tracing algorithms. Work by Ed Jenner.

A simple, linear relationship does not exist between the results for a model such as that in Ed's tests and those for the sinusoidal model in this thesis. The results shown in Figure 7.2, however, indicate a reduction in the magnitude of the short-wavelength spectral components of the time-distortions in the finite-difference-generated data, similar to the high cut filtering action seen for short offsets in the sinusoidal model (e.g., Figure 4.3). Also similar to other results of the present work, ray-tracing modeling fails to reproduce this wave-theoretical reduction in the magnitude of short-wavelength components of the distortions. These results support the claim that despite the nonlinearity of the problem of near-surface-induced time-distortions, the results from simple models such as the sinusoidal models used in this thesis should give insight into the problem that is useful in understanding the results for more complicated models that

address more realistic situations.

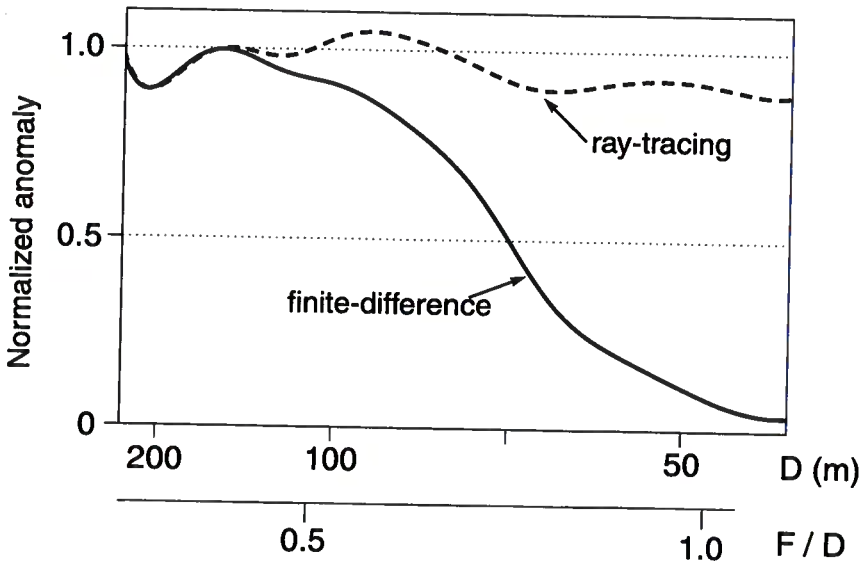

FIG. 7.2. power spectra of the time-distortions in the data generated for a model with pseudo-random variations in the shape of the base of the weathering, using finite-difference and ray-tracing algorithms. The time-distortions are shown in Figure 7.1. Work by Ed Jenner.

To parallel the work here, it remains to be seen to what extent the time-distortions for the model with pseudo-random variations in the shape of the base of the weathering conform to those expected under the assumption of surface-consistency. A critical matter when analyzing data from models with non-periodic base-of-weathering is that of how to devise a measure of the departure from surface-consistency if, as in the work in this thesis, practical limitations allow us to generate only a limited amount of data. The simplicity and regularity of the sinusoidal models studied in this thesis, which allowed for surface-consistency in the time-distortions to be identified with a repetition with offset of the sinusoidal pattern, is not available in that situation.

Lateral variations in velocity within the weathering can also introduce reflection-time distortions such as those observed in practice. Models with lateral velocity variation offer the potential benefit of yielding realistic levels of both time-distortions and strength of surface-associated multiples. If realism in the finite-difference simulation is sought by using a free-surface condition as boundary condition in the earth's surface, as we already saw, an unrealistically high level of surface-associated multiples is present in the generated data. A reduction in the vertical velocity-contrast at the base of the weathering yields a reduction in the level of multiples but also an undesired reduction in the magnitude of the time-distortions in the data. It is desirable to build a model which gives significant time-distortions while at the same time keeping the strength of the multiples at reasonable levels, as is common in land data. Including

lateral velocity variations in the near-surface in a model that also features a mild vertical velocity contrast at the base of the weathering (which could be flat for simplicity, at least in a first approximation) could give us the desired model. If this is to be pursued, the details of such a model have to be worked out. Once again, sinusoidal lateral variations in the velocity of the weathering could be considered. Also, it remains to be seen whether or not the results obtained with such a model are similar to those obtained here by considering lateral variations in the thickness of the weathering.

As previously acknowledged, one further respect in which the work here is simplistic is that it has involved study of only 2D earth models. Considering lateral variations in the near-surface and studying the character of the time-distortions in data generated for a 3D model is a challenging subject, not only in the computational and data-handling aspects of the problem, but also in the complexity added by including further variations in the dimension added to the problem. For example, a 3D study would require addressing issues such as the azimuthal dependence of variations in the character of the time-distortions and in the quality of the surface-consistency assumption, besides the dependence on offset already addressed in the present 2D study.

In the present work, an approximate characterization of time-distortions has been achieved by distinguishing between wave- and ray-theoretical influences on the character of those distortions. As with wave-theory, however, ray-theory can be formulated at several levels of generality or complexity. For example, we have postulated that ray-theoretical influence on the magnitude of the time-distortions would yield a monotonic increase in that magnitude with increasing offset, due to the increasing departure from the vertical of the raypaths in the weathering. Such behavior of the slant path of the rays, however, applies only to a situation in which the base-of-weathering interface is horizontal. The ray-theoretical behavior is more complex if the sinusoidal shape of the interface is taken into account in the ray tracing; the departure in the raypaths from those corresponding to a flat horizontal base of weathering is larger as D is smaller. The sinusoidal shape was indeed included in the ray-tracing simulations whose results were presented in Figures 3.6 and 3.7. As illustrated in Figure 3.7, even considering that shape does not lead to reproducing the reduction in the magnitude of the time-distortions observed in the finite-difference data. That reduction is certainly a wave-theoretical phenomenon. We observed, however, that considering the departure from the vertical of the rays in the weathering helped explained features such as the variations in the phase in the time-distortions (see the discussion in Section 4.2.4 even in situations in which there was reduction in the magnitude of the distortions. A comparison between the time-distortions present in the synthetic data and those predicted taking the slant path into account (either simplistically by using the flat horizontal base of weathering, or more precisely by using the sinusoidal shape) would help determine whether or not some other features in the behavior of those distortions can be explained by ray-theoretical considerations.

7.4 Are there other problems for surface-consistency?

Since it is supported by a simplistic model of vertical-wave propagation in the near-surface, we expect the assumption of surface-consistency to be imperfect. Yet in this work, arguments are given in favor of the acceptability of the assumption for residual-statics problems for a number of situations. Moreover, residual-statics methods based on the assumption generally work at least acceptably in practice. Perhaps those expectations are too pessimistic. Also, we should look for significant departure from surface-consistency elsewhere.

A portion of the time-deviations present in reflections is removed by the NMO-correction performed prior to any residual-statics estimation effort. This is specially significant for long-wavelength anomalies (i.e., those with a wavelength comparable to the spreadlength). For such long-wavelength anomalies, NMO-correction compensates for a large portion of the deviation from the vertical of raypaths in the near-surface. Alternative methods to residual-statics estimation (e.g, "field statics" or refraction statics) do not include the prior NMO-correction step. In those approaches, a vertical correction is applied and then NMO-correction is performed, optionally followed by residual statics estimation. NMO-correction should then remove most the influence of non-vertical propagation not taken care of by the previous static corrections, at the expense of possible distortion in the estimated velocities (since the velocity analysis is based on a distorted timing of the reflections resulting from the limitations of the vertical correction).

Using surface-consistent statics to correct for near-surface-induced distortions as opposed to other methods which allow for consideration of non-vertical raypaths in the near-surface, might have a significant influence on the performance of imaging processes. As shown in the work of Salinas (1996), in situations of large lateral and vertical velocity variations in the near-surface, surface-consistent static corrections might contribute to less-than-optimum quality in prestack depth migration images from data that have undergone such corrections (see his discussion in Section 5.3.1 and specifically Figures 5.5 through 5.7). It is also shown in the work of Salinas (1996) that the application of surface-consistent static corrections might lead to errors in conventional stacking-velocity analysis (see his Section 5.6).

BIBLIOGRAPHY

Alford, R. M., K. R. Kelly, and D. M. Boore (1974). Accuracy of finite-difference modeling of the acoustic wave equation. *Geophysics*, **39**, no. 6, 834–842.

Berkhout, A. J. (1984). *Seismic resolution: resolving power of acoustical echo techniques.* Geophysical Press.

Berryhill, J. R. (1979). Wave equation datuming. *Geophysics*, **44**, no. 8, 1329–1344.

Berryhill, J. R. (1984). Wave equation datuming before stack (short note). *Geophysics*, **49**, no. 11, 2064–2067.

Bleistein, N. (1984). *Mathematical methods for wave phenomena.* Academic Press, New York.

Bloor, R. (1996). Near-surface layer traveltime inversion: a synthetic example. *Geophysical Prospecting*, **44**, 197–213.

Cerveny, V. and J. E. P. Soares (1992). Fresnel volume ray tracing. *Geophysics*, **57**, no. 7, 902–915.

Clayton, R. W. and B. Engquist (1977). Absorbing boundary conditions for acoustic and elastic wave equations. *Bulletin of the Seismological Society of America*, **67**, no. 6, 1529–1540.

Combee, L. (1994). Wavefield scattering by a 2-d near-surface elliptic anomaly. In *64th Annual Internat. Mtg., Soc. Expl. Geophys., Expanded Abstracts*, Volume 94, pp. 1306–1309.

Combee, L. (1995). Scattering of the source-generated wavefield by a 2-d near-surface elliptic anomaly. In *65th Annual Internat. Mtg., Soc. Expl. Geophys., Expanded Abstracts*, Volume 95, pp. 1325–1328.

Docherty, P. (1991). Documentation for the 2.5-d common shot program cshot. Technical Report CWP-U08R, Center for Wave Phenomena.

Farrell, R. C. and R. N. Euwema (1984). Refraction statics. *Proc. Inst. Electr. Electron. Eng.*, **72**, 1316–1329.

Fei, T. and K. Larner (1995). Elimination of numerical dispersion in finite-difference modeling and migration by flux-corrected transport. *Geophysics*, **60**, no. 6, 1830–1842.

Fornberg, B. (1988). The pseudospectral method - accurate representation of interfaces in elastic wave calculations. *Geophysics*, **53**, no. 5, 625–637.

Gouveia, W. (1996). Sudref: A distributed elastic reflectivity modeling algorithm. Technical Report CWP-215, Center for Wave Phenomena.

Hileman, J. A., P. Embree, and J. C. Pflueger (1968). Automated static corrections. *Geophys. Prosp.*, **16**, no. 3, 326–358.

Kin, A. R. and C. A. Jacewitz (1984). Interactive model-based weathering corrections. In *54th Annual Internat. Mtg., Soc. Expl. Geophys., Expanded Abstracts*, Volume 84, pp. Session:S1.4.

Larner, K., G. Perez, E. Jenner, and T. Salinas (1996). The quality of the surface-consistency assumption in residual-statics estimation. In *66th Annual Internat. Mtg., Soc. Expl. Geophys., Expanded Abstracts*, pp. 1646–1649.

Marsden, D. (1993a). Static corrections-a review, part 1. *The Leading Edge*, **12**, no. 1, 43–49.

Marsden, D. (1993b). Static corrections-a review, part 2. *The Leading Edge*, **12**, no. 2, 115–120.

Marsden, D. (1993c). Static corrections-a review, part 3. *The Leading Edge*, **12**, no. 3, 210–216.

McMechan, G. A. and H. W. Chen (1990). Implicit static corrections in prestack migration of common-source data. *Geophysics*, **55**, no. 6, 757–760.

Muir, F., J. Dellinger, J. Etgen, and D. Nichols (1992). Modeling elastic fields across irregular boundaries (short note). *Geophysics*, **57**, no. 9, 1189–1193.

Rajasekaran, S. and G. A. McMechan (1995a). Prestack processing of land data with complex topography. *Geophysics*, **60**, no. 6, 1875–1886.

Rajasekaran, S. and G. A. McMechan (1995b). Tomographic estimation of the spatial distribution of statics. *Geophysics*, **61**, no. 4, 1198–1208.

Rice, J. A., C. E. Krohn, and L. M. Houston (1991). Shallow near-surface effects on seismic waves. In *61st Annual Internat. Mtg., Soc. Expl. Geophys., Expanded Abstracts*, Volume 91, pp. 747–749.

Salinas, T. (1996). The influence of near-surface time anomalies in the imaging process. M.Sc. Thesis. Colorado School of Mines.

Schneider, William A., J., L. D. Phillip, and E. F. Paal (1995). Wave-equation velocity replacement of the low-velocity layer for overthrust-belt data. *Geophysics*, **60**, no. 2, 573–579.

Sheriff, R. E. (1980). Nomogram for fresnel-zone calculation (short note). *Geophysics*, **45**, no. 5, 968–972.

Sheriff, R. E. (1991). *Encyclopedic Dictionary of Exploration Geophysics*. Society of Exploration Geophysicists.

Snieder, R. and A. Lomax (1996). Wavefield smoothing and the effect of rough velocity perturbations on arrival times and amplitudes. *Geophys. J. Int.*, **125**, 796–812.

Stefani, J. P. (1995). Turning-ray tomography. *Geophysics*, **60**, no. 6, 1917–1929.

Taner, M. T., F. Koehler, and K. A. Alhilali (1974). Estimation and correction of near-surface time anomalies. *Geophysics*, **39**, no. 4, 441–463.

Taner, M. T., L. Lu, and E. Baysal (1988). Unified method for 2-d and 3-d refraction statics with first break picking by supervised learning. In *58th Annual Internat. Mtg., Soc. Expl. Geophys., Expanded Abstracts*, Volume 88, pp. Session:S5.1.

Tjan, T. (1995). Residual statics estimation for data from structurally complex areas using prestack depth migration. M.Sc. Thesis. Colorado School of Mines.

Tsvankin, I. (1995). *Seismic wavefields in layered isotropic media.* Samizdat Press.

Vasco, D. W., J. Peterson, John E., and E. L. Majer (1995). Beyond ray tomography: Wavepaths and fresnel volumes. *Geophysics*, **60**, no. 6, 1790–1804.

White, J. E. (1983). *Underground Sound, Application of Seismic Waves.* Elsevier, New York.

Wiggins, R. A., K. L. Larner, and R. D. Wisecup (1976). Residual statics analysis as a general linear inverse problem. *Geophysics*, **41**, 922–938.

Yilmaz, O. (1988). *Seismic Data Processing; Investigations in Geophysics 2.* Society of Exploration Geophysicists.

Zhu, X., D. P. Sixta, and B. G. Angstman (1992). Tomostatics: Turning-ray tomography + static corrections. *The Leading Edge*, **11**, no. 12, 15–23.